Glaciers retreat, frogs advance:
rapid adaptation, genetic drift, and infection dynamics during the climate-driven range expansion
of an Andean frog

By

Emma C. Steigerwald

A dissertation submitted in partial satisfaction of the

requirements for the degree of

Doctor of Philosophy

in

Environmental Science, Policy, and Management

in the

Graduate Division

of the

University of California, Berkeley

Committee in charge:

Professor Rosemary Gillespie, Chair
Professor Rasmus Nielsen
Professor Erica Bree Rosenblum
Professor Eileen Lacey

Summer 2023

ABSTRACT

Glaciers retreat, frogs advance:
rapid adaptation, genetic drift, and infection dynamics during the climate-driven range expansion
of an Andean frog

by

Emma C. Steigerwald

Doctor of Philosophy in Environmental Science, Policy, and Management

University of California, Berkeley

Professor Rosemary Gillespie, Chair

All over the world, species are shifting their geographic distributions in response to climate change. We know from studies of other range expansion and contraction scenarios—like those driven by species invasions or by the end of the last Ice Age—that they affect ecological interactions and the evolutionary trajectories of species. The impacts of range expansions and contractions driven specifically by contemporary climate change, though, are still profoundly uncertain. Understanding these ecological and evolutionary impacts will be important for biodiversity conservation and management under rapid global change. To address this critical knowledge gap, I combine fieldwork, molecular work, and analyses of population genetics and disease ecology over the course of three dissertation chapters. My research illuminates how the whole genome diversity, genetic adaptation, and infection dynamics of a host species were affected by its climate-driven range expansion. Specifically, my dissertation examines the expansion of the Marbled four-eyed frog (*Pleurodema marmoratum*) into upslope, mountain pass habitat that deglaciated over the last 150 years in the Cordillera Vilcanota, Peru.

To my parents, who are the reason I get to do something I care about.

TABLE OF CONTENTS

INTRODUCTION

The three fundamental ways in which a species may respond to rapid contemporary climate change are to evolve their environmental tolerance limits, shift their distributional range, or decline towards extinction. Yet these three possibilities are not mutually exclusive (Parmesan, 2006). To illustrate their dynamic interaction, consider distributional shifts—specifically, range expansion. Clearly species may need to adapt to novel environmental conditions as they colonize new habitats (Kirkpatrick & Barton, 1997; Polechová & Barton, 2015). The process of range expansion might, through high genetic drift in small founding populations and rounds of founder events bottlenecking genomic diversity (Slatkin & Excoffier, 2012; Willi et al., 2020), impact the future evolutionary possibilities and likelihood of decline for newly founded populations. Range expansion might also influence interspecific relationships by introducing both players to a novel environment and perhaps favoring one species to the detriment of the other (Scholthof, 2007). If we aim to conserve biodiversity in a rapidly changing world, we must improve our understanding of the interplay of distributional change, adaptation, and decline in species' climate change responses.

The Cordillera Vilcanota, a portion of the eastern Andes located in southern Peru, has been designated a critical climate refuge promoting the long-term persistence of global biodiversity due to its situation high atop a megadiverse portion of the Andes-Amazon region (Young et al., 2015). Among the species already documented to have expanded their upslope elevational range into the rapidly deglaciating mountain passes of the Vilcanota are three amphibians: the Marbled four-eyed frog (*Pleurodema marmoratum*), the Andean toad (*Rhinella spinulosa*), and the Marbled water frog (*Telmatobius marmoratus;* Seimon et al., 2007). Their upslope expansion in the Vilcanota was marked by outbreaks of the devastating fungal pathogen of amphibians *Batrachochytrium dendrobatidis* (*Bd;* Seimon et al., 2007). With my dissertation work, I studied how climate-change driven range expansion affected (1) the population genomic diversity of *P. marmoratum*, (2) this species' adaptation to the novel environment colonized, and (3) the dynamics of all three species with the *Bd* pathogen.

Chapter 1: Range expansions may have an array of possible impacts on genetic diversity (e.g., Klopfstein et al., 2006; Peischl et al., 2015; Razgour et al., 2013), with potential implications for the fitness and evolvability of leading-edge populations. Although climate-driven range expansions are both taxonomically and spatially widespread (e.g., Chen et al., 2011; Moritz et al., 2008; Freeman et al., 2018; Raxworthy et al., 2008), we have not yet observed how they impact whole-genome diversity. By assembling a *de novo* reference genome for *P. marmoratum* and doing low-coverage, whole-genome resequencing for 192 frogs across the study landscape, we discover that expansion has both driven declines in genomic diversity and novel opportunities for gene flow that can ameliorate these declines. These results illuminate how considering changing patterns of gene flow under climate change affects the anticipated impacts of range expansions on the heterozygosity and evolutionary potential of wild populations.

Chapter 2: Enhanced genetic drift may interfere with selection efficacy during range expansion (Willi et al., 2018). If this is true for climate-driven range expansions, there may be repercussions for the long-term persistence of leading-edge populations. We studied the

adaptation of *P. marmoratum* to extreme high elevations and what happened to the putatively adaptive alleles detected along the course of the range expansion front. By functionally annotating the *P. marmoratum* genome and performing genotype-by-environment association tests on our low-coverage resequencing dataset, we find that *P. marmoratum* does appear to have a suite of genetic adaptations to high elevation life. However, allele frequencies for these candidate genes behave unpredictably in the upslope habitat colonized over just the last 150 years, suggesting that the genetics of species undergoing climate-change driven range expansions may indeed be ruled by genetic drift at the cost of selection efficacy.

Chapter 3: Climate change impacts emerging infectious disease events through multiple mechanisms, but the influence it exerts through driving host range shifts has been little explored. Not only might we expect range shifts to affect pathogen transmission by altering the connectivity of host populations (Haddad et al., 2014), but range expanding hosts and pathogens will have different physiological responses to the suites of novel conditions they are exposed to, influencing infection outcomes (Scholthof, 2007). We studied the fungal pathogen *Batrachochytrium dendrobatidis* (*Bd*) on three amphibians in the Vilcanota: *Pleurodema marmoratum*, *Telmatobius marmoratus*, and *Rhinella spinulosa*. We analyzed *Bd* genetics, infection metrics, and apparent sublethal impacts along the colonization front to explore how elevational range expansion affected host-pathogen dynamics. Amphibian range shifts have enabled their new connectivity across the once continuously glaciated Vilcanota, but genetic evidence suggests that *Bd* disperses so frequently and extensively that this novel connectivity has not contributed significantly to overall *Bd* dispersal. Although amphibians have not escaped *Bd* infection outright through upslope expansion in the Vilcanota, *Bd* growth does appear to be constrained at the highest elevation reaches. Finally, we present evidence that *Bd* infection has different sublethal costs for amphibians at the new elevations they have colonized, though whether the costs are mitigated or exacerbated by extreme elevation may be moderated by amphibian microhabitat use.

ACKNOWLEDGEMENTS

CHAPTER 1

Climate-driven range expansion depletes genetic diversity but also creates new opportunities for gene flow

Emma Steigerwald, Diana Aguilar-Gomez, Lydia Smith, Juan Carlos Chaparro, Rasmus Nielsen

Abstract

In the first chapter, I use whole genome data to describe what happens to population genetic diversity over the course of contemporary, climate-change driven range expansion. We know that population genetic diversity may decline over space in some range expansion scenarios, sometimes with important implications for the fitness of individuals and for the evolutionary potential of populations. By assembling a *de novo* reference genome for *P. marmoratum* and sequencing 192 frogs sampled from across the study landscape to low coverage, we examine structure, demography, and genetic statistics for *P. marmoratum* populations across the Vilcanota. We find that metrics of genetic diversity initially decline along the elevational expansion front, though gladly we do not observe a corresponding buildup of deleterious mutations. However, we also find that the elevational range expansion of these frogs appears to have created new opportunities for them to interbreed between differentiated watersheds, with restorative impacts on genetic diversity.

1.1 Introduction

The persistence of biodiversity under climate change demands that species undergo evolutionary adaptation and distributional changes (De Meester et al., 2018; Parmesan, 2006). Many species have already shifted their distributions in recent decades (Kusrini et al., 2017; Moritz et al., 2008; Parmesan et al., 1999). While these shifts can allow species to better track the climatic conditions to which they evolved, they will have repercussions for population genomic diversity—particularly closest to changing range limits (Razgour et al., 2013; Rehm et al., 2015). For example, though we might consider a range expansion a successful response to climate change, serial founder events and high genetic drift along an expansion front sometimes causes declines in genetic diversity and the buildup of deleterious genetic variants (Gilbert et al., 2018; Peischl & Excoffier, 2015; Slatkin & Excoffier, 2012). Additionally, we expect range expansions to lead to changing opportunities for gene flow (Hoffmann et al., 2011). The action of these various forces along range expansion fronts may have important implications for the fitness of populations and for their evolvability in the face of continued environmental challenges (Edelaar & Bolnick, 2012; González-Martínez et al., 2017; Pearman & Garner, 2005; Willi et al., 2018).

Knowledge of the characteristics of leading-edge populations may be particularly important to understanding and predicting how climate-driven range expansions will shape the adaptation and demographic trajectories of species (Rehm et al., 2015). Not only do populations at the leading edge of an expanding range tend to serve as the source of the first founders colonizing new habitat, but frequently their descendants can exclude genotypes that arrive later (priority effects; Peter & Slatkin, 2015; Slatkin & Excoffier, 2012). Accentuating the influence of the leading edge is the possibility that many trailing edge populations are undergoing demographic decline and fragmentation or are prevented from contributing migrants by landscape barriers (Hampe & Petit, 2005; Rehm et al., 2015).

Without prior knowledge of the most important genes for the genetic health and adaptation of a species to the new habitat they colonize, any signature of range expansion detected from only a few loci may have little relevance to the persistence or evolvability of that species (Forester et al., 2022). Therefore, documenting the consequences of climate-driven range shifts for whole-genome diversity provides a more relevant and generalizable way to manage countless wild populations to promote their long-term persistence. However, among the few studies that have examined the genomic consequences of climate-change driven range expansions, most employed only a few markers from throughout the genome, and we are aware of none that have employed whole genome sequences (Bi et al., 2019; Garroway et al., 2010; Garroway et al., & Wilson, 2011; Grupstra et al., 2017; Ramos et al., 2018; Rubidge et al., 2012).

To study the genomic signature of contemporary, climate-driven range expansion, we studied amphibians in the Cordillera Vilcanota, Peru. Until the end of the Little Ice Age (1500 – 1900; (Thompson et al., 1986), the Vilcanota would have formed a continuously glaciated, approx. 80 km-long barrier across the landscape. In the intervening years, the Vilcanota has undergone rapid deglaciation, freeing vast areas of upslope habitat, particularly along mountain passes. These passes have been rapidly colonized by the Marbled four-eyed frog (*Pleurodema marmoratum;* Seimon et al., 2007) as it expanded its upper elevational range limit into the newly deglaciated habitat. Whereas the recent range expansions of many species cannot be absolutely confirmed,

fifteen years of herpetological surveys and extensive local glaciological studies lend certainty that *P. marmoratum* actually expanded its upslope distributional limit in the Vilcanota (Seimon et al., 2017). Moreover, this species' robust populations across the Vilcanota make it easy to sample at regular intervals across the landscape (Seimon et al., 2007). We use low-coverage, whole genome sequencing to study the climate-driven elevational range expansion of *P. marmoratum*. Considering how recent and rapid this range expansion has been, we tested the hypothesis that it is characterized by declining heterozygosity, increasing inbreeding coefficients, the accumulation of deleterious genetic variants, and the increasing genetic differentiation of frogs along the range front with increasing distance from source populations. We also tested the hypothesis that this range expansion has provided new opportunities for gene flow across the Vilcanota via now deglaciated mountain passes. Collectively, these results generate important insights into the genome dynamics of species experiencing range expansions that should prove helpful for predicting and potentially managing the genetic consequences of such expansions in other taxa.

1.2 Methods

1.2.1 Field sampling

Frogs were sampled from 3967 to 5303 m a.s.l. in the Cordillera Vilcanota (13.7°S, 71.1°W), a portion of the eastern Peruvian Andes located approximately 100 km ESE of the city of Cusco. Precipitation in the Vilcanota is highly seasonal, with the wet season occurring from October to April and the dry season from May to September (Perry et al., 2014). Fieldwork was timed to coincide with the end of the breeding season for *P. marmoratum* reproductive activity, such that the depth of daily precipitation was abating but adults could still be easily found near water bodies. This placed our sampling from March to May of 2018 and 2019. We searched for post-metamorphic stages visually by inspecting pools and riparian areas as well as manually by feeling for frogs moving under rocks or in mud and along the edges of bodies of water. A total of 10-15 *P. marmoratum* were sampled per site (Fig. 1), with a preference for adults, which were supplemented first with juveniles and then with tadpoles. Sampling sites were generally about 5km apart, but along the two deglaciated mountain passes, Osjollo and Chimboya Pass, we invested in a more concentrated sampling effort (Fig. 1).
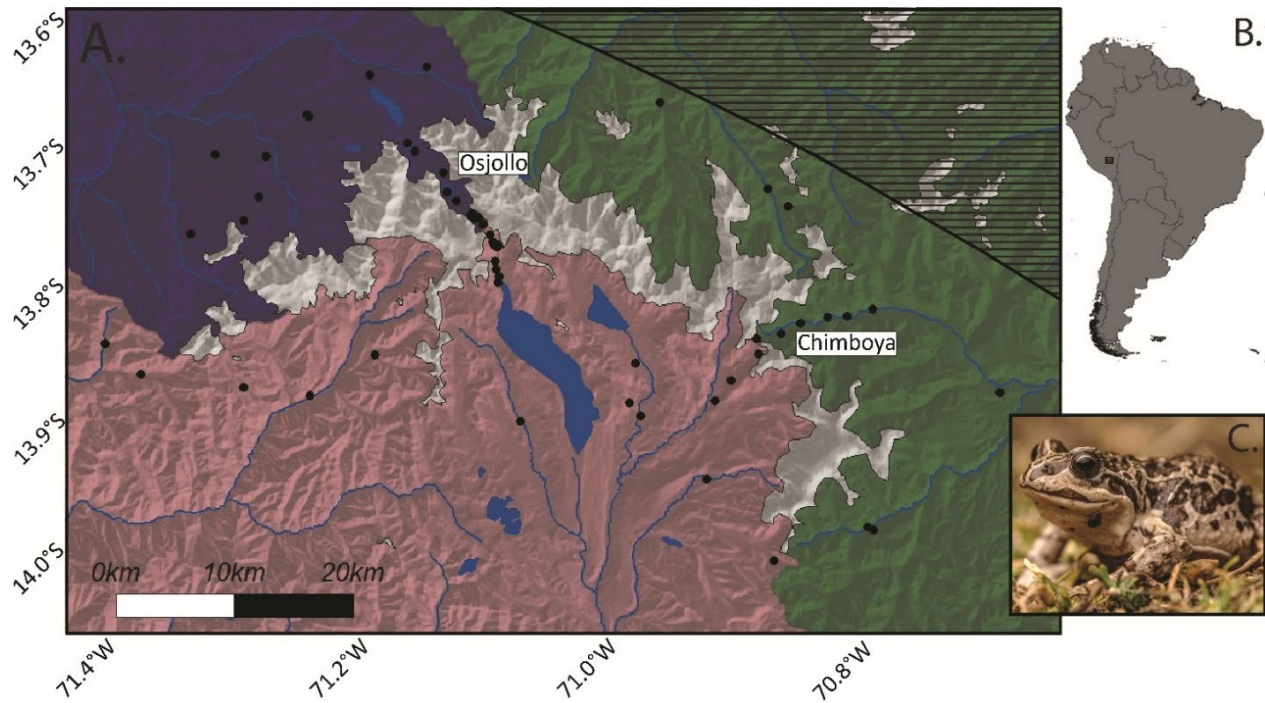
Figure 1. (A) Map of *P. marmoratum* sampling sites (black points) shown over a hill-shaded map of the Cordillera Vilcanota, colorized by the three watersheds on this study landscape. The white hill-shaded polygons show the current glacial extent in the Vilcanota. The deglaciated mountain passes of Osjollo and Chimboya are labelled. The hashed polygon to the northeast shows the area beyond the distributional range margin of *P. marmoratum.* (B) The inset map shows the location of the study site in Peru. (C) The study species, *Pleurodema marmoratum.*

All frogs had one to two toes clipped to provide non-destructive samples for genomic analyses, which were stored in ethanol. Frogs were also dry swabbed (MW113, Medical Wire & Equipment Co., Ltd., Corsham, Wiltshire, UK) to assess the presence of *Bd* infection (Boyle et al., 2004; Hyatt et al., 2007). Body size, mass, and sex were recorded for each animal, as was any evidence of illness or deformity. We determined the developmental stage of each tadpole captured using standard techniques (Gosner, 1960). In December 2019, a single *P. marmoratum* was captured and transported live to Lima. There, it was sacrificed, dissected by tissue type, flash frozen, and transported on dry ice. All samples were transported to the University of California, Berkeley for storage in a -80˚C freezer until DNA extraction, sequencing, and analysis.

1.2.2 Genome assembly

High molecular weight DNA was extracted from muscle of the *P. marmoratum* individual that was flash frozen and tissued. The extract was used to prepare sequencing libraries with the 10X Genomics microfluidic platform, and then sequenced on an Illumina NovaSeq with PE150 reads to a raw coverage of 62x and an effective coverage of 39x. These linked reads were adapter-trimmed with Trimmomatic (v0.39; Bolger et al., 2014), assembled with Supernova (v2.1.1; Weisenfeld et al., 2017), and cleaned of duplicate sequences using SeqKit (v2.1.0; Shen et al., 2016). The contiguity of the assembly was assessed using Assemblathon statistics

(https://github.com/KorfLab/Assemblathon/blob/master/assemblathon_stats.pl; Bradnam et al., 2013) and the completeness of the assembly with respect to genes expected to be single-copy orthologs was assessed with BUSCO (v4.1.2; Simão et al., 2015). Repetitive regions of the genome were identified with RepeatModeler2 (v2.0.3; Flynn et al., 2020) and then masked with RepeatMasker (v4.1.2; Smit et al., 2022). Scaffolds in the mitochondrial genome were identified and suffixed with 'mito' via alignment with MUMmer4 (v4.0.0; Marçais et al., 2018) to mitochondrial genomes from *Melanophryniscus moreirae* (vNC_037378.1) and *Telmatobius chusmisensis* (vNC_030333.1), and a partial mitochondrial genome from *Pleurodema thaul* (vJX564888).

1.2.3 Whole genome resequencing

DNA was extracted from toe clips from 192 adult *Pleurodema marmoratum* using the Omega Bio-Tek Mag-Bind Blood and Tissue plate extraction kit. A subset of the adult frogs sampled were selected for sequencing to represent a range of *Bd* infection intensities (see Chapter 3) and to maximize geographic representation of sequencing data (Fig. 1). Libraries were prepared using the KAPA Hyper Prep Kit and then sequenced on two Illumina Novaseq lanes to an average sequence depth of 3X. Raw data were adapter-trimmed with Trimmomatic (v0.3.9; Bolger et al., 2014) and cleaned of over-represented sequences with Prinseq (v0.20.4; Schmieder & Edwards, 2011), after which their quality was assessed with FastQC (https://github.com/s-andrews/FastQC). These preprocessed sequences were aligned with BWA-MEM (v0.7.17; Li, 2013) to the genome assembly, with the repeat regions of the assembly left unmasked in order to reduce the potential for sequence misalignment. Final BAM files excluded unmapped reads, reads where the mate-pair read was unmapped, reads that were not the primary alignment, reads that failed platform or vendor quality checks, and reads that were either PCR or optical duplicates.

The resulting BAM alignment files and a version of the genome with both simple and complex repeats hard-masked were processed in ANGSD (v0.941-11-g7a5e0db; Korneliussen et al., 2014) to call a list of sites throughout the genome not embedded in repetitive regions and where data are available for at least 50 individuals. The likelihood ratio that each of those sites was mis-mapped was calculated in ngsParalog (v1.3.2; Linderoth, 2018) and sites with a Bonferroni-corrected p-value of less than 0.05 were discarded. ANGSD (Korneliussen et al., 2014) was used to calculate genotype likelihoods for the remaining sites using the GATK model and store them in beagle format. Genotype likelihoods contain probabilistic information about genotypes across the genome and are important to use in the context of low-coverage whole genome sequencing given the high uncertainty of genotype calls. Two files were generated, the first containing all sites (variable and invariable; 615,668,560 sites), while the second file included only variable sites (SNP p-value $< 1 \cdot 10^{-6}$; 15,746,373 sites). The final data was filtered to retain only the following: (i) base calls with a Phred quality exceeding 20; (ii) reads where both pairs of sequences derived from sequencing a given DNA molecule from opposite sides (mate pairs) aligned to the reference genome, where their alignment with the reference genome had a mapping quality exceeding 20, and where there was a single best alignment hits; (iv) individual frogs with a sequencing depth between one and 25; and (v) genomic sites that were biallelic and had a p-value of larger than 10^{-4} in a test for Hardy-Weinburg equilibrium.

1.2.4 Structure analysis

To estimate the number of genetically distinct populations present in our sample, the beagle file containing only variable sites was used to calculate a covariance matrix of individual admixture proportions in PCAngsd (v1.10; Meisner & Albrechtsen, 2018). This matrix was imported to R for eigenvalue decomposition and plotting in gpplot2 (Wickham, 2011). To examine population structure further and understand geographic areas where these populations are admixing, we then used OHANA (Cheng et al., 2017; https://github.com/jade-cheng/ohana). For OHANA analyses, we rarefied data to ensure even geographic representation of samples across the landscape, given that the individuals sequenced overrepresented the two mountain pass transects on the landscape (compare sampling sites plotted in Fig. 1 and 3). Evidence for genetic differentiation by watershed was explored for $k = 2$ through $k = 6$ possible ancestry components using the OHANA qpas command. The output allele frequency inference was then used to estimate component covariances, which was approximated into a component tree, using the OHANA nemeco and cov2nwk commands. In the resulting newick tree file, branch lengths are represented by the genetic distances between ancestry components as calculated from the covariance matrix:

$$Dist\ (p_1,\ p_2) = Var\ (p_1) + Var\ (p_2) - 2 \times Cov\ (p_1,\ p_2)$$

The contribution of ancestry components to the genotypes of individual frogs as well as trees representing the relationship among those ancestry components were plotted in ggplot2 (Wickham, 2011). Additionally, OHANA ancestry components for $k = 3$ were projected as pie charts onto the genetic PCA and onto a hill-shaded DEM of the Vilcanota.

1.2.5 Demographic analysis

The folded site frequency spectrum (SFS), which represents the distribution of genetic variation across different allele frequencies, was estimated in ANGSD (Korneliussen et al., 2014) from the total set of variable and invariable sites and then plotted in R with gpplot2 (Fig. S 1; Wickham, 2011). The folded SFS was used to estimate heterozygosity across sampled frogs using the following formula, where a_i is the probability mass in the ith category of the folded SFS (standardized to sum to one including fixed sites) and n is the total number of individuals sampled (here, 192):

$$\sum_{i=1}^{n-1} 2(\frac{i}{2n})\left(1 - \frac{i}{2n}\right) a_i$$

For demographic analyses, frogs were treated as three populations, largely based on the watershed from which they were sampled. The one exception was a sample of six individuals from the southern watershed (the leftmost six in Fig. S 3 B) that were obtained from the two westernmost sites (Fig. 3); these animals were most genetically similar to samples from the northwestern watershed and were thus grouped together with them. LD (r^2) across the set of ANGSD-filtered variable sites was first calculated in ngsLD (v1.1.1; Fox et al., 2019) from genotype likelihoods for every pair of variable sites in the genome no more than 300 kb apart, using an expectation maximization algorithm. LD decay was visualized using the R script

fit_LDdecay.R. Based on the resulting plots, SNPs were removed from the dataset if they were less than 50 kb apart in the genome and had an LD of more than 0.5 using prune_graph (Fox et al., 2019), leaving a set of just over six million LD-pruned SNPs.

A random subset of 500,000 of these LD-pruned sites was used to construct a 3-D SFS for these populations in ANGSD (Korneliussen et al., 2014). A demographic model was estimated based on the SFS using GADMA (2.0.0rc25; Noskova et al., 2023) and the likelihood function calculated in DaDi (Gutenkunst et al., 2009) with BFGS local optimization and 50 replicate optimization attempts. The model assumed one time interval between each split, to facilitate the convergence of this complex, three-population model. The parameters estimated were t_1, the time interval between the two different population splits; t_2, the time interval since the split between populations 2 and 3; nu_1, the size of population 1; nu_2, the size of population 2; nu_3, the size of population 3; $m_{1\_2,3}$, the migration rate from population 3 to 2 during t_1; m_{1_32}, the migration rate from population 2 to 3 during t_1; $m_{2\_1,2}$, the migration rate from population 2 to 1 during t_2; and $m_{2\_2,1}$, the migration rate from population 1 to 2 during t_2. Model convergence was assessed by inspecting the models every 150 iterations and the log likelihood values for each of the 50 repeats over successive iterations. When the model and log likelihood value stabilized, the model was considered to have converged. Genetic time units were converted to years by specifying a theta of 7.15 ($\theta = 4L\mu$; where assembly length, L, was 1.788 Gb and the mutation rate per base per generation, μ, was $1 \cdot 10^{-9}$) and a generation time of 3.5 years. The mutation rate employed was based on a nuclear mutation rate estimate derived from six frog species (Crawford, 2003), and the generation time estimated from age structure data collected for a high-altitude, geographically proximal congeneric (Iturra-Cid et al., 2010).

To refine inference of population history since these populations split, ANGSD was also used to construct a 2D-SFS of each the southern and northwestern population pair and the southern and northeastern population pair. These joint SFS were used in GADMA/DaDi with the same specifications as previously, except this time a more complex model structure was permitted with two time intervals before and after the population split. The parameters estimated were t_1, the more recent time interval before the population split; t_2, the time interval immediately after the population split; t_3, the more recent time interval since the population split; s_1, the fraction of the effective population size that goes into each population during the split; $nu_{1,1}$, the size of the population during t_1; $nu_{2,1}$, the size of population 1 during t_2; $nu_{2,2}$, the size of population 2 during t_2; $nu_{3,1}$, the size of population 1 during t_3; $nu_{3,2}$, the size of population 2 during t_3; $m_{2\_1,2}$, the migration rate from population 2 to 1 during t_2; $m_{2\_2,1}$, the migration rate from population 1 to 2 during t_2; $m_{3\_1,2}$, the migration rate from population 2 to 1 during t_3; and $m_{3\_2,1}$, the migration rate from population 1 to 2 during t_3. Model convergence was assessed as previously.

1.2.6 Assessing genomic statistics along the expansion front

Both individual expected heterozygosity (H_e) and individual breeding coefficient (F) were calculated using a subset of 500,000 SNPs randomly sampled from the total set of ANGSD-filtered variable sites. Individual heterozygosity was examined by generating a folded SFS for each frog in ANGSD (Korneliussen et al., 2014) and dividing the count of singleton mutations by the total number of sites in the subset. Individual inbreeding coefficients were estimated in ngsF (v1.2.0-STD; Vieira et al., 2013) for one hundred replicates, each time first running the

approximating algorithm and feeding its estimates into the non-approximating algorithm with a stopping criterion of $1 \cdot 10^{-9}$. The inbreeding coefficients used were those calculated from the replicate achieving the highest log likelihood value.

Expansion load was examined by aligning pre-processed *P. marmoratum* reads for each frog to the *E. pustulosus* genome (v1.0; Bredeson et al., 2021) as an outgroup. These BAM alignment files were used to generate beagle genotype likelihood files using the same ANGSD inclusion criteria used to filter reads, loci, and individuals in resequencing above (section 1.2.3), including the same SNP *p*-value filter. The resulting set of sites was used in bcftools (v1.15.1; Danecek et al., 2021) to generate first an mpileup and then a VCF file, which was filtered for variants with a minor allele frequency of less than 5 % (rare variants). The *E. pustulosus* genome and annotation files (Bredeson et al., 2021) were used to generate a custom SNPeff database (v5.1d; Cingolani et al., 2012), which was then deployed to annotate the VCF file. With the annotated VCF, for each frog we summed the total number of high-impact mutations—variants assumed to have disruptive impact in the protein according to the classification of SNPeff, and thus having a high probability of being deleterious. The VCF was also used to calculate the average depth of sequencing coverage per frog at the sites of these high-impact mutations. In R, linear regression was used to model the relationship between the count of high-impact mutations for a frog as a response variable and, as predictor variables, the depth of sequencing coverage at those mutations and individual-level heterozygosity of that frog. The residuals of this model were used as a representation of expansion load. It is important to use the residuals of this model rather than the raw counts of high impact mutations because we expect that loci sequenced at higher coverage have a higher likelihood of being called as genetic variants (Lefouili & Nam, 2022) and that individual frogs with higher genetic diversity will generally have more genetic variants (Mathur & Dewoody, 2021; Yang et al., 2015).

Individual heterozygosity, inbreeding statistic, and expansion load (the residuals of the regression model above) were mapped on a hill-shaded DEM of the Vilcanota using R. The statistics were first averaged between individuals at a single sample site. Then, a geostatistical model of the genetic statistic was created using the gstat function from the package gstat (v2.0.9), using a maximum of four data points for each interpolation and an inverse distance weighting parameter of 0.5. Finally, we performed raster interpolation with the raster package (v3.5.21) command interpolate using the geostatistical model as the input. This raster was visualized with ggplot2 (Wickham, 2011). The values of these statistics for individual frogs were also visualized along the two major mountain pass transects using a ggplot2 scatterplot.

Pairwise genetic differentiation between sampling sites was calculated in ANGSD (Korneliussen et al., 2014) for sampling sites where three or more frogs had been sequenced. To do this, a joint SFS was first generated for each sampling site pair, then F_{st} was calculated using the realSFS fst index and fst stats command. Pairs of sites were examined along the deglaciated mountain pass transects and between sites sampled downslope towards the core range of the frogs in the southern watershed. Data were visualized as a pairwise heatmap as well as a scatterplot of distance versus linearized F_{st} $\left(\frac{F_{st}}{1-F_{st}} \right)$ generated in ggplot2 (Wickham, 2011).

1.3 Results

1.3.1 Assembly

The Supernova assembly algorithm estimated the genome size of *Pleurodema marmoratum* at about 2.04 Gb, of which 1.79 Gb was assembled into scaffolds. The scaffold N50 was 2.38 Mb and the contig N50 was 17.9 kb, which compares positively with the contiguity of other published landmark anuran genome assemblies (Table S 1). 63.5 % of BUSCOs were complete and in single copy, 1.5 % were complete and duplicated, 14.7 % were fragmented, and 20.3 % of BUSCOs were missing; these metrics are comparable to those for other landmark anuran genome assemblies (Table S 1).

1.3.2 Structure

In the genetic PCA, PC1 explained 15.9 %, PC2 explained 9.4 %, PC3 explained 3.4 %, and PC4 explained 1.7 % of variation in the genetic data. PC1 and PC2 largely separated frogs by watershed (Fig. 2), while PC3 separated frogs by elevation (Fig. S 2). OHANA analysis also effectively split frogs by watershed at $k = 3$, with frogs from each watershed being characterized by a different composition of ancestries with a different ancestry component being dominant in each (Fig. S 3). The mountain passes represent zones of rapid turnover in ancestry components (Fig. 3), with those mountain pass individuals being arrayed along the two major arms of the PCA running parallel to PC2 (Fig. S 4). According to the OHANA-generated phylogenetic tree for $k = 3$, the pairwise genetic distance was largest between the ancestry components dominating the northwestern and northeastern watersheds (*Dist* $(p_{nw}, p_{nw}) = 1.38$) and smallest for southern and northeastern watersheds (*Dist* $(p_s, p_{nw}) = 0.83$), with the distance between northwestern and southern watersheds being intermediate between those values (*Dist* $(p_{nw}, p_s) = 0.91$).
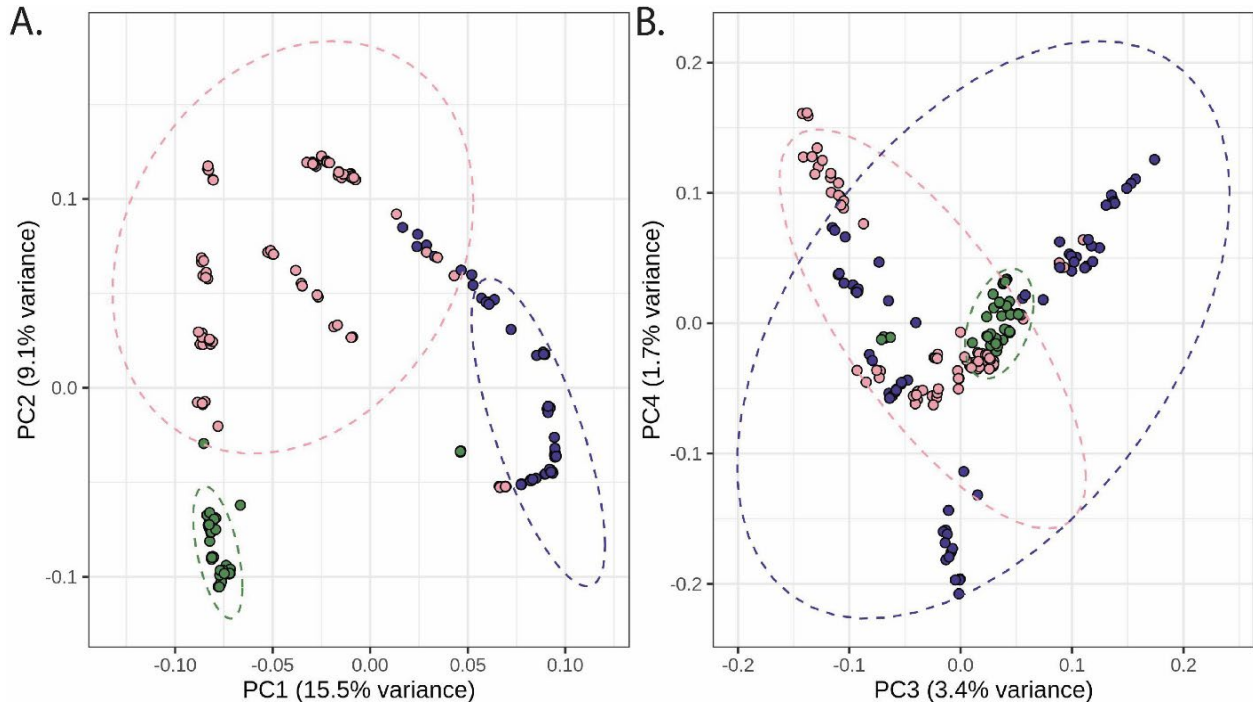
Figure 2. PCA of genomic sequencing data. Individuals are colored by the watershed from which a frog was sampled: purple represents the northwestern, pink the southern, and green the northeastern watersheds. Results are shown for PCs (A) one and two and (B) three and four.
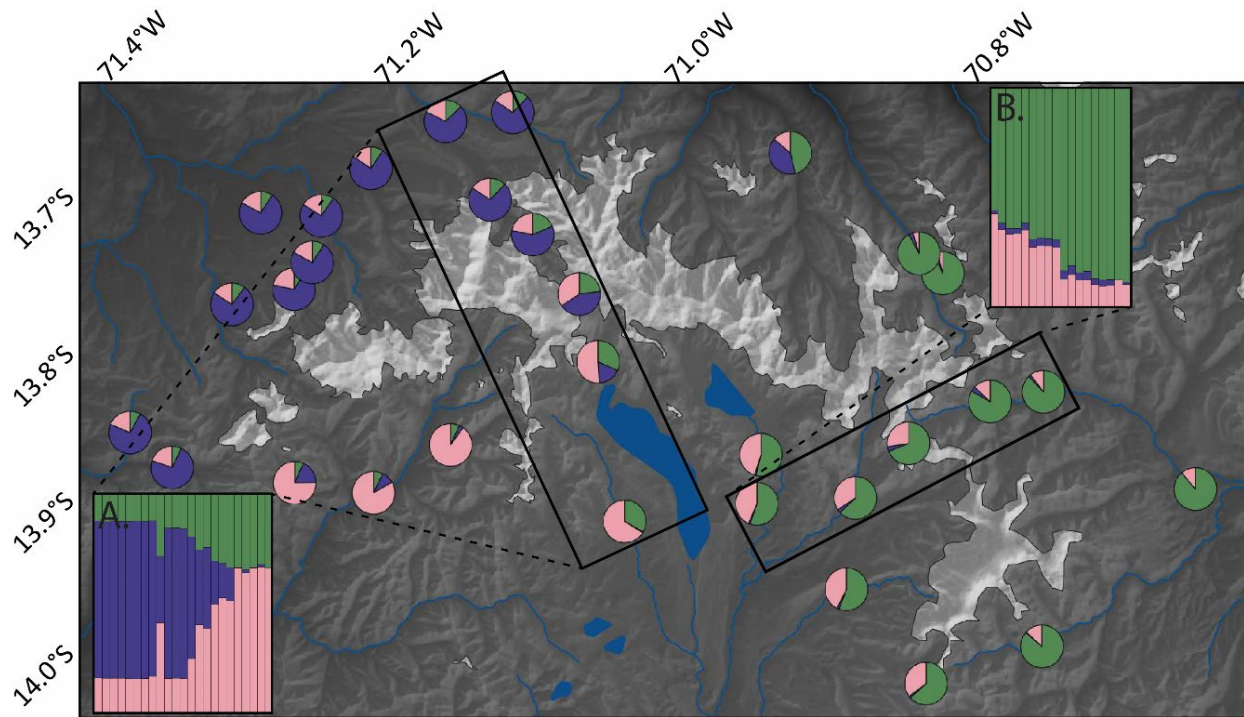
Figure 3. OHANA ancestry components for $\underline{k}$ = 3 depicted as pie charts, averaged across individuals at each sampling site, and overlaid on a hill-shaded map of the Vilcanota. The hill-shaded white polygons show current glacial extent in the Vilcanota. Insets show the ancestry components for individual frogs arrayed along the deglaciated mountain passes of (A) Osjollo and (B) Chimboya.

1.3.3 Demography

The 1-D SFS generated from the complete set of 192 *P. marmoratum* whole genome sequences (Fig. S 1) shows that most of the diversity in these frogs is segregating at low frequencies. About 38 % of the variants in the 1-D SFS were single-copy mutations. Expected heterozygosity across the full data set was 0.19 % (Table S 2).

The demographic model of the three populations that maximized the log likelihood in GADMA/DaDi supports that the *P. marmoratum* population from which frogs currently inhabiting the Vilcanota are descended first colonized the northwestern watershed (Fig. 4). The split between the frog populations now inhabiting the northwestern and southern watersheds is estimated to have occurred 22 thousand years ago. The northwestern population is inferred to have maintained a stable population size until about ten thousand years ago, at which time it began to grow exponentially. The population now inhabiting the southern watershed is inferred to have started at a much smaller effective population size, growing linearly and very gradually until it split with the population now inhabiting the northeastern watershed about 15 thousand years ago. After this split, the southern population is inferred to have maintained a stable population size until about three thousand years ago, at which time it would have begun growing exponentially. The population now inhabiting the northeastern watershed started at a smaller effective population size and grew linearly and gradually until about three thousand years ago, at which time it is inferred to have undergone a sudden population contraction. Migration pulses have been asymmetrical, and they are estimated to have occurred particularly regularly over the last ten thousand years of these populations' history.
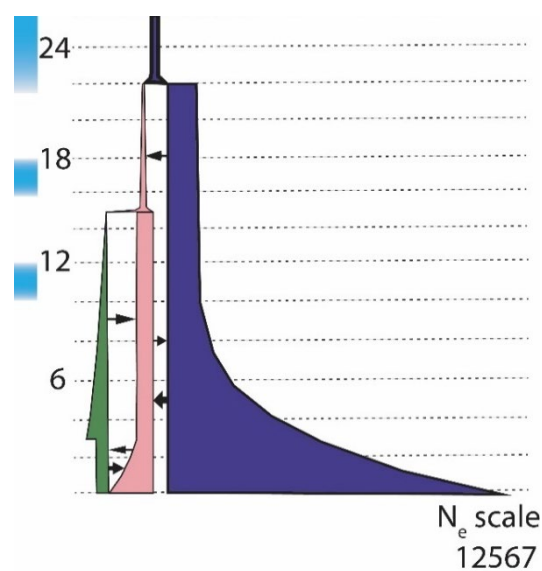
Figure 4. The demographic history of the three *P. marmoratum* populations sampled in this study. Time in thousands of years before the present is shown along the *y*-axis. Effective population size is shown along the *x*-axis, and is relative to the included scale bar. Populations are colored according to their corresponding watershed as in Fig. 1 A. The blue bars show periods of glacial expansion according to regional glaciological studies (Farber et al., 2005; Mark et al., 2004; Thompson et al., 1986).

1.3.4 Genomic statistics along the expansion front

For individual frogs in the Vilcanota, expected heterozygosity ranged from 0.02 to 0.11, with a mean of 0.05. Inbreeding coefficients ranged from 0 to 0.66, with a mean of 0.29. Both depth of sequencing coverage and heterozygosity were significant predictors of the count of low-frequency, high-impact mutations ($p < 2.2 \cdot 10^{-16}$, adj. $r^2 = 0.41$). Residuals of this regression, our metric for expansion load, ranged from -31.83 to 49.68.

Overall, the northeastern portion of the study area was characterized by low values for expected heterozygosity, high values for inbreeding coefficients, and high values for the expansion load metric (Fig. 5 A, 5 D, and 5 H). In contrast, the northwestern portion of the study area was characterized by the highest values for expected heterozygosity, lowest values for inbreeding coefficients, and relatively low values for the expansion load metric. The southern mouth of Osjollo Pass was additionally characterized by low values of the inbreeding coefficient and expansion load metric (Fig. 5 D and 5 H).

Focusing on values for these metrics for individual frogs along the mountain passes, we find a trend of increasing inbreeding coefficients for frogs moving from the northern towards the southern mouth of Osjollo (Fig. 5 E). Concomitantly, heterozygosity generally declines along this same transect (Fig. 5 B). In the southern mouth of Osjollo where inbreeding coefficient and load drop to low values for many individuals, we also see a small peak in heterozygosity (Fig. 5 B, 5 E, and 5 I). Patterns in Chimboya Pass are less clear, but we generally see heterozygosity gently declining and both inbreeding coefficient and expansion load gently increasing in the south-to-north direction (Fig. 5 C, 5 F, and 5 J). Near to the northern mouth of Chimboya Pass there is a small peak in heterozygosity values and a small trough in inbreeding coefficient values (Fig. 5 C and 5 F).

Pairwise estimates of F_{st} for sampling sites along Osjollo and Chimboya Passes were characterized by the greater rate of differentiation of demes over distance relative to the rate observed for downslope populations towards the core range of *P. marmoratum* (Fig. 6). Whereas linearized pairwise F_{st} $\left(\frac{F_{st}}{1-F_{st}}\right)$ increased by about $7 \cdot 10^{-3}$ / km for core downslope site pairs, it increased by $1.3 \cdot 10^{-2}$ / km for Chimboya and $3.4 \cdot 10^{-2}$ / km for Osjollo site pairs (Table S 3).
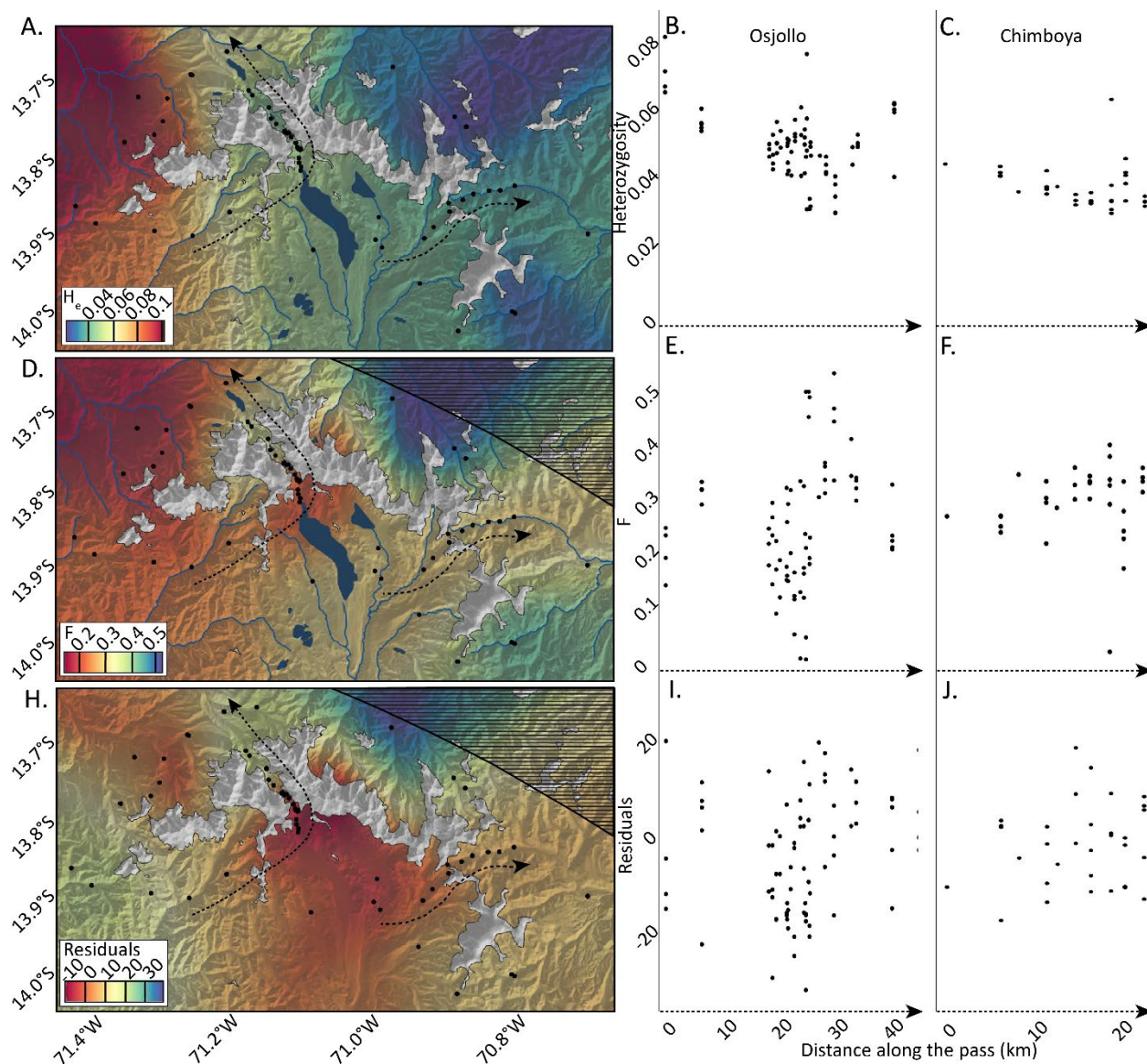
Figure 5. Individual-level heterozygosity, inbreeding coefficients, and expansion load across the landscape. In the hill-shaded maps, the hill-shaded white polygons show current glacial extent in the Vilcanota, while the broken lines across Osjollo and Chimboya Passes demonstrate the transects featured in the scatterplots. (A) A map of the individual heterozygosity of frogs, averaged over individuals sampled per site and interpolated between sites. (B) The heterozygosity of individual frogs shown relative to their distance from the mouth of Osjollo Pass. (C) The individual heterozygosity of frogs shown relative to their distance from the mouth of Chimboya Pass. (D) A map of inbreeding coefficient for frogs averaged over individuals sampled per site and interpolated between sites. (E) Individual inbreeding coefficients shown relative to their distance from the mouth of Osjollo Pass. (F) Inbreeding coefficients for individual frogs shown relative to their distance from the mouth of Chimboya Pass. (G) A map of the residuals of the linear regression of counts of high-impact mutations relative to depth of sequencing coverage and individual heterozygosity, averaged over individual frogs sampled per site and interpolated between sites. (H) The residuals of the linear regression of counts of high-impact mutations relative to depth of sequencing coverage and individual heterozygosity shown relative to their distance from the mouth of Osjollo Pass. (I) The residuals of the linear regression of counts of high-impact mutations

relative to depth of sequencing coverage and individual heterozygosity shown relative to their distance from the mouth of Chimboya Pass.
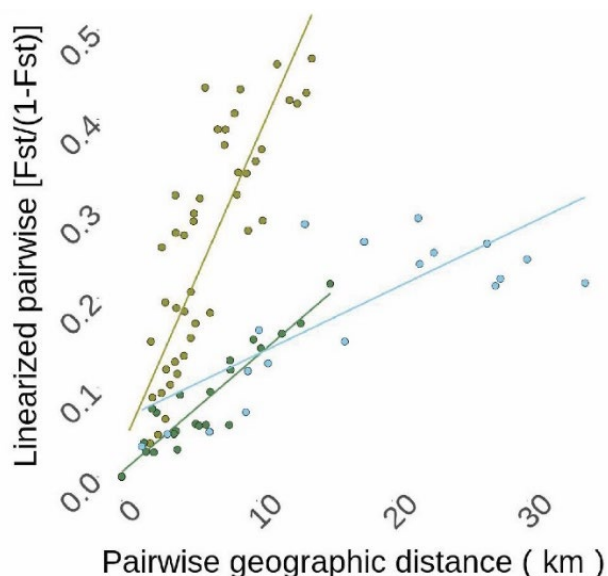
Figure 6. Site linearized pairwise F_{st} versus geographic distance for Osjollo Pass, Chimboya Pass, and core downslope sampling sites. Osjollo site pairs are in gold, Chimboya site pairs are in green, and core downslope site pairs are in light blue.

1.4 Discussion

The upslope expansion of *Pleurodema marmoratum* into recently deglaciated mountain passes of the Cordillera Vilcanota, Peru, provides a well-documented example of climate-driven elevational range expansion taking place on a contemporary timescale. Using low-coverage, whole-genome resequencing data, we have demonstrated that this recent, rapid range expansion left behind a detectable genomic signature in frog populations. Although the direct impact of upslope range expansion was the genetic depletion of frogs along the colonization front, expansion also created new opportunities for gene flow across the mountain passes, providing frogs with opportunities for the restoration of eroded diversity. Our results make clear the important role that changing patterns of landscape connectivity will have for understanding how climate-driven range expansions will shape the evolutionary potential of wild populations.

1.4.1 After the Little Ice Age, frogs could colonize deglaciated mountain passes bi-directionally

Determining the genomic consequences of the climate-driven range expansion of *P. marmoratum* requires first establishing the directions in which the colonization of new mountain pass habitats proceeded. Frogs are assumed to have colonized the narrow band of habitat suitable for *P. marmoratum* to the north of the Vilcanota at some point prior to the Little Ice Age (LIA, ~ C.E. 1500 – 1900; Thompson et al., 1986), but from there two scenarios are possible. On one

hand, populations to the north of the Vilcanota might have persisted during the LIA, such that as contemporary deglaciation commenced mountain passes could have been colonized bi-directionally (from both north and south). On the other hand, *P. marmoratum* might not have persisted in the habitat directly to the north of the Vilcanota, as the LIA drove the upslope bound of their already narrow range to contract downslope. In this case, mountain passes may have been colonized almost entirely by frogs dispersing northwards from populations in the watershed to the south of the Vilcanota.

Results from demographic modelling provide clear evidence that frogs persisted in all three watersheds during the LIA, as they date the split times between the three populations to thousands of years before the LIA. In the Peruvian Andes, the Last Glacial Maximum (LGM, 20—26 kya) was comprised of two separate time intervals of glacial expansion, occurring from about 16 – 18 kya and then from about 22 – 30 kya (Farber et al., 2005). During these intervals, the sites sampled in the present study would have been covered by glacial ice (Fig. S 5), which would have excluded *P. marmoratum* from the northeastern watershed and severely limited their connectivity to the south. However, portions of the northwestern and southern watershed would have been accessible to frogs (Fig. S 5), and the first split time derived from GADMA/DaDi models suggests that the split between the northwestern and southern populations would have occurred about 22 kya, between these two LGM intervals of glacial expansion. The relative effective population sizes of these populations after their split suggest that frogs inhabited the northwestern watershed first and colonized the southern watershed from there. In the last three to ten thousand years or so, the southern but particularly the northwestern populations have undergone periods of exponential population growth, perhaps fostered by the decreasing aridity and increasing stability of the South American climate at that time (Riris & Arroyo-Kalin, 2019). The inference that the northwestern population is both the largest and oldest of the three is corroborated by northwestern frogs today being characterized by the highest heterozygosities and lowest inbreeding coefficients sampled anywhere on the landscape (Fig. 5 A and Fig. 5 D). This area of the landscape is also characterized by a low load metric (Fig. 5 G), which could be due to relatively efficient selection being able to act against deleterious variants of additive effect in this area of high effective population size.

Similarly, demographic modelling suggests that the northeastern population split from the southern population well before the LIA, about 15 kya. This split time corresponds with the time interval between the younger LGM interval of glacial expansion (16 – 18 kya) and a post-LGM period of glacial re-expansion that would have occurred from about 10 – 12 kya in the Peruvian Andes. Unlike the northwestern and southern populations, the northeastern population appears to have undergone a population contraction in recent millennia. The inference that the northeastern population is the youngest of the three watershed populations and has the smallest effective size is supported by it having the lowest heterozygosities and highest inbreeding coefficients sampled anywhere on the landscape (Fig. 5 A and Fig. 5 D). This part of the landscape is also characterized by a high load metric (Fig. 5 G), which could be consistent with a reduced efficacy of selection against deleterious variants due to low effective population size.

1.4.2. Reduced genetic diversity at the expansion front

Studies of other examples of range expansion (invasive species, expansion out of ice age refugia, etc.) suggest that increasing distance along a colonization front is typically associated with declining heterozygosity, increasing inbreeding coefficients, and increasing differentiation of successive demes from the source population (Arenas et al., 2012; Dlugosch & Parker, 2008; Hewitt, 2004). Documenting whether such an erosion of available genetic diversity along the range front is observed in species undergoing climate-driven range expansion is of interest on conservation biology given the profound importance of genetic variation in providing the substrate for evolutionary change Fisher, 1930; Lewontin, 1974). As we hypothesized, we do observe this same genomic signature of range expansion in the Cordillera Vilcanota, particularly along Osjollo Pass in the north to south direction. This 150-year-old expansion front is characterized by decreasing heterozygosity and increasing inbreeding coefficients. These trends can be observed continuing up to the highest part of Osjollo at 5400 m a.s.l., nearly at the southern mouth of the pass, where the last glacial ice melted and made Osjollo a continuously deglaciated corridor in 1980. Osjollo Pass is also characterized by increasing deme differentiation in excess of what we observe in parts of the landscape that have instead been stably populated over the last 150 years (Fig. 6).

Chimboya Pass, which reaches a maximal elevation of 5100 m a.s.l. and would have become continuously deglaciated sooner than Osjollo Pass, does not exhibit as strong a signature of the post-LIA expansion. However, a gentle decline in heterozygosity and increase in the inbreeding coefficient is also evident along Chimboya along the south-to-north transect (Fig. 5 C, Fig. 5 F). Once again, we also see a pattern of increasing deme differentiation over space in excess of the pattern observable in the downslope, stable part of the range, though that relationship is not as dramatic as for Osjollo (Fig. 6).

1.4.3 Expansion has provided frogs with novel opportunities for gene flow

Changes in species distributions may also be associated with changing patterns of gene flow across the landscape (Flantua et al., 2019; Hoffmann et al., 2011). While range contractions can sever existing connections between populations, range expansions can forge new points of contact between them. Many studies have modelled how gene flow within species' ranges might be altered by climate-driven distributional changes (Velo-Antón et al., 2013; Wasserman et al., 2013) but we have only just begun to quantify these patterns in natural populations (Bi et al., 2019; Garroway et al., 2011; Ramos et al., 2018). *P. marmoratum* offers an important exemplar of climate-driven distributional change that has created new opportunities for gene flow, with deglaciated mountain passes becoming movement corridors for frogs across the barrier once presented by the heavily-glaciated Cordillera Vilcanota. Admixture in these passes is evidenced by a peak in heterozygosity and trough in the inbreeding coefficient towards the southern mouth of Osjollo Pass (Fig. 5 B, Fig. 5 E) and towards the northern mouth of Chimboya Pass (Fig. 5 C, Fig. 5 F). The recency with which frogs from northern and southern watersheds have met in Osjollo Pass is evident in the steep clines of ancestry proportions observed in that area (Fig. 3 A), though relatively steep clines in ancestry are still observable in the older Chimboya Pass populations (Fig. 3 B).

Although our demographic models suggest that frogs were living both to the north and south of the Vilcanota and so could colonize mountain passes bidirectionally after the LIA, the final

glacial ice to melt before Osjollo became a continuously deglaciated corridor in about 1980 was near to its southern mouth, where Osjollo Pass peaks at 5400 m a.s.l. (Seimon et al., 2007). Our data from the southern mouth of Osjollo is consistent with what we would expect if frogs from the differentiated populations north and south of the mountains were meeting and breeding there: low inbreeding coefficients and higher heterozygosity (Fig. 5 B, Fig. 5 E). The southern mouth of Osjollo also has the lowest values of our expansion load metric of any part of the study landscape, indicating relatively few high-impact mutations circulating in this zone relative to the heterozygosity of the frogs there (Fig. 5 G). This finding is contrary to our stated hypothesis, that populations along the expansion front should accumulate rare, deleterious mutations. Our interpretation is that, since this expansion occurred over less than 150 years, there was insufficient time for the accumulation of deleterious mutations of additive effect. Meanwhile, any deleterious, recessive mutations of large effect that may have been circulating in the ancestral, downslope populations could have been purged by the low effective population sizes at the leading edge of the upslope expansion (Gilbert et al., 2018).

1.5 Conclusion

Genetic diversity is considered an essential variable that we must monitor if we are to keep track of the integrity of our biosphere under rapid global change (Pereira et al., 2020; Steffen et al., 2015). Here, we have focused on what is happening along the leading edge of a climate-change driven range expansion to understand its consequences for genomic diversity. As hypothesized, genetic diversity was depleted along the colonization front, with heterozygosity declining and inbreeding coefficients increasing—even though, contrary to our expectations, we did not see the buildup of mutational load. However, as we anticipated, expansion also created new opportunities for gene flow across the mountain passes, providing opportunities for the restoration of eroded diversity. These genomic consequences of climate change are critical given direct links between population heterozygosity and fitness (Reed & Frankham, 2003). Their implications for the adaptive potential of populations on the leading edge of range expansions may be of particular significance (González-Martínez et al., 2017; Pennington et al., 2021). Future studies will reveal how the repercussions of climate-driven range expansions for genetic diversity and opportunities for gene flow may impact their adaptive potential and the efficacy of selection in range edge populations.

1.6 Acknowledgements

1.7 Supplementary materials

Table S 1. Statistics representing the contiguity and completeness of the *Pleurodema marmoratum* genome compared to other published, landmark anuran genomes.

Genome assembly	*Pleurodema marmoratum* (v1.0)	*Nanorana parkeri* (v2.0)	*Rana catesbeiana* (v2.1)	*Rana marina* (v2.2)	*Xenopus tropicalis* (v9.1)	*Xenopus laevis* (v9.2)
Total length (Gb)	1.79	2.07	6.25	2.55	1.44	2.72
Technology	10X	Illumina, RNA-seq	Illumina, 10X	PacBio, Illumina	PacBio, Illumina	PacBio, Illumina
No. scaffolds	110,000	135,000	1,540,000	31,000	7,000	108,000
Scaffold N50 (kb)	2,380	1,060	39	168	135,000	137,000
BUSCO (%)						
Complete single copy	63.5	83.4	42.3	80.9	87.5	52.9
Complete duplicate	1.5	1.6	0.9	2.2	1.0	39.8
Fragment	14.7	7.2	22.3	7.5	6.0	3.2

Table S 2. Estimated heterozygosity (H_e) across sampled *Pleurodema marmoratum* individuals in the Cordillera Vilcanota, compared to H_e for other species of frogs where H_e was calculated based on whole-genome data.

Species	Estimated heterozygosity (H_e)	Data type	Reference
Cane toad (*Rhinella marina*)	0.05-0.21 %	ddRAD	(Mittan-Moreau et al., 2022)
Cerro Campana stubfoot toad (*Atelopus zeteki*)	0.16-0.27 %	Whole exome	(Byrne et al., 2021)
Marbled four-eyed frog (*Pleurodema marmoratum*)	0.19 %		
Variable harlequin frog (*Atelopus varius*)	0.27-0.31 %	Whole exome	(Byrne et al., 2021)
High Himalaya frog (*Nanorana parkeri*)	0.43 %	Whole genome sequencing	(Sun et al., 2015)

Table S 3. Linearized F_{st} $\left(\frac{F_{st}}{1-F_{st}}\right)$ over distance (km) for site pairs in mountain pass habitat versus habitat in downslope habitat that has been inhabited more stably over time.

Site pairs	Intercept	Coefficient	Adj. r^2
Osjollo Pass	$3.3 \cdot 10^{-2}$**	$3.4 \cdot 10^{-2}$***	0.78
Chimboya Pass	$5.2 \cdot 10^{-3}$	$1.3 \cdot 10^{-2}$***	0.87
Core downslope	$6.4 \cdot 10^{-2}$*	$7.3 \cdot 10^{-3}$***	0.54

Figure S 1. Folded site frequency spectrum
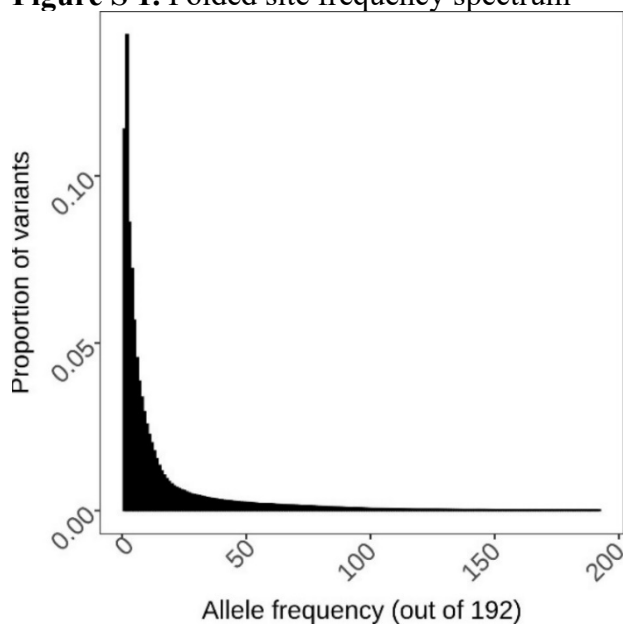
Figure S 2. The relationship between genetic principal components (PCs) and elevation. (A) PC1 and PC2, and (B) PC3 and PC4, colored by the elevation at which frogs were sampled. (C) PC3 shown in relationship to the elevation of sampled frogs.
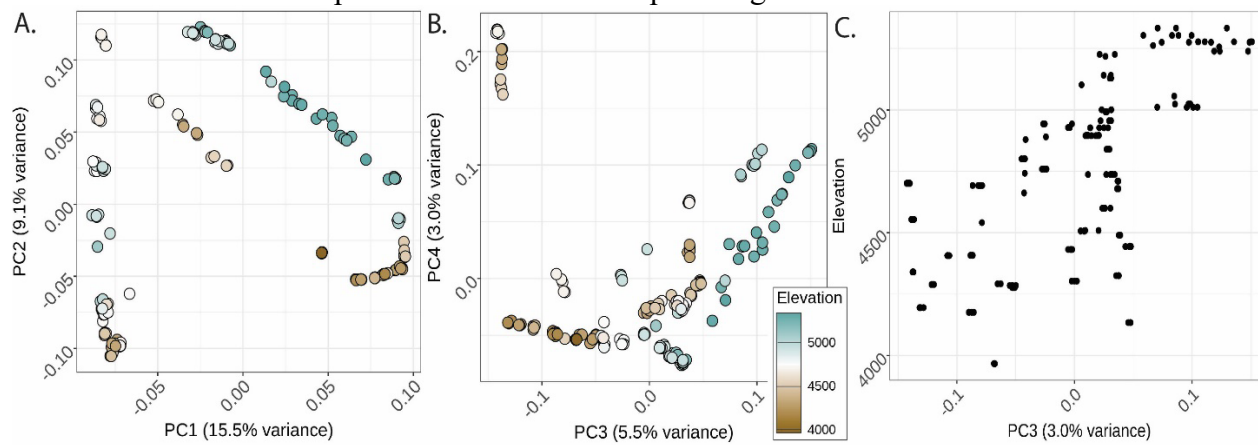
Figure S 3. OHANA plots showing ancestry components for frogs, organized by the three watersheds from which frogs were sampled (south, northwest, and northeast), as well as unrooted trees showing the relationship between these components. The structure plots are displayed for (A) $k = 2$, (B) $k = 3$, (D) $k = 4$, (F) $k = 5$, and (H) $k = 6$. The unrooted trees are displayed for (C) $k = 3$, (E) $k = 4$, (G) $k = 5$, and (I) $k = 6$. Both structure plots and unrooted trees are colored so that the primary ancestry component at $k = 3$ matches the colors assigned to watersheds in Fig. 1.

Figure S 4. OHANA ancestry components of individual frogs displayed as pie charts on the genetic PCA (Fig. 2).
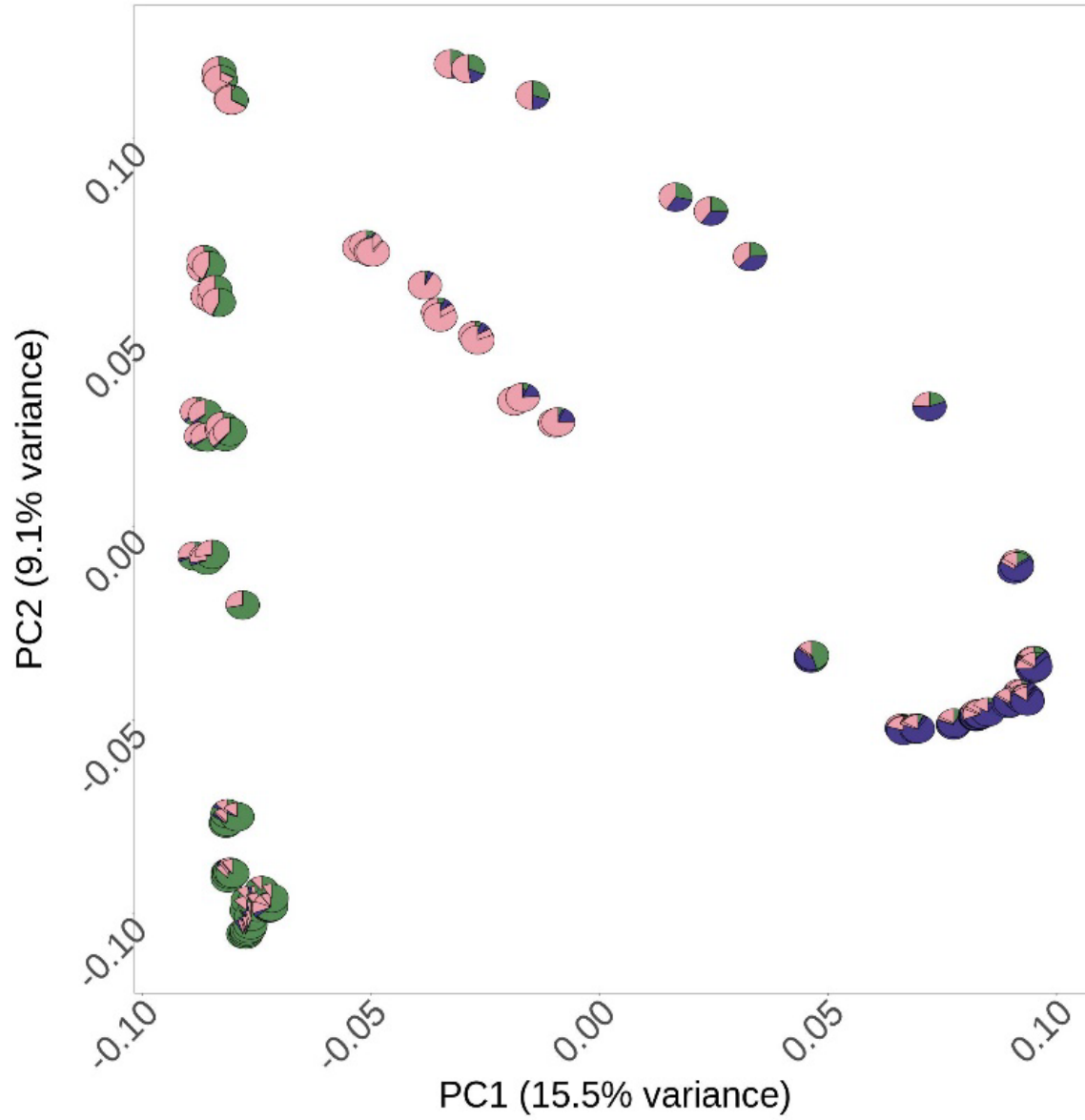
Figure S 5. (A) The range of *Pleurodema marmoratum* (grey polygon) in South America (black polygon) in relationship to the extent of glacial ice during the Last Glacial Maximum (LGM, white polygon). The red rectangle shows the bounding box for the Cordillera Vilcanota. (B) An inset of the Cordillera Vilcanota, showing the extent of glacial ice during the LGM (white polygon), the current extent of glacial ice (detailed black outline), sites where frogs were sampled for this project (red points), and the area beyond the range of *P. marmoratum* (black hashing).
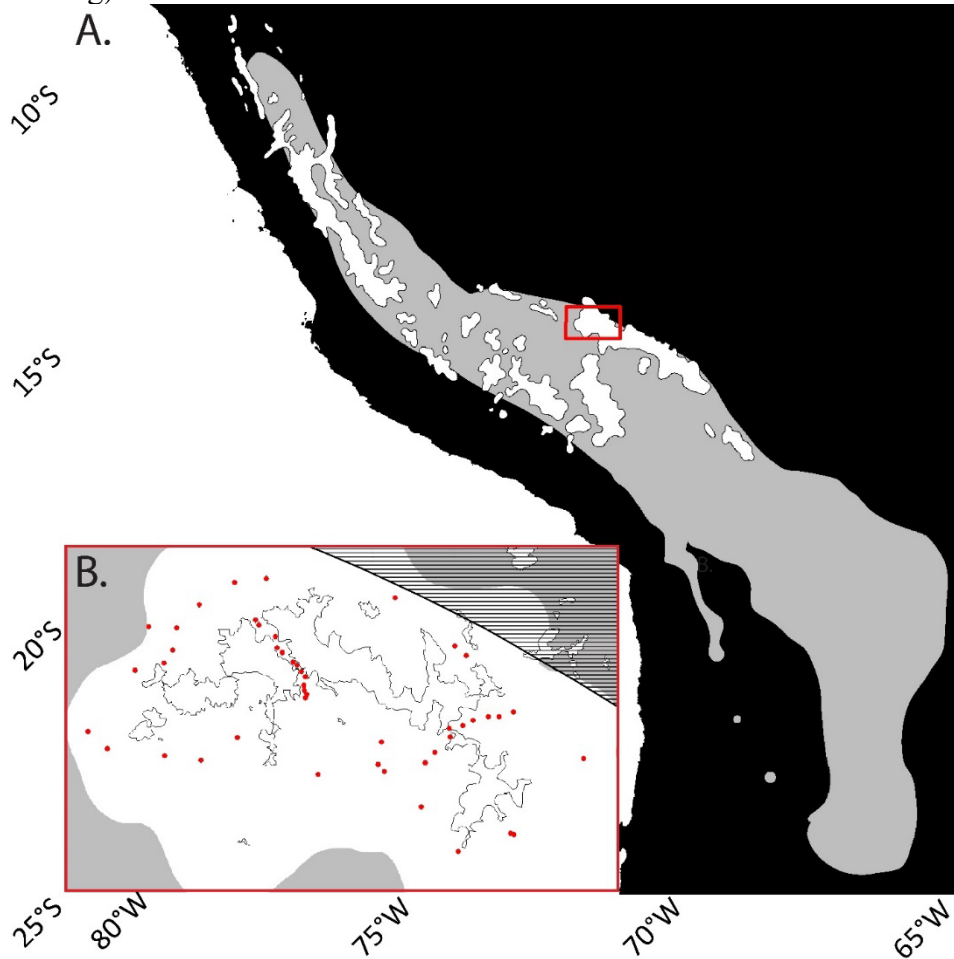
CHAPTER 2

Rapid genetic adaptation during climate-change driven range expansion of the Marbled four-eyed frog (*Pleurodema marmoratum*)

Emma Steigerwald, Diana Aguilar-Gomez, Lydia Smith, Juan Carlos Chaparro, Rasmus Nielsen

Abstract

My second chapter uses field-collected temperature data and the low-coverage genome sequencing dataset to detect putative genetic adaptation to high elevation. Enhanced genetic drift may impact selection efficacy at changing distributional limits, and if this is true for climate-driven range expansions then leading-edge populations may be more adaptively mismatched to their environment than ancestral populations. After functionally annotating the *P. marmoratum* genome, we use genotype-by-environment association tests to identify putative high elevation adaptation genes and examine allele frequencies at the relevant outlier loci along the elevational gradient. We show that the new elevations *P. marmoratum* colonized expose them to their critical thermal limits, and identify candidate genes putatively involved in their adaptation to high elevation conditions. Finally, we see that allele frequencies for these candidate genes behave unpredictably in the newly-colonized landscape. Our results suggest that selection may be relatively ineffective during the course of a rapid, climate-change driven range expansion.

2.1 Introduction

Range expansions can allow species to alleviate the stress of anthropogenic climate change (Cahill et al., 2012). In the course of colonizing new habitat, species often encounter novel environmental conditions and biotic interactions, to which they must adapt if they are to successfully establish themselves (Kirkpatrick & Barton, 1997; Polechová & Barton, 2015). Their adaptation may be based on changes in genetic sequences or gene expression, but ultimately plasticity will be insufficient to support range expansions in many cases (Gunderson & Stillman, 2015). Therefore, studies scrutinizing how populations along contemporary climate-change-driven range expansion fronts are, or are not, rapidly genetically adapting to their novel environments will be important for understanding the implications of climate change for the persistence of biodiversity (Urban et al., 2016).

Different scenarios of range expansion can be useful for informing our expectations of genetic adaptation during climate-change-driven range expansion. For example, many studies have documented local adaptation along environmental gradients by species expanding postglacially out of Ice Age refugia (Eidesen et al., 2015; Lai et al., 2019; Mörch et al., 2019) or by invasive species expanding into non-native habitats (Bossdorf et al., 2005; Sakanari & Moser, 1990; Wilson-Rich & Starks, 2010). Generally, these studies indicate that these populations are subject to accelerated genetic drift and thus decreased selection efficacy relative to populations within the stable distribution of a species (González-Martínez et al., 2017; Willi et al., 2018). However, in the case of expansions out of Ice Age refugia, the velocity of that climate change was much slower than the velocity of anthropogenic climate change (Loarie et al., 2009). Slower climate velocity allows for slower range expansions in climatic niche-tracking species, and consequently larger effective population sizes that are less subject to genetic drift (Garnier & Lewis, 2016). Also, these expansions are old enough—typically up to twenty thousand years old—that using contemporary samples we do not know whether species' initial adaptation may have relied on plasticity, with any molecular sequence-based changes now observable along those expansion fronts having instead accrued in the intervening millennia (Price et al., 2003). In the case of the expansions of invasive species, many expansions are comprised of admixed genotypes originating from the interbreeding of individuals introduced from multiple source localities, producing artificially elevated diversity on which evolution may act (Bossdorf et al., 2005; Dlugosch & Parker, 2008). Invasive species also tend to be characterized by a subset of ecological traits conferring high evolutionary capacity, like high mutation rates, high fecundity, and short generation times (Urban, 2020). Thus, although other scenarios of range expansion can help inform our expectations for contemporary, climate-change driven range expansions, each analogy has important limitations as a basis for comparison.

To understand whether species undergoing climate-change driven range shifts may be rapidly genetically adapting to the environments they colonize, we studied the Marbled four-eyed frog (*Pleurodema marmoratum*) in the Cordillera Vilcanota, Peru. There, this species has expanded its upslope range in response to deglaciation since the end of the Little Ice Age (1850 AD), exposing the animals to extreme high elevation conditions (Seimon et al., 2007). In fact, this species' expansion upslope has made it the highest living amphibian in the world, reaching up to 5,400 m a.s.l.—hundreds of meters higher than the highest living amphibians in the Himalayas (Wang et al., 2018). At 5,400 m a.s.l., frogs contend with a suite of novel, intense abiotic

selective pressures: intense UV, a partial oxygen pressure 50-60 % of that at sea level, and the fastest soil freezing rates in the world (Schmidt et al., 2009; Seimon et al., 2017; Wang, Hiderma, et al., 2014). We employed a low-coverage, whole genome resequencing approach. This approach is particularly advantageous for studying this very young landscape, since signatures of selection can be highly localized within the genome (Lowry et al., 2016; Tiffin & Ross-Ibarra, 2014) and even sequencing approaches that use a reduced representation approach leave a large portion of the genome unsampled (Lou et al., 2021).

We tested the following hypotheses relating to the genetic sequence-based high elevation adaptation (HEA) of *Pleurodema marmoratum*:

(H1) At their new upslope range limit, *P. marmoratum* are more frequently exposed to their thermal limits relative to other parts of their sampled range; demonstrating a component of the selective pressure they are under at extreme high elevations.

(H2) Based on other studies of HEA in amphibian systems (Muiret al., 2014; Sun et al., 2018; Wang et al., 2018; Weber et al., 2002; Yang et al., 2012), we expect that candidate genes involved in high elevation adaptation (HEA) will be associated with biological functions relating to oxidative stress response; hypoxia response; DNA repair; functioning of the cardiovascular, nervous, and immune systems; tissue integrity; and metabolism. Oxidative stress, hypoxia, and DNA damage increase with altitude, while the various physiological responses catalogued are largely responses to these stressors, to decreasing nutrients availability, and to changing light regimes (Cheviron & Brumfield, 2012).

(H3) Due to strong genetic drift during rapid range expansion (Excoffier et al., 2009), allele frequencies will undergo larger changes in newly colonized habitats (5,100 – 5,400 m. a.s.l.) relative to more stationary parts of the range, but not necessarily in an adaptive direction. Therefore, candidate high elevation adaptation alleles that we identify may even decline in frequency or be lost across the elevational range expansion front in *P. marmoratum*.

(H4) Since the end of the last glacial maximum (LGM), frogs have experienced multiple rounds of glacial expansion and deglaciation, which we expect resulted in repeated downslope range contraction and upslope range expansion (Martini et al., 2017). Therefore, candidate HEA loci in genes associated with response to oxidative stress, DNA damage repair, and hypoxia will be under balancing selection due to temporally variable selection pressures.

This study provides an exciting opportunity to examine whether and to what extent species are undergoing extraordinarily rapid adaptation to climate-change driven elevational range shifts.

2.2 Methods

2.2.1 Quantifying exposure to temperature extremes

To obtain data regarding the environmental conditions experienced by *P. marmoratum* in our study area, DS1921G Thermocron Temperature Loggers (OnSolution Pty Ltd, Sydney, Australia; hereafter, 'iButtons') were placed at a 20 sampling sites during the March—May 2018 field season, with paired iButtons deployed to measure temperature every four hours in adjacent aquatic and terrestrial microhabitats. Aquatic iButtons were protected with rubber spray sealant, glued to the inside of a 3 cm-diameter PVC tube of 12 cm length, and placed in ephemeral ponds

containing *P. marmoratum* tadpoles. Terrestrial iButtons were glued to the inside of a 10 cm funnel, which was placed upside down and covered with rocks in a location where adult *P. marmoratum* occurred. Data were downloaded from recovered iButtons during the March—May 2019 sampling season.

2.2.2 Reference genome annotation

To enable description of the location of outlier SNPs from subsequent selection tests relative to known genes, the genome of *P. marmoratum* (see Chapter 1, section 1.3.1) was structurally and functionally annotated. The structural components—predicted genes, intergenic regions, exons, UTR, etc.—were first annotated with GeMoMa (v1.9; Keilwagen et al., 2019). As input data, reference genome annotations from *Engystomops pustulosus* (v1.0); from the model frog species *Xenopus laevis* (v10.1); from an amphibian species used in many genomic studies of extreme high elevation adaptation, *Nanorana parkeri* (v1.0); and from the model tetrapod species, *Mus musculus* (GRCm39) and *Homo sapiens* (GRCh38), were downloaded from the NCBI Assembly database. Additionally, RNA sequence data from *Engystomops pustulosus*, the closest-related organism for which substantial RNAseq data was available, were downloaded from the NCBI Sequence Read Archive (SRR10362873, SRR10362870, SRR10362872, SRR10362875, SRR10362876, SRR10362877, SRR10362878, SRR10362879, SRR10362887, SRR10362888, SRR10362889, SRR10362890, SRR10362891, SRR10362892, SRR10362893, SRR10362894, SRR10362895, SRR10362883, SRR10362884, SRR10362886, SRR10362881, SRR10362882, SRR10362880). RNAseq FASTQ files were aligned to the unmasked *P. marmoratum* reference genome using STAR (v2.7.10b; Dobin et al. 2013), then in samtools (v1.16.1) were converted to BAM format while excluding reads as follows: unmapped reads, reads where the mate-pair read was unmapped, reads that were not the primary alignment, reads that failed platform or vendor quality checks, and reads that were either PCR or optical duplicates. Finally, BAM were sorted by leftmost coordinates and indexed.

Next, we annotated functional aspects of the genome—proteins, hypothetical proteins, GO terms, etc. using Funannotate (v1.8.15; Palmer & Stajich, 2016). This pipeline aggregates predictive information about protein function from databases accessed with InterProScan, a tool that searches protein databases to identify conserved protein domains, motifs, and functional sites (v95.0; Jones et al., 2014); Eggnog-mapper, a database providing orthologous groups and functional annotations for proteins (v2.1.10; Cantalapiedra et al., 2021); Pfam, a database of protein families and domains (v2.1.10; El-gebali et al., 2019); CaZy, a database of carbohydrate-active enzymes (v11; Drula et al., 2022); MEROPS, a database of peptidases and proteases (v12.0; Rawlings et al., 2018); and the BUSCO tetrapoda_odb10 database, a database of genes we expect to be highly conserved in single-copy across tetrapod diversity (v1.0; Simão et al., 2015). For any protein annotated as "hypothetical protein" and containing a fully-resolved EC number (i.e., resolved to 4-digits), the "hypothetical protein" annotation was replaced with the EC number's product in the ExPASSY Enzyme database (28 June 2023 release; Bairoch, 2000). If the EC number was only resolved to three digits or fewer, the "hypothetical protein" annotation was kept and the EC number removed. To evaluate the annotation for completeness, the proportion of conserved, single-copy orthologs expected to be present across tetrapods (tetrapoda_odb10 database; Simão et al., 2015) was calculated for the final annotation and

compared to the statistics already calculated for the assembled genome (see Chapter 1, section 1.3.1).

2.2.3 Genotype-by-environment association tests

These analyses made use of the field and whole genome resequencing data described in Chapter 1, sections 1.2.1 and 1.2.3. To identify candidate loci for high elevation adaptation, three separate genotype-by-environment association (GEA) tests were conducted: one using redundancy analysis (RDA), one using latent factor mixed models (LFMM), and one using ANGSD doAsso (Caye et al., 2019; Forester et al., 2018; Oksanen, 2012; Skotte et al., 2012). Each of these GEA tests has its strengths and weaknesses, so comparing the outliers may lend additional insight into HEA in *P. marmoratum.*

To create the input file for the former two tests, the sites obtained by applying filters through ANGSD and ngsParalog (15,746,373 sites, see Chapter 1, section 1.2.3) were used to create an mpileup file. Genetic variants were called in a VCF with bcftools using this mpileup file as the input (v1.15.1; Danecek et al., 2021). With plink2, first a pgen and then a RAW format version of this VCF was created (v1.90b6.7; Chen et al., 2019). In this final step, a minor allele frequency filter removing variants with a frequency of <5 % was applied, resulting in a final set of 626,493 sites. This minor allele frequency filter is imposed because inferences about very low frequency variants are more impacted by sequencing error, and the lowest frequency variants are less likely to be highly functionally significant while greatly increasing computational burden.

Both RDA and doAsso can use externally-produced principal components (PCs) of genetic structure to account and control for the underlying genetic structure of the data. A scree plot was used to select the first four PCs of the eigen decomposition of the covariance matrix produced by PCAngsd (see Chapter 1, section 1.2.4) as adequately representing population genetic structure. The eigenvectors for individuals along each of these four PCs were saved to a text file as input for RDA and doAsso.

RDA was conducted using the R package vegan (v2.6-4; Oksanen, 2012). This GEA approach can achieve higher power than LFMM when sample sizes are very small and in cases of weak, multilocus selection, since it considers how sets of SNPs may covary in response to an environmental variable of interest (Forester et al., 2018; Rellstab et al., 2015). First, bioclim variables were extracted from Wordclim at the coordinates of resequenced frogs and the resolution of 0.5 minutes of a degree (Fick & Hijmans, 2017). Retained environmental variables were elevation and any bioclim variables that did not covary with elevation, did not covary with one another, and had clear biological significance for the study species. RAW formatted genotype data was imported to R using the package adegenet (v2.1.10; Jombart, 2011). Partial RDA was then used to model the relationship between genotypes and environmental predictors with multivariate linear regression (Forester et al., 2018). The four genetic PCs from PCAngsd were included as conditioning variables in this partial RDA, such that variation in the genetic data could be partitioned as being attributable to shared ancestry or population history rather than environment, removing possibly false positive signals. From this RDA, the loadings of loci for the two ordination axes were used to identify outliers following an established procedure (Capblancq et al., 2018), first calculating Mahalanobis distances between each site and the center

of the RDA distribution using two degrees of freedom in the R package robust (v0.7-2; Wang, Zamar, et al., 2014) and then converting these distances to a p-value. SNPs were considered outliers when their p-value was less than the Bonferroni-adjusted threshold of 0.05 ($p < 1.93 \cdot 10^{-8}$). Outlier SNPs were associated with the predictor variable with which they were most highly correlated.

LFMM was conducted using the R package lfmm (v1.0; Caye et al., 2019). This GEA approach uses latent factors to control for the confounding effects of population structure and unobserved demographic processes, reducing the likelihood of allele frequency signatures being falsely attributed to structure alone through the simultaneous estimation of the impacts of environmental variables and of genetic structure on allele frequencies (Caye et al., 2019). For this approach, RAW genotype data was again imported to R with adegenet (Jombart, 2011). The LFMM ridges estimation was used to fit a model of the association between these genotypes and the elevation of sampled frogs, specifying that four principal components of genetic structure should be included as latent factors in the model. The association test was then performed using the resulting fitted model, calibrating the test using the genomic inflation factor (GIF). Again, SNPs were considered outliers when their p-value was less than the Bonferroni-adjusted threshold of 0.05 ($p < 1.93 \cdot 10^{-8}$).

An additive model using a generalized linear framework was used to test for genetic association with elevation in ANGSD with -doAsso 2 (v 0.941-11-g7a5e0db; Skotte et al. 2012). This GEA approach is specifically designed for low-depth sequencing data, and so accounts for genotype uncertainty by modelling unobserved genotypes as latent variables (Jørsboe, 2022). This set required the BAM alignment files of processed reads against the *P. marmoratum* reference genome (see Chapter 1, section 1.2.3) as input genotypes, the elevation of sampled frogs as input phenotypes (yQuant), and the text file of the first four genetic PCs from PCAngsd as input covariates (cov). The filters applied to sites included those applied to the sites used in RDA and LFMM, but additionally a filter that excluded sites with fewer than 30 highly credible genotypes across the 192 sampled frogs (-minHigh 30), resulting in a final set of 373,176 sites. Output likelihood ratios were converted into p-values, with SNPs again considered outliers when their p-value was less than the Bonferroni-adjusted threshold of 0.01 ($p < 2.68 \cdot 10^{-8}$), with a more stringent threshold implemented due to a higher recovery of outlier loci with this test.

Outlier SNPs from all tests were annotated in SNPeff (v5.1d; Cingolani et al., 2012) to determine SNPs genomic location relative to genes, the identity of these genes, and the predicted impact of mutations at these sites. To use this program, a custom SNPeff database was first built from final functional annotation GFF file.

2.2.4 Genome-wide selection scans

To differentiate the type of selection affecting the portions of the genome containing outlier SNPs, Tajima's D (Tajima, 1989) was calculated for sliding windows across the entire genome in ANGSD (Korneliussen et al., 2014). The value of D summarizes the distribution of allele frequencies. An excess of intermediate-frequency variants and thus positive value of D may indicate balancing selection, though could also be attributable to a population bottleneck event, population structure, or other factors. Meanwhile, an excess of low-frequency variants and thus a

negative value of D may indicate a recent selective sweep or purifying selection, though could also be driven by recent demographic expansion, low-frequency variants recently entering the population by migration, or other factors. However, D is still useful to provide insight into genomic outliers that GEA methods have already suggested to be under selection. To this end, site allele frequency likelihoods were calculated using doSaf -1 of all the sites that passed the SNP filters and the invariable sites that passed the mapping and read quality filters. Then the maximum likelihood estimate of the folded site frequency spectrum was calculated (realSFS), and thetas estimate for each site using saf2theta (Korneliussen et al., 2013). Tajima's D was calculated according to the formula described in (Tajima, 1989), using windows of 600 base pairs and a step size of 100 base pairs. Outlier SNPs from GEA tests were assigned the average D of all windows overlapping them.

2.2.5 Visualizing outlier frequency across elevations

To visualize changes in SNP frequencies over the elevational gradient at sites identified as candidates for HEA, outlier sites were extracted from a VCF. Individuals were grouped into five equal elevational bins (3900-4200, 4200-4500, 4500-4800, 4800-5100, and 5100-5400). Within each bin, allele frequencies at outlier sites were calculated for RDA and LFMM by counting instances of whichever allele was the minor allele in the lowest elevational bin and dividing this sum by the total number of alleles in that bin. Allele frequencies at outlier sites were calculated for doAsso by multiplying genotype likelihoods for each frog by 0 for the homozygotes of the major allele in the lowest elevational bin, 1 for heterozygotes, and 2 for homozygotes of the minor allele in the lowest elevational bin; summing these values across the elevational bin; and dividing this sum by the total number of alleles in that bin.

2.2.6 Gene ontology enrichment analysis

Gene ontology (GO) enrichment analysis, a computational method used to determine the biological processes, molecular functions, and cellular components that are overrepresented or enriched within a particular gene set, was then conducted for variants held in common between the independent genotype-by-environment association analyses using topGo in R (v2.50.0; Alexa & Rahnenführer, 2009). For each GEA test, genes associated with identified outlier SNPs were considered a predetermined set of interesting genes. The gene universe was defined by reading in a file with a complete mapping of all the genes annotated in the *P. marmoratum* genomes and their accompanying GO terms recovered through the functional annotation pipeline. Hypergeometric tests were conducted to determine if the gene set of interest was significantly enriched with genes associated with specific Gene Ontology terms relative to the complete gene set annotated in the *P. marmoratum* genome. Separate tests were conducted for the molecular function (MF) and biological process (BP) categories of GO terms.

2.3 Results

2.3.1 Quantifying exposure to temperature extremes

With increasing elevation, average annual daily maximal temperatures stay relatively stable but annual average daily minimal temperatures decline in both terrestrial and aquatic microhabitats,

such that the annual average diel temperature range amplifies (Fig. 1 A). The proportion of time that iButtons spend outside of the critical thermal limits of *Pleurodema marmoratum* increases with elevation (Fig. 1 B), with increased occurrence of both temperatures exceeding this species' critical thermal maximum and dipping below its lower critical thermal limit (Fig. 1 A).

2.3.2 Reference genome annotation

Structural annotation predicted the presence and structure of 28,703 genes, 43,915 mRNAs, and 303,541 coding sequences (CDS) in the *P. marmoratum* genome. Of this final set of filtered genes, 19,234 were orthologous to genes in *E. pustulosus*; 12,543 were orthologous to genes in *X. laevis*; 9,940 were orthologous to genes in *N. parkeri*; 9,931 were orthologous to genes in *M. musculus*; and 10,474 were orthologous to genes in *H. sapiens*. In the process of functional annotation, 37,084 gene annotations were obtained from analysis with Interproscan; 38,780 from Eggnog; 30,759 from Pfam; 510 from CaZy; and 1,738 from MEROPS. A total of 33,012 GO terms were associated with annotated genes. The final genome annotation recovered 63.8 % of all complete genes in the BUSCO set. This statistic compares favorably to the 65 % initially recovered in the genome assembly (see Chapter 1, section 1.3.1).
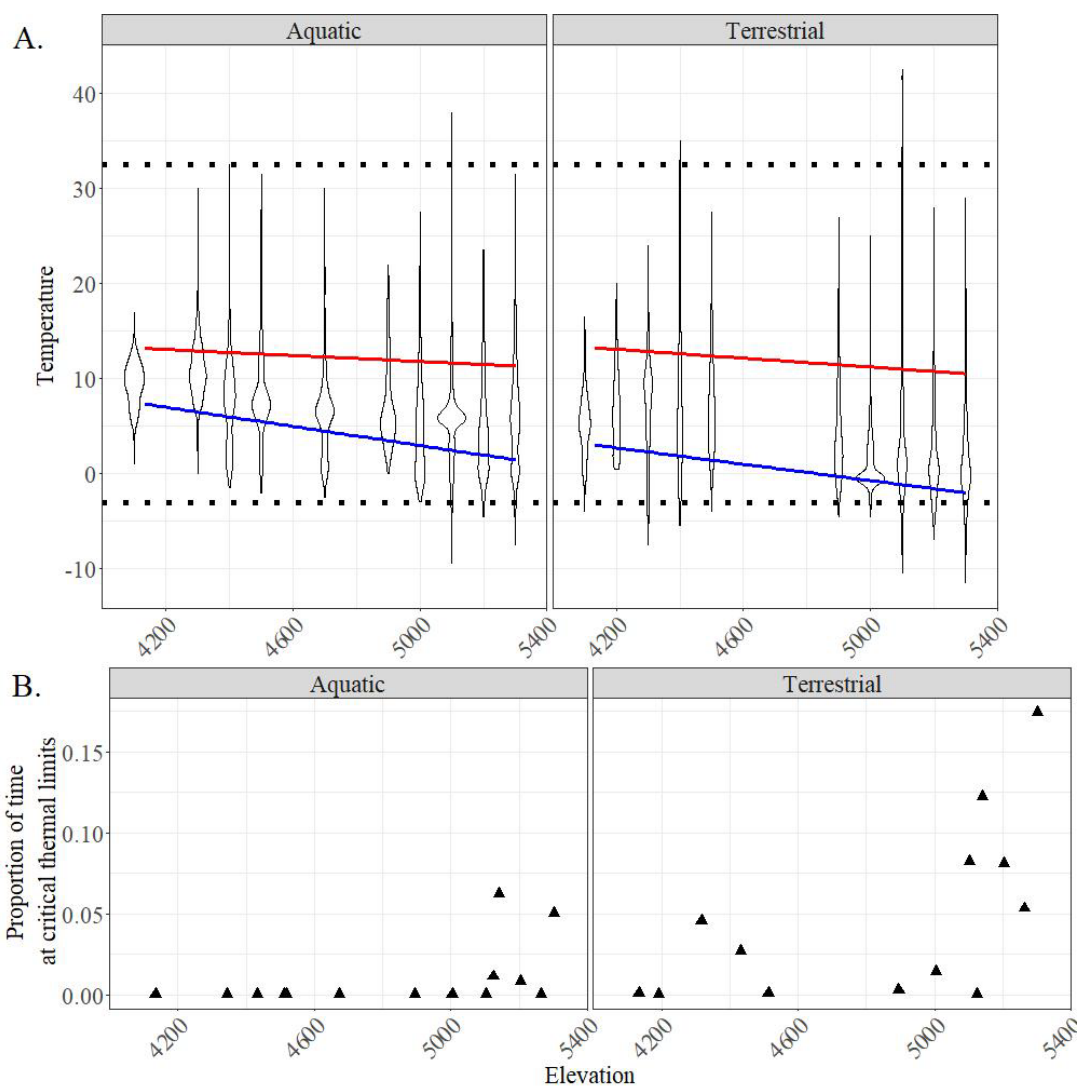
Figure 1. Exposure to temperature extremes along the elevational gradient. (A) Temperature data for terrestrially and aquatically-placed iButtons. Violin plots show the raw data, the red line represents average annual daily maximum temperatures, and the blue line shows average annual daily minimum temperatures. The upper black dotted line shows the critical thermal maximum for *P. marmoratum* and the lower black dotted line shows the mean temperature withstood by frogs that were able to recover after being frozen. (B) The proportion of time that terrestrially and aquatically-placed iButtons were outside of frogs' critical thermal limits across the elevational gradient.

2.3.3 Genotype-by-environment association tests, genome-wide selection scans, and gene ontology enrichment analysis

In RDA, only elevation and mean diurnal temperature range (BIO2) were retained as environmental axes. The model built with these axes and elevation data was significant, as were each of the environmental predictors ($p < 0.0001$). The model explained 1.00 % of variation in the genetic data, with elevation alone explaining 0.56 % of the variation. 30 outlier SNPs retained using the Bonferroni-corrected p-value threshold for significance ($p < 1.91 \cdot 10^{-8}$) were most correlated with elevation (Fig. 2), while 23 were instead most correlated with mean diurnal temperature range. Of the 30 candidate HEA outlier SNPs, 18 SNPs could be associated with

annotated genes, with the remaining 12 SNPs either associated with hypothetical genes, too distant from known genes to be annotated, or on scaffolds too small to contain annotated genes. Meanwhile, of the 32 outlier SNPs from LFMM retained using the Bonferroni-corrected p-value threshold for significance ($p < 1.91 \cdot 10^{-8}$), 15 could be associated with annotated genes; and of the 64 outlier SNPs from doAsso retained using the Bonferroni-corrected p-value threshold for significance ($p < 2.83 \cdot 10^{-9}$), 28 could be associated with annotated genes. Outlier SNPs and candidate genes identified did not overlap between doAsso, RDA, and LFMM.
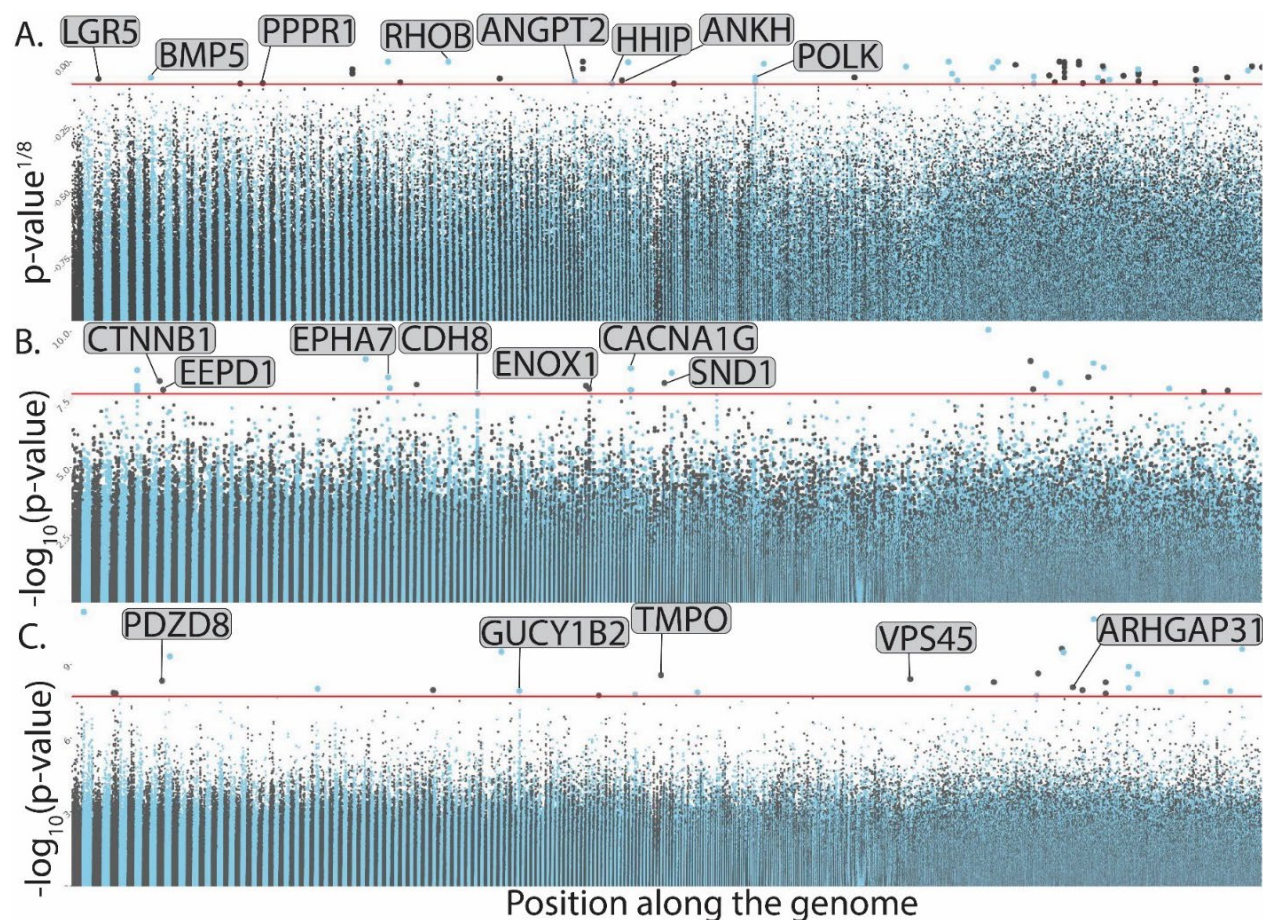
Figure 2. Manhattan plots showing outliers from GEA tests from (A) doAsso, (B) RDA, and (C) LFMM. The Bonferroni-adjusted significance threshold is shown with the horizontal red line, and alternating scaffolds along the genome are shown in grey and blue. Outlier SNPs featured in Table S 2 are annotated with the relevant gene name.

Most outlier SNPs were in portions of the genome characterized by negative Tajima's D values (Table S 2). Among the annotated genes associated with outlier SNPs from RDA, LFMM, and doAsso, those having known associations with HEA in other studied systems or else clear links to biological processes involved in HEA are catalogued in the supplements (Table S 2). These genes were enriched for GO terms with strong associations to hypoxia sensing and response pathways; energy metabolism; cardiovascular and neural functioning; immune and inflammatory responses; response to oxidative stress; DNA repair; the regulation of gene expression, tissue

integrity, growth, and repair; the regulation of hormone secretion; the maintenance of ion balance; and the promotion of protein stability and regulation of protein activity (Table S 3).

2.3.4 Visualizing outlier frequency across elevations

The different GEA tests detected outlier SNPs characterized by different frequency changes relative to elevation (Fig. 3). LFMM outliers were characterized by monotonic allele frequency changes relative to elevation—uniformly increasing or decreasing in frequency relative to elevation. LFMM outliers were also characterized by the most dramatic changes in allele frequencies relative to elevation (Fig. 3 C). RDA outliers were characterized by the most subtle allele frequency changes relative to elevation (Fig. 3 B). Both doAsso and RDA not only captured SNPs that monotonically increased or decreased in frequency relative to elevation, but also a substantial number of outliers that initially increased in frequency relative to elevation and then dramatically declined again in the highest elevational bins (Fig. 3 A-B).
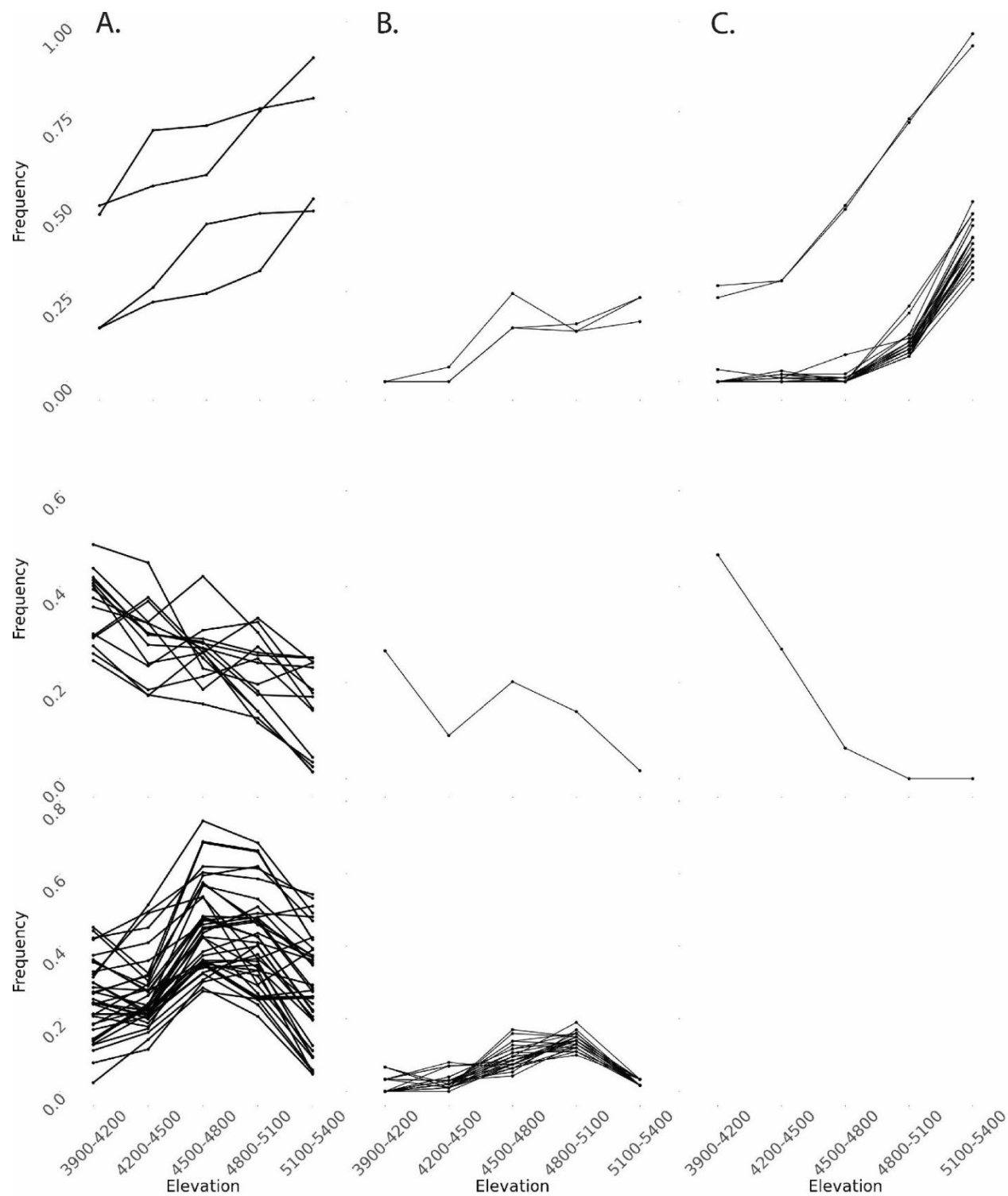
Figure 3. Allele frequencies along the elevational gradient for outlier SNPs identified with (A) doAsso, (B) RDA, and (c) LFMM. The top row shows outlier SNPs from each approach where the major allele at the lowest elevations sampled (3900-4200 m. a.s.l.) increases with elevation, the middle row shows SNPs where it decreases, and the bottom row shows SNPs that first increase and then decline.

2.4 Discussion

In this study of genetic adaptation during climate-change-driven range expansion, the Marbled four-eyed frogs (*Pleurodema marmoratum*) are found to be exposed to their critical thermal limits at the expanding edge of their range. Candidate loci that are putatively involved in enabling high elevation adaptation (HEA) of frogs along the elevational gradient examined in the Vilcanota were identified. However, we saw evidence of genetic drift impacting selection efficacy across the upslope elevational expansion front (those sites above 5,100 m. a.s.l.) of *P. marmoratum*, where putatively adaptive alleles often declined rapidly in frequency.

2.4.1 Candidate genes may be subject to temporally fluctuating selection and do not overlap between GEA tests

The three GEA approaches employed in this study have no overlap in the candidate genes they identify for HEA. Overlapping detections can increase confidence in high true positive and low false negative rates for tests. However, detections are only expected to overlap in the case of genes that have been subject to strong, hard selective sweeps (Corre & Kremer, 2012; François et al., 2016), and we don't expect hard sweeps to play an important role in the rapid HEA of *P. marmoratum*. In other words, all GEA methods will perform well in identifying candidate genes when a new mutation arose and was subject to strong selection pressure so quickly that it sweeps to high frequency on a single genetic background. However, in the case of *P. marmoratum*, given how quickly recent elevational expansion has occurred, we expect that selection would have relied on standing genetic variation and polygenic adaptation, resulting in multiple mutations and multiple different genetic backgrounds rising to frequency (Hermisson & Pennings, 2017). Additionally, we expect that cyclical glacial expansion and contraction in the zone will have resulted in temporally fluctuating selection on HEA loci—this proposition is supported by candidate HEA genes occurring in regions of the *P. marmoratum* genome characterized by relatively large, negative values of Tajima's D. Given our expectations that selection in the Vilcanota was polygenic, temporally fluctuating, and acting on standing genetic variation, it is unsurprising that the three GEA tests employed uncovered different sets of candidate loci and associated genes.

2.4.2 Candidate high elevation adaptation genes play roles in stress response, metabolism, and the cardiovascular, neural, and immune systems

As expected from previous studies of HEA in amphibians, candidate loci for HEA in *P. marmoratum* are not at the same genomic positions or even in the same genes as the loci identified in studies of HEA in other amphibian systems. Rather, candidate loci are involved in the same molecular pathways and biological functions that have been found to play a role in the HEA of other amphibian species (Sun et al., 2018). Broadly, the literature on the specific genes identified and the recovered GO enrichment terms were strongly associated with hypoxia and oxidative stress response pathways; DNA repair; energy metabolism; cardiovascular functioning; neural functioning; immune and inflammatory responses; tissue integrity, growth, and repair; and gene expression and epigenetic regulation (Table S 3).

Given the dependable relationship between altitude and hypoxia, it is perhaps unsurprising that many of the significantly enriched GO terms are closely associated with pathways that sense and respond to cellular oxygen concentrations. Particularly evident are associations with pathways of hypoxia inducible factors (HIF). HIFs are master transcription factors which coordinates a broad array of organismal responses to hypoxic conditions through communication with specific protein-hormone receptors ('Protein hormone receptor activity'): the formation of new blood vessels, the production of red blood cells, metabolism, and tissue repair and regeneration, among others (Cheviron & Brumfield, 2012; Lee et al., 2004). HIF pathways have already been characterized as responding to freezing and anoxia in wood frogs, *Rana sylvatica*; appear to be under selection in very high elevation Asiatic toads (*Bufo gargarizans*); and seems to be involved in the convergent evolution of four high-elevation frogs of the Tibetan Plateau (Lu et al., 2020; Storey et al., 2023; Yang, Qi, & Fu., 2016). Candidate genes in this study were enriched for terms relating to protein phosphatases ('protein phosphatase regulator activity'/'protein phosphatase binding'), which are key regulators of HIF (Pyo et al., 2018). Other GO terms are related to other key interactants with HIF pathways ('G protein-coupled receptor activity', 'Protein serine/threonine kinase inhibitor', 'Positive regulation of kinase activity', 'Protein phosphorylation', and 'Wnt signaling pathway'; Majmundar et al., 2015; Mottet et al., 2005; Olechnowicz et al., 2012).

A second critical aspect of adaptation to extreme high elevations reaffirmed by the candidate gene set from this study is the importance of genes involved in the response to oxidative stress. Oxidative stress can be more intense at high altitudes—not only due the lower oxygen levels (hypoxia), leading to an overproduction of reactive oxygen species (ROS) as byproducts of cellular metabolism relative to the availability of the oxygen required to neutralize them; but also due to increased metabolic demand as organisms attempt to compensate for reduced oxygen availability, leading to higher rates of ROS production; cold temperatures, which impair antioxidant defense systems; higher UV radiation, which directly induces oxidative damage; and limited nutrient availability, including essential antioxidants (Dosek et al., 2007; Wang, Hiderma, et al., 2014). Antioxidant activity has already been linked to high elevation adaptation in several high elevation amphibian species (Fu et al., 2022; Gao et al, 2019; Sun et al., 2018; Yang, Wang, et al., 2016). Among significantly enriched GO terms from this study were three tightly associated with cellular maintenance of oxidation-reduction balance: two involved in the generation of NADPH, an essential component of the antioxidant defense system, and one that helps protect proteins from irreversible oxidative damage ('6-phosphogluconolactonase'/'Pentose Phosphate Shunts' and 'Protein-disulfide reductase activity'; Jiang & Zhang, 2002; White & Someya, 2023).

The candidate gene set also confirms the increasing importance of DNA repair mechanisms with increasing altitude, as increased UV radiation, oxidative stress, and exposure to extreme weather conditions tend to lead to single-strand breaks and oxidative lesions in DNA (Lundby et al., 2003; Sinha & Häder, 2002). Genes associated with outlier SNPs were enriched for several GO terms related to DNA repair. Two terms were associated with the generation of ribose-5-phosphate, an essential molecule for DNA repair ('6-phosphogluconolactonase'/'Pentose Phosphate Shunts'; Habibi et al., 2022; Li et al., 2019). The remaining three terms were associated with binding damaged DNA, nucleotide excision and repair, and with assisting DNA polymerase in being capable of bypassing lesions or damage in the DNA template during

replication ('DNA-directed DNA polymerase activity', 'Damaged DNA binding', and 'Translesion synthesis'; Yasbin et al., 1993). Similarly, selection on DNA repair systems have been implicated in the high elevation adaptation of *Nanorana* genus frogs and *Rana kukunornis* (Sun et al., 2018; Yang et al., 2012).

We expect that high elevation adaptation may require adjustments in cellular metabolism to cope with reduced oxygen availability and changing nutrient availability, and indeed aspects of metabolism are clearly subject to selection along the elevational gradient in the Vilcanota. Indeed, selection on metabolic pathways is one of the most consistent signals identified in genomic studies of the high elevation adaptation of amphibians (Lu et al., 2020; Sun et al., 2018; Wang et al., 2018; Yang et al., 2012, 2016). Candidate genes were enriched for GO terms associated with metabolic functioning. Four of these GO terms were directly related to phosphorylation and dephosphorylation, processes critical to metabolic pathways like glycolysis and oxidative phosphorylation ('Phosphate ion transmembrane transporters', 'Protein phosphatase binding', 'Positive regulation of kinase activity', 'Protein phosphorylation', and 'Protein serine/threonine kinase inhibitor'; Scallen & Sanghvi, 1983; Shacter et al., 1984). Other GO terms enriched in the gene set are related to the provision of intermediates in glycolysis and other metabolic pathways ('6-phosphogluconolactonase'), and perhaps the modulation of the rhythm of metabolism ('Ultradian rhythm') or mitochondrial fission ('Membrane fission') in response to the changing environmental cues and energy demands at extreme high elevations.

As prior studies lead us to expect, the cardiovascular, nervous, and immune system appear to be involved in the HEA of *P. marmoratum*. Their role in HEA is expected, as these stressful environments increase demands on cardiovascular performance, impair neural development and cognitive functioning, and trigger immune responses and inflammatory reactions (Miscio et al., 2009; Mishra & Ganju, 2010; Naeije, 2010). Three enriched GO terms relate to the messenger molecular cGMP and are involved in the regulation of heart rate, vessel tone, neuronal function, and synaptic plasticity ('cGMP biosynthetic process', 'Guanylate cyclase activity', and 'cGMP-mediated signaling'; Lincoln et al.). Eight enriched GO terms are involved in regulating neuronal excitability and blood vessel tone through modulating action potential generation ('Action potential', 'Sodium channel activity', 'Voltage-gated calcium channel activity', 'Calcium ion binding', 'Calmodulin-lysine N-methyltransferase activity', ' G protein-coupled receptor activity', 'Chemical synaptic transmission', and 'Positive regulation of secretion by cell'; Raghavan et al., 2019). Three additional GO terms have simultaneous implications for the formation of new blood vessels, for vascular remodeling, and for neural crest migration during embyogenesis ('Transmembrane receptor protein tyrosine phosphatase activity', 'Cadherin binding', and 'Adherens junction organization'; Dejana et al., 2008; Monier-Gavelle & Duband, 1997), which are functions putatively under selection in the HEA of Nanorana frogs (Sun et al., 2018). Two enriched GO terms relate to exocytosis. This process plays a vital role in neural signaling through neurotransmitters and immune signaling through molecules like cytokines and chemokines ('Regulation of exocytosis' and 'Calcium-ion regulated exocytosis'; Hirashima & Zasshi, 2000), and has also been highlighted as functionally important in Nanorana (Sun et al., 2018). Final GO terms associated with these systems are terms related to the modulation of neurotransmitter and ion channel function ('Adenosine to inosine editing') and to promoting neuroprotection and plasticity through the production of myelin ('Oligodendrocyte differentiation'; Domingues et al., 2018).

Candidate genes for HEA in *P. marmoratum* also highlight the importance of tissue integrity, growth, and repair in the face of low oxygen availability, temperature fluctuations, and increased cellular demands. Five enriched GO terms were associated with cell-cell and cell-extracellular matrix adhesion ('Cadherin binding', 'Adherens junction organization', 'Plasma membrane organization', 'Positive regulation of protein polymerization', and 'Transmembrane receptor protein tyrosine phosphatase activity'; Taddei et al., 2002). The other associated GO terms were involved in facilitating cell division, cell structure, and cell migration ('Cytokinetic process', 'Cytoskeleton-dependent cytokinesis', and 'Positive regulation of protein polymerization'; Fletcher & Mullins, 2010). Indeed, genes controlling these same functions –cell adhesion, migration, and proliferation—are known to be differentially expressed along the elevational gradient in the Asiatic toad (*Bufo gargarizans;* Chen et al., 2022).

Finally, several enriched GO terms are closely linked to gene expression and epigenetic regulation. Changes in gene expression and epigenetic regulation can have far-reaching implications across cellular and physiological functioning, so could help these frogs rapidly adjust to the stressors of extreme high elevations. Specifically, GO terms were associated to regulating gene transcription ('DNA-binding transcription repressor activity'), RNA translation ('Double-stranded RNA binding' and ' tRNA adenosine deaminases'), and chromatin accessibility and methylation ('Nucleosome organization', 'Nucleosome binding', 'ATP-dependent chromatin remodeler activity', and 'Calmodulin-lysine N-methyltransferase activity').

2.4.3 Allele frequencies of most candidate high elevation adaptation loci do not change monotonically along the recent, rapid, upslope expansion of *P. marmoratum*

The three different GEA approaches employed identified outlier SNPs characterized by different relationships between allele frequency and elevation, highlighting the differences in how these approaches operate. LFMM outliers were characterized by monotonic allele frequency changes relative to elevation and by the most dramatic overall changes to allele frequencies. Most of the outliers identified undergo these dramatic allele frequency changes largely in the highest elevation portion of the study landscape (5,100-5,400 m. a.s.l.), elevations which were only sampled in one portion of the landscape: Osjollo Pass (see Chapter 1, Fig. 1). RDA and doAsso conservatively rule out such loci as potentially being attributable to shared ancestry (genetic PCs) alone, however LFMM is better able to avoid false negatives in this situation through the simultaneous estimation of the impacts of elevation on both genetic structure and allele frequencies (Caye et al., 2019). The strength of doAsso is that it is specifically designed for low-depth sequencing data (Skotte et al., 2012). Meanwhile, RDA outlier SNPs were characterized by the most subtle allele frequency changes relative to elevation. These subtler signatures make some sense considering the strengths of RDA as a GEA tool: RDA is particularly powerful in uncovering weak, multilocus selection, since it considers how sets of SNPs may covary in response to an environmental variable of interest (Forester et al., 2018; Rellstab et al., 2015). However, the fact that RDA did not additionally yield variants with stronger signatures requires further scrutiny.

Both RDA and doAsso identified many loci that initially increased in frequency with elevation, only to decline again in the highest elevation portion of the landscape. This dropout of putatively

adaptive alleles may relate to the accentuated genetic drift experienced by the populations range expanding over the newest, highest elevation portions of the landscape (Slatkin & Excoffier, 2012). The apparent inefficacy of selection during the climate-change driven range expansion of *P. marmoratum* raises concerns for the future fitness and adaptive potential of this species in the newly colonized portions of its range.

2.5 Conclusion

The upslope range expansion of *P. marmoratum* into upslope habitat deglaciated over the last 150 years provided an exciting opportunity to test for rapid contemporary adaptation in natural populations responding to climate change. Our work uncovers candidate genes likely contributing to this species' establishment at the highest elevations ever colonized by any amphibian, but also provides some evidence that populations undergoing climate-change driven range shift may be experiencing enhanced genetic drift and consequently the dropout of beneficial alleles.

2.6 Acknowledgements

2.7 Supplementary materials

Table S 1. Comparison of BUSCO statistics calculated from the *Pleurodema marmoratum* genome assembly compared to those calculated from the final functional genomic annotation of the genome.

	Complete, single copy	Complete, duplicate	Fragment	Missing	N
Assembly	63.5	1.5	14.7	20.3	5310
Annotation	43.4	20.4	11.9	24.3	5310

Table S 2. Candidate HEA SNPs in *Pleurodema marmoratum* from doAsso, RDA, and LFMM, highlighting SNPs in genes that are candidate HEA genes in other studied systems and a subset of genes with clear connections to biological processes involved in HEA.

Gene name	Outlier SNP impact, location	Tajima's D	Association with high elevation adaptation (HEA) in other systems and/or putative functional link to HEA.	Citation
doAsso				
bone morphogenetic protein 5 (BMP5)	Modifier, upstream gene variant	-1.89	Strong expression differences between individuals developing acute mountain sickness and not. Candidate gene in hypoxia tolerance in catfish. Involved in vasculogenesis and angiogenesis.	(Cai et al., 2020; Lu et al., 2016; Yuan et al., 2016)
angiopoietin 2 (ANGPT2)	Modifier, upstream gene variant	-1.06	Candidate gene in HEA of domesticated pigs. Plays an important role in vascular remodeling and angiogenesis. Has a broad range of effects on gas exchange, and is involved in inflammation and energy metabolism in response to acute hypobaric hypoxia. Regulated by the HIF-1 hypoxia response pathway.	(Chang et al., 2023; Hobohm et al., 2021; Wang et al., 2016; Zhang, Cheng, et al., 2019)
DNA polymerase kappa (POLK)	Modifier, intron variant	0.76	Candidate gene in HEA of lizards. Involved in organismal susceptibility to UV radiation.	(Takenaka et al., 2006; Yang et al., 2014)
ras homolog family member B (RHOB)	Modifier, intergenic variant (94467bp downstream)	0.72	Candidate gene in HEA of Andean humans. Candidate gene in hypoxia tolerance in mammals. Involved in cellular responses to oxidative stress. Regulates lung vascular permeability and vascular remodeling.	(Eichstaedt et al., 2015; Li et al., 2021; Zeng et al., 2016)
ANKH inorganic pyrophosphate transport regulator (ANKH)	Modifier, intergenic region (13507bp upstream)	-0.19	Candidate gene in HEA of domesticated pigs. Candidate gene in hypoxia tolerance of Tibetan, Sherpa, and Nepalese people. Contains two hypoxia-responsive elements (HREs) in proximity to its promoter region, and thus its expression is regulated by hypoxic factors (HIFs).	(Ai et al., 2014; Arciero et al., 2018; Sharma et al., 2022)
leucine-rich repeat containing G protein-coupled receptor 5 (LGR5)	Low, synonymous variant	-0.35	Candidate gene in HEA of humans and fruit flies. Regulated by the Wnt and HIF-2 hypoxia response pathways	(Emery, 2015; Zhou et al., 2021)
protein phosphatase 4 regulatory subunit 1 (PPP4R1)	Modifier, intron variant	0.13	Regulates multiple cellular events, including DNA damage response, immune response, stem cell development, and glucose metabolism. A key regulator of hypoxia response pathways.	(Wang et al., 2023; Winter et al., 2007)
hedgehog interacting protein	Modifier, intergenic	-0.72	Important role regulating the hedhog pathway, which plays a key role in the development of the lungs and other organs.	(Zhou et al., 2013)

(HHIP)	region (5189bp upstream)			
RDA				
catenin beta 1 (CTNNB1)	Modifier, upstream gene variant	-1.89	Candidate gene in HEA of fish, rodents, and domesticated sheep. Controls the development of several major organs like the lungs and heart, and controls heart size in mice. Activity moderated by hypoxic conditions.	(Heallen et al., 2011; Talaminos-Barroso et al., 2021; Wilkinson et al., 2015; Yang et al., 2021; Yuan et al., 2020; Zhang, Cheng, et al., 2021)
endonuclease/exon uclease/phosphatas e family domain containing 1 (EEPD1)	Modifier, intron variant	-1.74	Promotes repair of oxidatively-stressed replication forks. Regulated by the HIF-alpha pathway.	(Jaiswal et al., 2023; Solanki et al., 2019)
ephrin receptor A7 (EPHA7)	Modifier, intergenic region (33342bp downstream)	-1.64	Regulates lung vascular permeability.	(Larson et al., 2008)
calcium channel, voltage-dependent, T type, alpha 1G subunit (CACNA1G)	Modifier, intergenic region (50235bp upstream)	-1.68	Candidate gene in HEA of domesticated cattle and chickens. Plays a role in the HIF-α pathway and appears to be important in organismal hypoxia response.	(Verma et al., 2018; Wang et al., 2015)
ecto-NOX disulfide-thiol exchanger 1 (ENOX1)	Modifier, intergenic region (76409 bp upstream)	-1.76	Involved in response to oxidative stress.	(Zhang, Ji, et al., 2021)
cadherin 8 (CDH8)	Modifier, intergenic region (283229bp downstream)	-1.26	Candidate cold adaptation locus in high elevation Peruvian Quecchua people. Established links to body mass, metabolism, and cold response. Appears to play a role in fat deposition in sheep.	(Ahbara et al., 2019; Battista, 2022; Ferris et al., 2021)

staphylococcal nuclease and tudor domain containing protein 1 (SND1)	Modifier, intergenic region (3775bp downstream)	-1.93	Plays a role in hypoxia adaptation through negatively regulating hypoxia-related miRNAs and hypoxia-induced transcription, consistent with a role as stress response regulator.	(Saarikettu et al., 2023)
LFMM				
guanylate cyclase 1, soluble, beta 2 (GUCY1B2)	Modifier, intergenic region (16860bp upstream)		Candidate gene in HEA of Andean people. Helps neurons respond to hypoxia.	(Bleymehl et al., 2016; Eichstaedt et al., 2015)
Rho GTPase activating protein 31 (ARHGAP31)	Modifier, upstream gene variant		Critical for vascular development and angiogenesis.	(Caron et al., 2016)
vacuolar protein sorting 45 homolog (VPS45)	Modifier, intergenic region (4370bp upstream)		Important role in hematopoesis.	(Stepensky et al., 2013)
thymopoietin (TMPO)	Modifier, intergenic region (105098bp upstream)	-1.40	Affects heart muscle development.	(Gonzalez-Garrido et al., 2022)
PDZ domain containing 8 (pdzd8)	Modifier, intergenic region (16860bp upstream)		Candidate gene in HEA of domesticated sheep. Appears to play a role in fat deposition in sheep.	(Horvath et al., 2022; Yuan et al., 2016)

Table S 3. Significantly enriched GO terms among the candidate genes for HEA identified by doAsso, RDA, and LFMM.

doAsso			RDA			LFMM		
GO term	Annotated	Significant	GO term	Annotated	Significant	GO term	Annotated	Significant
Molecular functions								
Phosphate ion transmembrane transporter	1	1	Cadherin binding	61	2	Calmodulin-lysine N-methyltransferase activity	1	1
6-phosphogluconolactonase activity	2	1	tRNA-specific adenosine deaminase activity	7	1	Guanylate cyclase activity	22	1
Protein-hormone receptor activity	10	1	Protein serine/threonine kinase inhibitor	11	1	Calcium ion binding	484	2
DNA-directed DNA polymerase activity	23	1	Protein-disulfide reductase activity	15	1	Transmembrane receptor protein tyrosine phosphatase activity	67	1
Damaged DNA binding	28	1	Double-stranded RNA binding	21	1			
DNA-binding transcription repressor activity	46	1	Nucleosome binding	23	1			
G protein-coupled receptor activity	1396	4	ATP-dependent chromatin remodeler activity	26	1			
Protein phosphatase regulator activity	52	1	Voltage-gated calcium channel activity	37	1			
			Sodium channel activity	44	1			
			Protein phosphatase binding	63	1			
Biological processes								

Phosphate ion transmembrane transport	2	1	Ultradian rhythm	1	1	cGMP-mediated signalling	11	1
Pentose-phosphate shunt	3	1	Adenosine to inosine editing	6	1	Positive regulation of protein polymerization	17	1
Oligodendrocyte differentiation	6	1	Cytokinetic process	12	1	cGMP biosynthetic process	20	1
Translesion synthesis	7	1	Positive regulation of secretion by cell	22	1	Response to oxygen levels	22	1
Positive regulation of canonical Wnt signaling	17	1	Chemical synaptic transmission	314	2	Positive regulation of kinase activity	22	1
Non-canonical Wnt signaling pathway	23	1	Adherens junction organization	35	1	Protein phosphorylation	87	2
Negative regulation of transport	43	1	Cytoskeleton-dependent cytokinesis	38	1			
Negative regulation of Wnt signaling pathway	50	1	Nucleosome organization	42	1			
Signal transduction	3507	9	Plasma membrane organization	45	1			
			Action potential	46	1			
			Calcium ion import	47	1			
			Calcium-ion regulated exocytosis	48	1			
			Membrane fission	55	1			
			Regulation of exocytosis	68	1			

CHAPTER 3

Amphibians' expansion to record elevations influences *Batrachochytrium dendrobatidis* (Batrachochytriaceae) infection dynamics

Emma Steigerwald, Cassandra Gendron, Juan C. Chaparro, Rosemary G. Gillespie, Allie Byrne, Rasmus Nielsen, Bree Rosenblum

Abstract

The third chapter focuses on the transmission and infection dynamics of the globally-important amphibian pathogen *Batrachochytrium dendrobatidis* (*Bd*). Though the impacts of climate-change-driven range expansions on vector-borne pathogens have received much attention in recent years, the impact of such expansions on direct-transmission pathogens represents a significant gap in our understanding. We genotyped and quantified zoospore loads for *Bd* swabbed from the skin of almost 700 *P. marmoratum* frogs, and we combined that data with body size and condition data for those frogs and for hundreds of Andean toad (*Rhinella spinulosa*) and Marbled water frogs (*Telmatobius marmoratus*) that have co-colonized the new high elevation habitat. We learned that *Bd* is resilient to and can disperse extensively in the Vilcanota, which presents the highest elevations used by amphibians anywhere in the world. Finally, we found evidence that some site infection metrics and apparent sublethal impacts of infection are affected by elevation, suggesting that hosts' elevational range shifts have had implications for infection outcomes.

3.1 Introduction

The rising incidence of emerging infectious diseases (EIDs) is a critical issue in both conservation and public health (Fisher et al., 2012; Jones et al., 2008). Climate change may be contributing to increased outbreaks by providing pathogens with opportunities to switch hosts, expand geographically, or become more virulent (Harvell et al., 2002; Hoberg & Brooks, 2015; Liang & Gong, 2017), while climate-driven range shifts are also expected to influence the infection dynamics of several important pathogens. In Hawaii, the upslope range shifts of mosquitos are predicted to drive the continuing decline of endemic birds currently escaping avian malaria at high elevations (Zamora-Vilchis et al., 2012), and in Europe the northwards expansion of ticks is predicted to increase the spatial extent of Lyme infections (Jaenson & Lindgren, 2011). However, the data we currently have on the interaction of climate-driven range shifts and EIDs tends to come from vector-borne systems, as many vectors are highly sensitive to climate (Harvell et al., 2002). Though little documented, the infection dynamics of many pathogens that rely on direct transmission will presumably be affected by the widespread climate-driven range shifts of host species (e.g., Freeman et al., 2018; Moritz et al., 2008; Parmesan et al., 1999). As hosts undergo range shifts, their exposure to novel environments may alter host-pathogen dynamics—potentially exacerbating or mitigating infections, changing transmission patterns, or exposing hosts to new pathogens.

The emergence of *Batrachochytrium dendrobatidis* (*Bd*), the pathogen causing chytridiomycosis that has contributed to devastating global amphibian declines (Scheele et al., 2019; Skerratt et al., 2007), has been linked to climate change through a few proposed mechanisms (Li et al., 2013). Climate change could expand the spatial extent of optimal *Bd* growth conditions (Bosch et al., 2007). Meanwhile, more frequent droughts compromise amphibian immunity and enhance *Bd* transmission when amphibians aggregate in wet or humid microhabitats (Burrowes et al., 2004; Lampo et al., 2006). Higher climatic variability may also favor rapidly-adapting pathogens over hosts, resulting in worse infections (Raffel et al., 2013; Rohr & Raffel, 2010). Finally, as parasites generally have broader thermal tolerances than hosts, frogs are likely to be exposed to suboptimal temperatures before *Bd*, placing them at a disadvantage (Cohen et al., 2019, 2017). The mounting evidence of climate-driven amphibian range shifts (e.g., Bustamante et al., 2005; Enriquez-Urzelai et al., 2019; Raxworthy et al., 2008) suggests this as an additional mechanism that could connecting climate change and amphibian-*Bd* dynamics.

The Cordillera Vilcanota, in southern Peru, presents an ideal system for exploring how climate-driven range shifts impact EIDs. Field surveys of this heavily glaciated tropical mountain chain in the early 2000s documented the first known *Bd* infections in southern Peru (Seimon et al., 2005), but also revealed that three frog species had expanded their elevational ranges by hundreds of vertical meters into passes that had deglaciated since the end of the Little Ice Age (~150 years ago). The Marbled four-eyed frog (*Pleurodema marmoratum*) had expanded upslope to 5,400 m asl, making it the highest elevation amphibian in the world; the Andean toad (*Rhinella spinulosa*) and Marbled water frog (*Telmatobius marmoratus*) had expanded to 5,244 m asl (Seimon et al., 2007). Chytridiomycosis was recorded at the upper limits of these species distributions, and a die-off event was observed in *T. marmoratus* at 5,244 m asl (T. A. Seimon et al., 2007). Today, all three species persist at lower abundances in the Vilcanota. Host-pathogen

dynamics have transitioned into a more stable, enzootic state (Seimon et al., 2017), as can also be said of neighboring amphibian communities downslope (Catenazzi et al., 2017).

Moving upslope in the Vilcanota, *Bd* and frogs are challenged by progressively more intense UV, deep frozen precipitation, and a partial oxygen pressure 50-60 % of that at sea level (Poremba et al., 2015; Seimon et al., 2017; Wang, Hiderma, et al., 2014). At the apex of the mountain passes, soil temperature can fluctuate between –12° C at night and 25° C during the day, with a soil freezing rate exceeding that measured from any site on Earth (1.8° C/hr; Schmidt et al., 2009). Resident frogs are exposed to an even broader operative temperature range (−3.5 to 44° C; Reider, 2018). Here, we asked how range expansion into these new, challenging elevations may have influenced *Bd* infection dynamics. We used genetic data to inform our understanding of the local history of *Bd*, then examined site infection metrics and apparent sublethal infection impacts to understand how conditions at newly-colonized elevations might sway infection outcomes. We anticipate that *Bd* in the Vilcanota is from the global panzootic lineage (*Bd*GPL), the lineage largely responsible for *Bd* epizootics in South America (James et al., 2015), though these highest elevations inhabited by *Bd* presumably impose strong selective pressures that could conceivably result in a limited number of locally-adapted strains proliferating. If *Bd* remains dispersive despite extreme high-elevation conditions, and particularly if it was introduced to the Vilcanota just before local die-offs in the 2000s, *Bd* will be spatially unstructured, a common finding elsewhere *Bd* population genetics have been studied (e.g., Alvarado-Rybak et al., 2021; Basanta et al., 2021; Byrne et al., 2019). However, if the environmental persistence of *Bd* is depressed by harsh, high elevation conditions, the genetic structure of *Bd* is more likely to reflect its gradual spread between watersheds by way of host dispersal along the corridors provided by deglaciated passes (Haddad et al., 2014). The present study is the first to examine *Bd* infection dynamics above 4000 m asl (3,900—5,400 m asl); though *Bd* infection prevalence and intensity tend to initially increase with elevation, studies sampling to 4000 m asl suggest that these metrics may begin to decline again with increasing elevations (Catenazzi et al., 2011; Muths et al., 2008). For this reason, we expect *Bd* infection to have lower sublethal impacts for amphibians at newly-colonized, extreme high elevation sites. Alternatively, if the stress of high elevations and *Bd* infection impact amphibians synergistically, the sublethal impacts of *Bd* may increase with elevation. These analyses provide the first insights into how the climate-driven range shifts of hosts may influence EID events.

3.2 Methods

3.2.1 Fieldwork

The Cordillera Vilcanota (13° 44' 24"S, 71° 5' 24"°W) is an 80 km-long mountain chain in the southern Peruvian Andes, crossing the departments of Cusco and Puno. We sampled *P. marmoratum*, *R. spinulosa*, and *T. marmoratus* during the transition between the wet and dry seasons (March—May) in 2018 and 2019. *T. marmoratus* breed year-round, while *P. marmoratum* and *R. spinulosa* are in their final breeding months at this time. We sampled at 76 sites across three watersheds: the Alto Urubamba on the interandean versant and the Inambari and Yavero on the Amazonian versant. Sites ranged from 3,967—5,333 m asl, including transects across two deglaciated passes (Fig. S 1). We spent approximately equal person-hours at each site, capturing tadpoles by scoop net and searching for post-metamorphic stages under rocks

and along the edges of water bodies. We attempted to capture 15 adults per species per site. If we could not locate 15 adults, we supplemented first with juveniles and then with tadpoles. We sampled 695 P. marmoratum (317 adults), 173 *Rhinella spinulosa* (82 adults), and 232 *T. marmoratus* (23 adults).

Post-metamorphic individuals were dry swabbed 7X along the ventral surface of each limb and the vascular patch to assess *Bd* infection; tadpole mouthparts were swabbed 25X (MW113, Medical Wire & Equipment Co., Ltd., Corsham, UK; Hyatt et al., 2007). Swabs were air dried and stored dry or in 80 % ethanol. We collected 30 paired dry- and ethanol-stored swabs to compare their efficacy in preserving *Bd* DNA. We noted snout-vent length (SVL), mass, sex, and signs of disease in adults (lethargy, excessive sloughing, reddened skin). Individuals with nuptial pads were considered adult males. Adult male SVL were used to derive a lower-end size threshold for classifying adults, since males of these species are smaller than females: 19 mm for *P. marmoratum*; 30 mm for *R. spinulosa*; and 29 mm for *T. marmoratus*. Post-metamorphic individuals without nuptial pads that exceeded this threshold were classed as females. We also recorded SVL, mass, and signs of disease in juveniles; as well as SVL, mass, and Gosner developmental stage (Gosner, 1960) in tadpoles. Samples were transported to the University of California, Berkeley for -80˚C storage.

DS1921G Thermocron Temperature Loggers (OnSolution Pty Ltd, Sydney, Australia; hereafter, 'iButtons') were placed at a subset of 20 sampling sites during the 2018 sampling season, with paired iButtons deployed to measure temperature every four hours in aquatic and terrestrial microhabitats. Aquatic iButtons were protected with rubber spray sealant, glued to the inside of a 3 cm-diameter PVC tube of 12 cm length, and placed in ephemeral ponds containing P. marmoratum tadpoles. Terrestrial iButtons were glued to the inside of a 10 cm funnel, which was placed upside down and covered with rocks in location where adult P. marmoratum occurred. Data was downloaded from recovered iButtons during the 2019 sampling season.

3.2.2 *Bd* infection quantification

We focused on gaining a comprehensive understanding of *Bd* dynamics in our most widely-sampled frog, *P. marmoratum.* We dried ethanol-stored swabs by vacuum-centrifuge and extracted DNA from swabs with 50 uL of PrepMan Ultra reagent (Thermo Fisher Inc.). We quantified *Bd* zoospore load using real-time TaqMan PCR assay (Boyle et al., 2004; Hyatt et al., 2007). We combined 12.5 µL 2x TaqMan Master Mix (Applied Biosystems), ITS-1 Chytr3 and 5.8s Chytr PCR primers at a concentration of 900 nM, a Chytr MGB2 probe containing a FAM fluorescence reporter at 250 nM, and 5 µL of 1:10-diluted sample DNA. We ran triplicate reactions for each sample, with each 96-well plate including standard dilutions representing 100, 10, 1, 0.1, and 0 zoospore equivalents. Amplification was performed on an Applied Biosystems StepOnePlus Real-Time PCR System as follows: 2 min at 50° C, 10 min at 95° C, followed by 50 cycles of 95° C for 15 s and 60° C for 1 min. We determined *Bd* zoospore equivalents (ZE) in each swab by comparing sample C_t values relative to a standard curve, averaging across triplicates, and multiplying by 100.

3.2.3 *Bd* genotyping

We selected 96 *Bd+* extracts from adult *P. marmoratum* for sequencing to maximize the geographic representation of sampling. Within localities, we selected swabs with the highest ZE, since samples with more *Bd* DNA are sequenced more successfully (Byrne et al., 2017). *Bd* extracts were sequenced across the 16 nuclear chromosomes and mitogenome at 240 regions (150-200 bp-long) in an assay designed to maximally discriminate between major *Bd* clades, maximize resolution within *Bd*GPL (Global Panzootic Lineage), and allow for comparison with previous genetic studies of *Bd* (Byrne et al., 2017). Extracts were cleaned with isopropanol precipitation, pre-amplified to enrich template DNA, cleaned of excess primers and dNTPs with Exo-SAP-IT, and diluted 1:5. We attached dual barcodes and Illumina sequencing adaptors to samples using the Fluidigm Access Array, then sequenced libraries with Illumina 2×300 bp reads using a quarter MiSeq lane at the University of Idaho IBEST Core.

We used the reduce_amplicons.R script (https://github.com/msettles/dbcAmplicons) to process sequence data following Byrne *et al.* (2017). We demultiplexed reads, trimmed primer sequences, and merged paired Illumina reads with FLASH2 (Magoč & Salzberg, 2011). We aligned merged reads to reference amplicon sequences using the BWA-MEM algorithm (Li, 2013; v0.7.17-r1188). We filtered amplicons with an average read depth < 5 from the resulting BAM files for use in structure analyses. We also created an ambiguity sequence for each sample, retaining only the most frequent length variant per amplicon, and removing variants present in < 5 reads and in < 5 % of the total reads. We exported sequences with possible polymorphisms represented as IUPAC ambiguity codes to a FASTA for use in phylogenetic analyses.

3.2.4 Phylogenetic, structure, and redundancy analyses

Importing ambiguity sequences for Vilcanota samples and previously published sequence data representative of global *Bd* diversity (Byrne et al., 2019) into R, we removed one sample for each of six amplicons that resulted in > 5 bp length differences, samples with > 80 % missing amplicons, and amplicons with > 33.3 % missing samples. We aligned filtered ambiguity sequences in MUSCLE (v3.32; Edgar, 2004). In Geneious (v2021.1.1), we checked for alignment issues and estimated a ML gene tree for each amplicon using RAxML (v4.0) with the GTR substitution model and the rapid bootstrapping method for 100 bootstraps. We collapsed gene trees in Newick Utils (v. 1.6) by branches with <10 bootstrap support to improve tree accuracy, then estimated an unrooted species tree in ASTRAL (v5.7.4) and visualized in GGTREE (v3.0.2).

To examine standing genetic variation of Vilcanota *Bd*, we used BAM files to create a Site Frequency Spectrum (SFS) in ANGSD (v0.933-106-gb0d8011). BAMs were then processed separately for the subset of Vilcanota samples retained in phylogenetic analyses and the larger dataset including globally representative BdGPL samples (Byrne et al., 2019). We indexed BAMs in SAMtools (v1.11) and detected variants with a minimum coverage of 10X in FreeBayes (v1.3.2-46-g2c1e395). We conducted a principal component analysis with a NIPALS PCA based on an ANGSD covariance matrix (Korneliussen et al., 2014), a method only evaluating pairwise sets of individuals at loci for which they are both sequenced. We tested for population structure at the scale of sampling sites and watersheds, using a pegas-based, clone-corrected AMOVA in Poppr (Kamvar et al., 2014). We also assessed the proportion of genetic variance that could be explained by elevation in R by imputing missing genotypes with the random-forest method MissForest (v1.4), conducting a redundancy analysis in Vegan (v2.5-7),

and calculating the adjusted r2 value and predictor p-values of the resulting model with ANOVA in Stats (v4.1.1).

3.2.5 Analysis of *Pleurodema marmoratum* disease dynamics across elevations

Analyses of site-level effects and sublethal impacts of *Bd* on individuals were performed in R (v4.0.2). In subsequent regression analyses, all combinations of variables and their interactions were built. This model set always included the saturated model or the model retaining only the random effect for mixed effect models, as well as partial covariates being controlled for when relevant. Variables were log, square root, or Tukey power-transformed as needed to meet model assumptions; the model was selected that minimized the AIC; and coefficient estimates, null and residual deviances, r^2 values, and *p*-values were examined to interpret model importance.

3.2.6 Site-level dynamics

To ascertain whether frog population density might change substantially across elevations, influencing site-level infection dynamics, we used GLMs in MASS (v7.3-54) to examine the relationship between the elevation and counts of adults captured per species per site. We used counts of adult frogs captured because equivalent search effort was used to attempt to capture up to 15 adults per species per site. We used Poisson regression (link = log) to model the response of adult counts to elevation for *T. marmoratus*, whereas due to data overdispersion we needed to use negative binomial GLMs in MASS (v7.3-54) for adult *P. marmoratum* and *R. spinulosa*. So that sampling at sites with unsuitable habitat for a given species did not conflate our analysis, a site was only included in the model for a species if individuals of that species of any life stage were captured there. Adult counts per site did not correlate with elevation for *P. marmoratum* (n_{sites} = 63; Fig. S 2 a) or *T. marmoratus* (n_{sites} = 17; Fig. S 2 b), so though adult counts of *R. spinulosa* declined gently with elevation (n_{sites} = 25, $p < 0.001$, Fig. S 2 c, Table S 3), we did not include a proxy of frog density in subsequent models of site-level infection metrics. It is unlikely that sampling bias, relating to the timing at which different elevations were sampled, invalidate our analyses because an explicit effort was made during fieldwork to sample different elevations across the sampling period both within and between years (Fig. S 3).

To investigate whether elevation was a good predictor of site infection metrics, we tested the fit of linear and quadratic regression models at *Bd+* sites. The site infection metrics we selected to study represent three important characteristics of the distribution of infection intensities at a site: site prevalence, or the proportion of frogs that were actually infected at any given site; mean infection intensity, or the average infection intensity when considering only *Bd* infected frogs at a site; and site maximal infection intensity, representing how highest pathogen load spiked at each site. As has been recorded by other studies of landscapes where frog populations have transitioned to a *Bd* enzootic state, most individuals sampled were *Bd-*. Among infected individuals, the majority had very low infection intensity (tens of zoospore equivalents), with only a very few individuals showing infection intensities spiking wildly into the thousands or tens of thousands of zoospores. We did not record signs of disease like excessive sloughing with sufficient frequency to report relationships between these symptoms and elevation.

To work with swab *Bd* quantitation data, we first compared zoospore equivalents derived from paired dry- and ethanol-stored swabs with a Wilcoxon signed-rank test and did not find a

significant difference in the efficacy of these storage methods for preserving genomic DNA ($n =$ 60, $p = 0.10$). Individual infection intensity was calculated as the mean swab zoospore equivalents across triplicate qPCR reactions. *P. marmoratum* were considered *Bd+* when they had a mean infection intensity of > 1 and showed *Bd* DNA amplification for ≥ 2/3 triplicate qPCR amplifications. For the subset of sites where ≥ 10 post-metamorphic frogs were swabbed, site infection prevalence was calculated as the proportion of adult *P. marmoratum* that were *Bd+* at that site for *Bd+* sites, and the site mean and maximal infection intensity of *Bd+* frogs were also calculated. To explore whether elevation was a good predictor of site mean infection intensity, site maximal infection intensity, or site prevalence, we tested the fit of both linear and quadratic regression models.

3.2.7 Sublethal effects of *Bd* on individuals

Amphibian body size (SVL) can be used to evaluate the nutritional status of an amphibian across its development (Hector et al., 2012; Martins et al., 2013; Metcalfe & Monaghan, 2001). Meanwhile, Scaled Mass Index (SMI), a metric of body condition, can be used to evaluate the nutritional status of an amphibian in the recent past (Brodeur et al., 2020), and has been shown to be a good measure of energy stores in tadpoles and juveniles as well as adult amphibians (Maccracken & Stebbings, 2012). Individuals dedicating energy to mounting an immune response or whose foraging ability has been compromised by disease may, therefore, exhibit a lower SVL or SMI (Warne et al., 2011). We calculated SMI from body mass and SVL (following Peig & Green, 2009). The scaling exponent ($b_{P.\ marmoratum} = 2.57$, $b_{T.\ marmoratus} = 3.12$, $b_{R.\ spinulosa} = 3.04$) was calculated using a non-linear power regression to ensure that SMI was independent of SVL (Brodeur et al., 2020).

We explored whether SMI or SVL were predicted by putative site infection status (*Bd+/-*) and elevation using GLMMs in lme4. We built models for the species-life stage combinations for which we had sufficient data at sites assessed for *Bd* infection status: *P. marmoratum* adults, *P. marmoratum* tadpoles, and *T. marmoratus* tadpoles. We included site as a random effect in all models, and Gosner developmental stage as a partial correlate predicting tadpole SVL. Though we collected data on sex for adult individuals, we excluded this variable from our analyses as it was not a significant contributor to our models. Sites were considered putatively *Bd+* if ≥ 1 individual(s) were *Bd+*. Sites were considered putatively *Bd-* if ≥ 10 post-metamorphic *P. marmoratum* had their infection intensity quantified with qPCR with no individuals being classified as *Bd+*. It should be noted that sixty individuals per population need to be tested in order to be 95 % certain than a single positive frog in that population has been detected (Lee F. Skerratt et al., 2008). Here, we will use the terms putatively *Bd-* or *Bd+*, but what our approach definitively represents is powerful differences in *Bd* prevalence across populations. For instance, 10 negative samples means that prevalence in a population must be <10 %. Published literature does not yield expectations for how body size or condition relates to elevation in these species, so we examined samples at *Bd-* sites to establish baseline trends.

To explore how thermal regimes along the elevational gradient might relate to observed trends in infection metrics and apparent sublethal impacts, we plotted March-April temperature data from recovered iButtons relative to the temperature-dependent logistic growth rate (r) of a tropical *Bd* strain (Voyles et al., 2017), the CT_{max} of adult *P.*

marmoratum, and the mean temperature tolerated by *P. marmoratum* adults that recovered following freezing (Reider et al., 2020).

3.3 Results

3.3.1 Phylogenetic placement, spatial genetic structure, and local adaptation

Vilcanota *Bd* samples from *P. marmoratum* (n = 44) nest within the *Bd*GPL-2 clade of the *Bd*GPL lineage but do not cluster together relative to a panel of globally-derived *Bd*GPL genotypes in a consensus gene tree or PCA (Fig. 1, Fig. 2 a). Vilcanota *Bd* is geographically unstructured, with samples failing to cluster in a PCA (Fig. 2 b) despite containing many low-frequency variants after stringent filtering (73.4 % variants have an allele frequency of ~1 %). Watersheds or sites were not differentiated according to an AMOVA (p > 0.05, Table S 1). Elevation was a significant predictor of genetic variance according to redundancy analysis but only explained 1.2 % of genetic variance (p < 0.05, Table S 2).
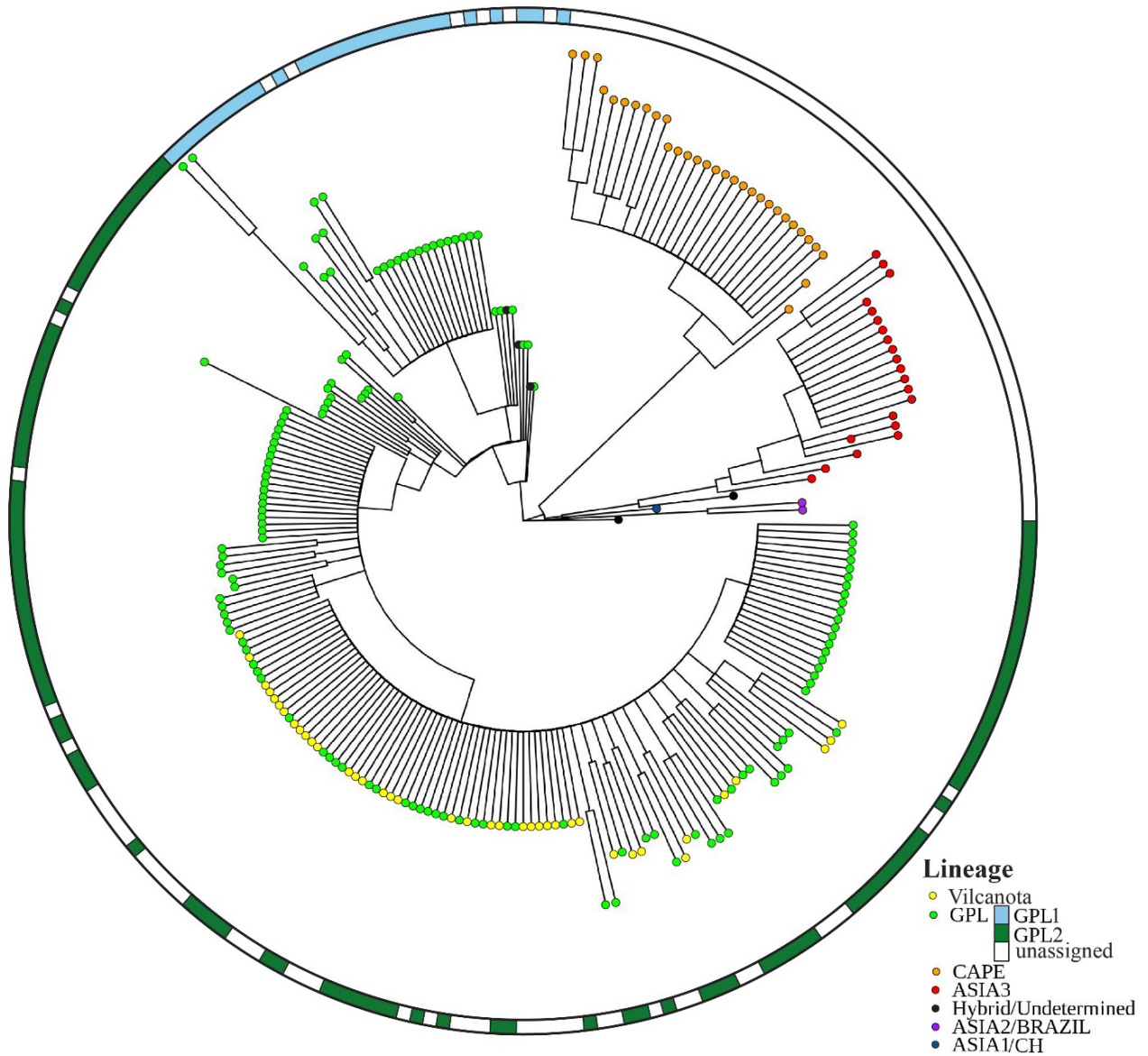
Figure 1. A midpoint-rooted consensus gene tree of Vilcanota *Bd* sampled from *Pleurodema marmoratum* (yellow tips) alongside previously-published samples representative of the five major *Bd* lineages (CAPE, ASIA3, ASIA2/BRAZIL, ASIA1/CH, GPL) and their hybrids (Byrne et al., 2019). This tree has a normalized quartet score of 0.807 and includes only nodes with a posterior probability ≥ 0.7. Assignment of *Bd*GPL samples to *Bd*GPL-1 or *Bd*GPL-2 is included whenever assigned by previous studies (James et al., 2015; Rothstein et al., 2021; Schloegel et al., 2012) and is shown in the concentric mosaic. This tree is included with sample names and the continent of swab origin in the supplements (Fig. S 2).
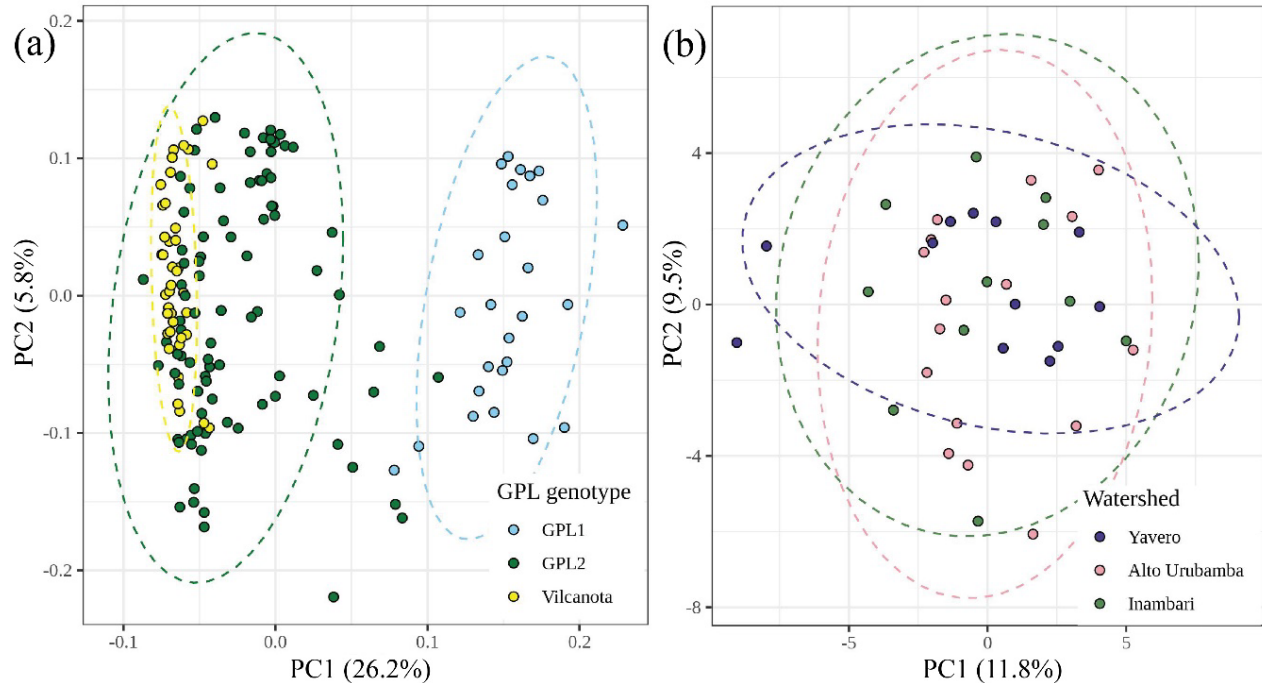
Figure 2. Principal component analyses (PCAs) of **(a)** global *Bd*GPL samples, demonstrating how *Bd* sampled from *Pleurodema marmoratum* in the Vilcanota is nested within the *Bd*GPL-2, and **(b)** Vilcanota samples, colored by watershed, showing their lack of spatial genetic structure.

3.3.2 Site infection metrics across elevations

We detected *R. spinulosa* up to 4,895 m asl. We recorded adult *Pleurodema marmoratum* and *Telmatobius marmoratus* at the highest part of the mountain passes, at a maximal elevation of 5,333 and 5,226 m asl respectively. We were able to sample *P. marmoratus* (but not the other species) at regular intervals across the entirety of both deglaciated mountain passes, suggesting that this species now has connectivity between populations north and south of the Vilcanota.

Bd prevalence in *P. marmoratum* was 30.0 % among juveniles ($n = 120$) and 24.0 % among adults ($n = 317$), but not detected in tadpoles ($n = 256$). The best model by AIC relating elevation to prevalence was a quadratic model, where prevalence peaked at approx. 4700 m asl (Fig. S 5 a, Table S 4). The predictors in this model were significant and explained 20 % of variance in prevalence ($n_{sites} = 18$, $p < 0.05$, Table S 4). Visual inspection of site infection intensity metrics against elevation suggested that these metrics declined with increasing elevation (Fig. S 5 b-c), but the data supported neither a linear nor a quadratic relationship ($n_{sites} = 18$).

3.3.3 Sublethal impacts across elevations

In *Telmatobius marmoratus* tadpoles, a full interactive model including elevation and putative site infection status explained 11 % of variance in body condition and minimized AIC ($n = 77$, $n_{sites} = 6$, Table S 5), though this model may be overfit. All predictors were significant ($p < 0.05$) except the slope of SMI against elevation at *Bd+* sites. This model suggested that tadpoles had

higher body conditions at lower elevations for *Bd-* sites but not *Bd+* sites (Fig. 3 a). Similarly, *T. marmoratus* tadpole body size (SVL) was best predicted by a full interactive model that included elevation, putative site status, and developmental stage. All predictors were significant, with fixed effects explaining 68 % of the variance ($n = 77$, $n_{sites} = 6$, $p < 0.001$, Table S 6). Consistent with our findings regarding SMI, this model suggested that tadpoles are longer relative to developmental stage at lower elevations but only at *Bd-* sites (Fig. 3 b). The relationships between *T. marmoratus* tadpole SMI or SVL and elevation cannot be attributed to differences in phenology across elevation (Fig. S 7 d).
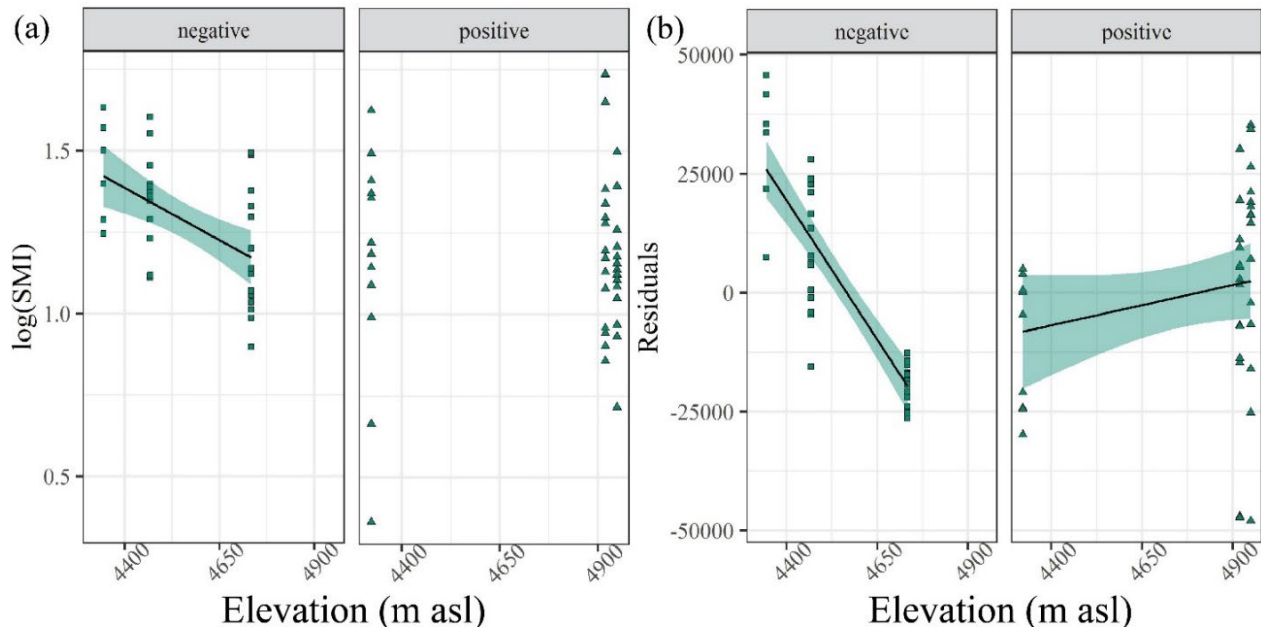
Figure 3. The relationship between elevation, site *Bd* infection status, and energetic status for *T. marmoratus* tadpoles. **(a)** Results of linear mixed model of *T. marmoratus* tadpole body condition (SMI) along the elevational gradient, displayed in separate panels for *Bd*-positive and *Bd*-negative sites as site infection status was a significant contributor to these models. **(b)** Results of linear mixed model of *T. marmoratus* tadpole residuals of body size (SVL) against Gosner stage, displayed in separate panels for *Bd*-positive and *Bd*-negative sites as site infection status was a significant contributor to these models. These trends do not appear to be attributable to differences in phenology across elevations (Fig S 7 D).

The model with lowest AIC predicting *Pleurodema marmoratum* tadpole SMI from elevation and putative site status included elevation only. According to this model, body condition declined with increasing elevation, but the model predictors were not significant, and the fixed effects explained only 4 % of variance in SMI ($n = 128$, $n_{sites} = 15$, $p > 0.05$, Table S 5). Visual inspection of these data revealed that SMI appeared reduced for lower elevation tadpoles at *Bd+* sites, similar to trends detected for *T. marmoratus* tadpoles (compare Fig. 3 a and Fig. S 6 a). Indeed, a model including site status and its interaction with elevation was within a ∆AIC of only 0.02 of the elevation-only model, explained 7 % of variance in SMI, and included a significant slope and intercept at *Bd-* sites (Table S 5). Meanwhile, *P. marmoratum* tadpole SVL was best predicted by elevation alone. Tadpoles were longer relative to developmental stage at higher

elevations regardless of putative site infection status (Fig. S 7 a). The model explained 18 % of variance in SVL, but not all predictors were significant ($n = 128$, $n_{sites} = 15$, $p > 0.05$, Table S 6). Differences in *P. marmoratum* phenology across elevations could potentially contribute to relationships between elevation and body condition (Fig. S 7 c), but this phenomenon would presumably impact *Bd+* and *Bd-* sites alike.

In *P. marmoratum* adults, the best model of SMI by AIC was an additive model that included elevation and putative site infection status, though these predictors were not significant and explained only 3 % of variance in SMI ($n = 339$, $n_{sites} = 53$, $p > 0.05$, Table S 5). Based on this model, adults had lower body conditions at high than at low elevations, and at *Bd+* than at *Bd-* sites. Visual inspection of these data reflects the trends that emerged for *T. marmoratus* tadpoles (compare Fig. 3 a and Fig. S 6 b): SMI was depressed for lower elevation tadpoles at *Bd+* sites. However, the full interactive model was not well supported by AIC-based model comparison (Table S 5).

In adult *P. marmoratum*, SVL was best predicted from a full interactive model of elevation and putative site infection status. Fixed effects in this model explained 9 % of variance in SVL, but though all the predictors were significant the intercept was not ($n = 339$, $n_{sites} = 53$, $p > 0.05$, Table S 6). According to this model, SVL in adult *P. marmoratum* increases with elevation, regardless of site infection status. However, while SVL increases rapidly at *Bd-* sites (6.5 mm per 1,000 m of elevation), SVL increases only gradually at *Bd+* sites (1.4 mm per 1,000 m; Fig. S 7 b).

Temperature data along the elevational gradient demonstrated that higher elevations were characterized by lower average daily temperatures and larger fluctuations in daily temperature (Fig. 4 a). Ephemeral pond habitats experienced less thermal variability than adjacent terrestrial habitats (Fig. 4 a). It follows that, at higher elevations, *Bd* is characterized by a lower average growth rate, but frogs also experience greater exposure to their physiological tolerance limits (Fig. 4 b).
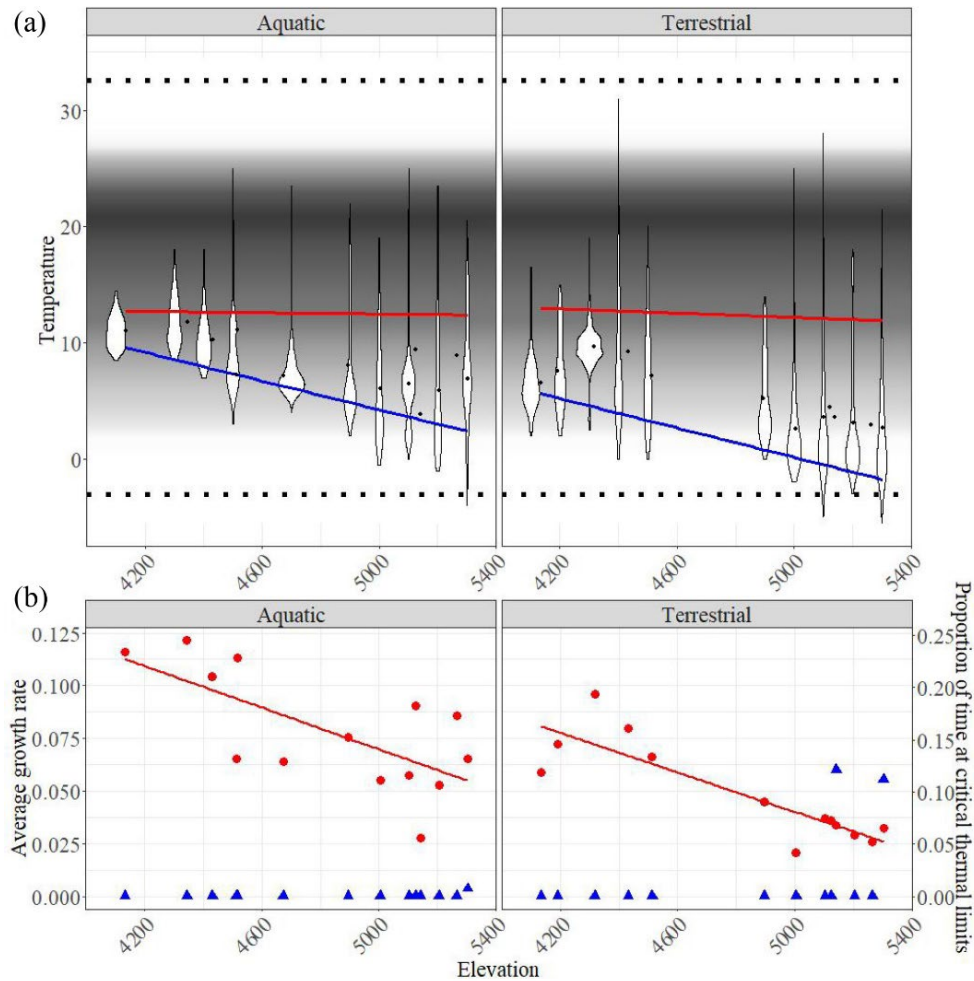
Figure 4. Thermal regimes along the elevational gradient and across microhabitats. **(a)** Violin plots of raw temperature data. Mean daily temperatures measured by a given iButton are displayed as black points. The red and blue lines represent linear regression of maximal and minimal daily temperatures, respectively. The greyscale gradient represents the logistic growth rate (r) of a tropical *Bd* strain quantified across temperatures (from Voyles et al., 2017). The upper black dotted line represents the CT$_{max}$ of adult *P. marmoratum* (32.56˚ C), and the lower dotted line represents the mean temperature tolerated by *P. marmoratum* adults that recovered following freezing (Reider et al., 2020). **(b)** Red points represent the average growth rate of *Bd* according to the temperatures recorded by a given iButton, and the red line represents a linear regression of this data. Blue triangles represent the proportion of time a given iButton was exposed to temperatures outside the physiological tolerance of *P. marmoratum* adults.

3.4 Discussion

Although how infection dynamics are influenced by pathogen or vector range shifts has been the subject of frequent study over the past decade (e.g. Dudney et al., 2021; Jaenson & Lindgren, 2011; Romanello et al., 2021; Zamora-Vilchis et al., 2012), we still know little about how they are influenced by the climate-driven range shifts of hosts. Here, we demonstrate that climate-

driven range shifts may impact the infection dynamics of direct-transmission pathogen systems, as well as vector-borne ones. We used genetic analyses and modeled the relationship among elevation, site infection metrics, and measures of individual energetic status to understand how the range expansion of three species may have impacted the course of their infection with a shared pathogen. We learned that one of the species studied is using mountain passes cleared by contemporary deglaciation as a new dispersal corridor, and that *Bd* is resilient to, and can disperse extensively at, the highest elevations used by amphibians. Finally, we found evidence that some site infection metrics and apparent sublethal impacts of infection are affected by elevation, suggesting that hosts' elevational range shifts have had implications for infection outcomes.

3.4.1 Genetic evidence suggests the recent introduction and extensive dispersal of *Bd*GPL-2

Whether global *Bd* epizootics were provoked by a novel or endemic pathogen remains an open question (Rosenblum et al., 2013). *Bd* was often present in areas long before recorded outbreaks (e.g., Basanta et al., 2021; De León et al., 2019). Indeed, the earliest known *Bd* was swabbed from a Titicaca water frog (*Telmatobius culeus*) collected 300 km southeast of the Cordillera Vilcanota in 1863 (P. Burrowes & De la Riva, 2017). Detections of *Bd* that predate epizootic events are often hypothesized to represent local *Bd* strains, with regional *Bd*-associated declines instead being attributed to the introduction of a novel strain in the 1990s (Becker et al., 2016; Burrowes & De la Riva, 2017)—usually the global panzootic lineage (*Bd*GPL), the lineage most frequently associated with disease outbreaks, whose lack of genetic structure even at global scales suggests its recent expansion (James et al., 2015; O'Hanlon et al., 2018; Rosenblum et al., 2013; Schloegel et al., 2012).

Bd samples sequenced in this study belong to *Bd*GPL, consistent with previous studies genotyping South American *Bd* west of the Brazilian Atlantic Forest (Alvarado-Rybak et al., 2021; Byrne et al., 2019; O'Hanlon et al., 2018; Russell et al., 2019). Further, Vilcanota *Bd* was all *Bd*GPL-2, the more derived and globalized of two *Bd*GPL sub-clades (James et al., 2015). However, it is worth noting that *Bd*GPL can outcompete other strains during coinfections, so may have displaced potentially pre-existing endemic strains in the Vilcanota (Farrer et al., 2011; Jenkinson et al., 2018). Additionally, selecting the highest intensity swabs to sequence at each site could introduce bias against less-virulent strains (Byrne et al., 2017; Farrer et al., 2011).

We found Vilcanota *Bd*GPL-2 to be spatially unstructured using our genetic markers, consistent with most previous genetic studies of *Bd*GPL, which have found it to be spatially unstructured from local to continental scales (Alvarado-Rybak et al., 2021; Basanta et al., 2021; Byrne et al., 2019; Rothstein et al., 2021; Velo-Antón et al., 2012). This lack of structure has often been interpreted as evidence for its recent introduction to the sampled area, though might simply indicate high rates of dispersal. One exception to the general lack of spatial structuring in *Bd* has been the Sierra Nevada of California, suggesting the western U.S.A. as a potential origin for *Bd*GPL (Rothstein et al., 2021). Sierran *Bd* demonstrates that *Bd*GPL can develop spatial structure, even despite cool, high-elevation conditions that may constrain rates of evolutionary change.

Though unstructured, Vilcanota *Bd* has substantial low-frequency variation, representative of the global variation in *Bd*GPL-2. Our data cannot exclude the possibility that *Bd*GPL circulated in

the Vilcanota prior to local epizootics of the early 2000s, but in the context of prior regional studies (Burrowes et al., 2020; Catenazzi et al., 2011; Lips et al., 2008) it is more likely that *Bd*GPL-2 housed substantial standing genetic variation upon its introduction or was introduced multiple times. Our analyses place Vilcanota *Bd* in a large, global polytomy in *Bd*GPL-2, so we cannot determine whether *Bd*GPL spread from Ecuador via the Andes (Lips et al., 2008) or from Brazil via Bolivia (Burrowes et al., 2020; Catenazzi et al., 2011). However, the timing of *Bd*GPL-2's arrival likely coincides with the amphibian die-offs in the Vilcanota in the early 2000s (Seimon et al., 2007; Seimon et al., 2005), as this corresponds to declines in adjacent lowland and cloud forest regions (Catenazzi et al., 2011).

Regardless of the provenance and timing of introduction, our data demonstrates that *Bd*GPL-2 has undergone extensive local dispersal. Its movement across the Cordillera Vilcanota would not have been limited to transmission by frogs along the terrestrial corridors provided by deglaciated passes. Processes facilitating its dispersal might include the trade of *T. marmoratus* for urban consumption (Catenazzi et al., 2010), the aquaculture of nonnative fish (Martín-Torrijos et al., 2016; Ortega & Hidalgo, 2008), the movements of Andean waterbirds (Burrowes & De la Riva, 2017), or even precipitation (Kolby et al., 2015).

3.4.2 Amphibians cannot escape *Bd* by range shifting upslope

Early studies generally found that *Bd* infection prevalence or intensity increased with elevation (Brem & Lips, 2008) and epizootics impacted highland sites more severely (Berger et al., 2004). These relationships are consistent with the preference of *Bd* for cool temperatures (Piotrowski et al., 2004; Woodhams et al., 2008) and the impaired function of amphibian immune systems and skin microbiomes at colder, more thermally variable high elevations (Daskin et al., 2014; Jackson & Tinsley, 2002). Early field studies did not sample above 2,500 m asl, but empirical work demonstrating that suboptimal temperatures retard *Bd* growth led to a hypothesis that *Bd* pathogenicity was restricted to below 4,000 m asl (Piotrowski et al., 2004; Pounds et al., 2006; Ron, 2005; Woodhams et al., 2008). Subsequent studies of *Bd* dynamics up to 4,000 m asl reported declining infection prevalence or intensity with increasing elevation (Catenazzi et al., 2011; Muths et al., 2008), perhaps due as much to increasing aridity as to decreasing temperatures (De la Riva & Burrowes, 2011).

The idea that *Bd* pathogenicity had an upslope bound was later undermined by severe infections documented above 4,000 m asl in the Vilcanota and other sites (Knapp et al., 2011; Seimon et al., 2007). Here, we find limited evidence that elevational extremes constrain *Bd* growth. *Bd* infection metrics appear to decline at the upper reaches of the elevational gradient colonized by Vilcanota frogs (3,967—5,333 m asl)—both for the significant and well-fit quadratic model of prevalence and for the inherently noisy infection intensity data. Such declines would be consistent with our expectations following from our iButton temperature data, considered in light of a study profiling the thermal dependence of *Bd* growth (Voyles et al., 2017): *Bd* likely grows more slowly at higher elevations in the Vilcanota (Fig. 4).

3.4.3 Upslope range shifts may mediate infection outcomes through exposure to thermal variability

We investigated whether extreme elevations compounded or ameliorated the apparent sublethal impacts of *Bd* by comparing frog body size and condition at putatively *Bd+* and *Bd-* sites. Body size and condition signal important information about nutritional history in amphibian larvae, juveniles, and adults; and can predict important fitness components such as fecundity, the ability to respond effectively to environmental stress, and lifespan (Brodeur et al., 2020; Hector et al., 2012; Maccracken & Stebbings, 2012; Martins et al., 2013; Metcalfe & Monaghan, 2001). To call sites as *Bd-* we required infection intensities for at least 10 postmetamorphic frogs at that site, with individual frog infection statuses being called from triplicate qPCR reactions; therefore, though we lacked longitudinal sampling that would more definitely classify site infection status, we believe our protocol minimizes the risk of both false negatives and false positives.

At *Bd-* sites, *Telmatobius marmoratus* tadpole condition and size declined with increasing elevations, which our examination of adult counts across elevations suggests we cannot attribute to increased competition. *T. marmoratus* tadpoles have a protracted larval development relative to *P. marmoratum* and *R. spinulosa*. During the estimated 5—19 months until metamorphosis (Lobos et al., 2018), they rely upon the resources of their natal stream (Catenazzi et al., 2013a; Rubio, 2019). Therefore, declines in stream primary productivity with increasing elevation (Jacobsen, 2008) might explain this trend in tadpoles. An alternative explanation could be that *T. marmoratus* tadpoles metamorphose more quickly at higher elevations, attaining a smaller size in the process (Licht, 1975).

For larval *T. marmoratus*, circulating *Bd* was associated with lower body condition and size relative to developmental stage, but only at low elevations. This interaction is consistent with expectations from our temperature data. Aquatic microhabitats at extreme elevations are frequently at no- or low-growth temperatures for *Bd*, resulting in a depressed average growth rate, but at low elevation remain steadily at temperatures conducive to *Bd* growth (Fig. 4, Fig. S 8). Studies of other amphibian species have shown that *Bd* infection can result in smaller, lighter tadpoles (Catenazzi et al., 2013b; Parris & Cornelius, 2004). Infected tadpoles may sacrifice body size and condition by diverting energy towards immune response or by accelerating metamorphosis (Warne et al., 2011). We expect that, for slow-developing *T. marmoratus*, the impact of *Bd* on tadpole mouthparts is particularly important: *Bd* infects keratinized tissues, which in tadpoles limits *Bd* growth to their mouthparts and causes oral deformities over time (Berger et al., 1998; Vredenburg & Summers, 2001), as has been demonstrated for congenerics (Rubio, 2019). Damaged mouthparts can reduce tadpole feeding efficiency and retard their growth (Rachowicz & Vredenburg, 2004; Rowe et al., 1996; Rubio, 2019).

Shared mechanisms may contribute to a similar trend in larval *P. marmoratum* body condition. Their body condition declines with increasing elevations at *Bd-* sites, but *Bd* infections appear to take a larger energetic toll on *P. marmoratum* tadpoles at lower elevations. Unlike larval *T. marmoratus*, larval *P. marmoratum* increase in body size relative to developmental stage with elevation regardless of putative site infection status. This trend may reflect a reproductive strategy that is advantageous in harsh environments and has been documented in several frog species (e.g., Liao et al., 2014; Lüddecke, 2002; Räsänen et al., 2005), that females produce fewer offspring of higher quality in harsher environments, or given the decline in abundance of *R. spinulosa* with increasing elevations could possibly result from decreasing competition since these species can share larval habitat.

Adult *P. marmoratum* body size also increases with elevation, perhaps owing to reduced competition with *R. spinulosa* or selection for larger size at metamorphosis and/or larger females capable of greater maternal investment (Chen et al., 2013; Liao et al., 2014; Womack & Bell, 2020). However, adult *P. marmoratum* body size increases dramatically with elevation at *Bd*-sites, while only gradually at *Bd*+ sites (6.5 mm vs. 1.4 mm per 1,000 m of elevation), suggesting that *Bd* may have a larger sublethal toll at higher elevations. While terrestrial frogs experience lower average *Bd* growth rates at extreme elevations, they are also not as thermally buffered from harsh temperature extremes as frogs inhabiting aquatic microhabitats. Indeed, we found that adult *P. marmoratum* are more exposed to their thermal tolerance limits at extreme high elevations (Fig. 4, Fig. S 8), placing them at a fitness disadvantage relative to the *Bd* pathogen (Cohen et al., 2019, 2017). Their failure to respond phenotypically to high-elevation conditions could compromise their fecundity and survivorship, suggesting that extreme elevations may compound rather than ameliorate the stress of *Bd* infection for *P. marmoratum* adults.

It is important to note that all association between *Bd* site status and apparent sublethal impacts to individuals are correlative in this study. We did not conduct trials and cannot know the *Bd* exposure history of any individual frog. One important implication is that we do not know the direction of causality: we interpret that *Bd* could be incurring sublethal impacts, but alternately *Bd* might be more likely to affect amphibian populations with lower energy reserves. If this were the case, observed interactions between body condition or size, elevation, and site *Bd* status require different mechanistic explanations.

3.5 Conclusion

Climate change will continue to drive range shifts, with many species expanding into more thermally-variable regions like the Vilcanota. It is important that we understand how the stress of novel, frequently less optimal, habitats impact host-pathogen systems, particularly in the face of increasingly common emerging infectious disease challenges. In the case of amphibian-*Bd* systems, hosts cannot escape infection by range shifting upslope: *Bd* infects amphibians and disperses readily even at the edges of their physiological tolerances, though factors like exposure to thermal variability may mediate infection outcomes. This work can help inform and stimulate further questions around how host range shifts might in some cases exacerbate and in others mitigate emerging infectious disease events.

3.6 Acknowledgements

3.7 Supplementary materials

Figure S 1. The study system. **(a)** Sites where amphibians and *Batrachochytrium dendrobatidis* were sampled in the Cordillera Vilcanota, colored to represent their watershed location and plotted over a hill-shaded digital elevation model (DEM). The two deglaciated mountain passes, Osjollo and Chimboya, are labeled. The study species **(b)** *Pleurodema marmoratum*, **(c)** *Telmatobius marmoratus*, and **(d)** *Rhinella spinulosa* are also pictured. Photos courtesy of Anton Sorokin.
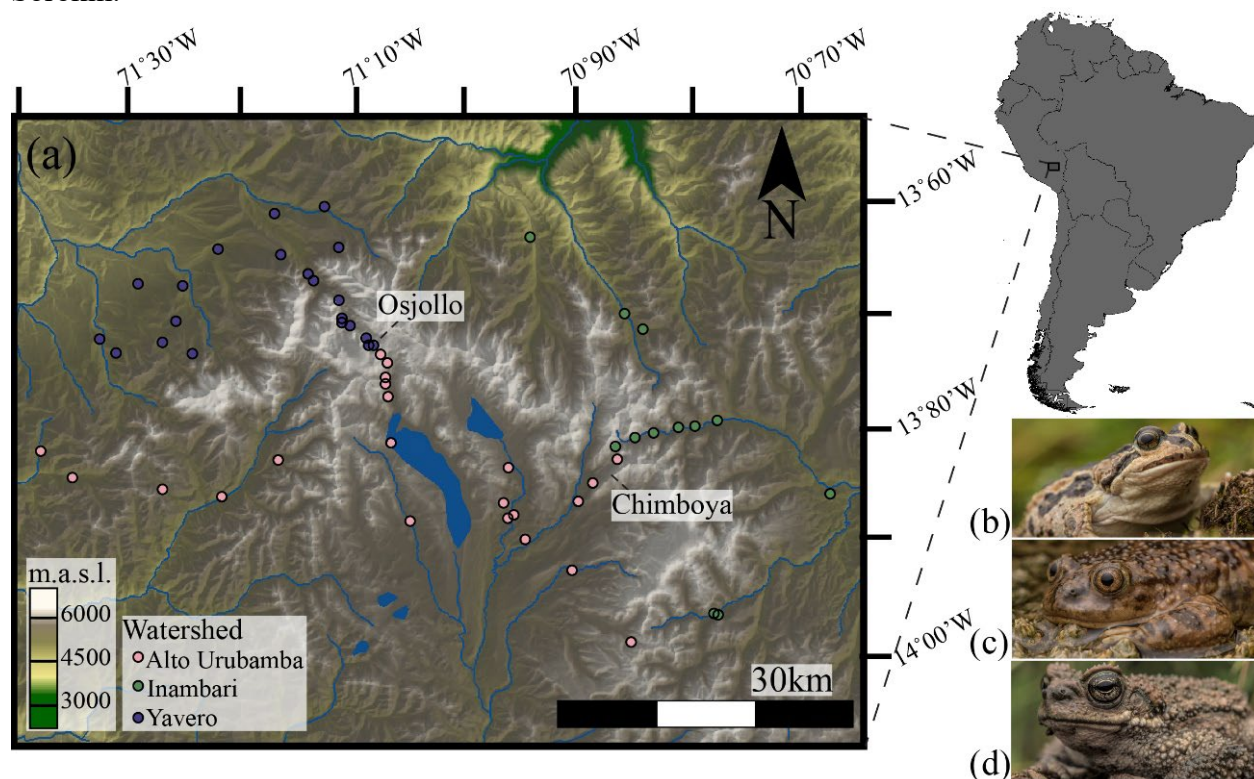
Table S 1. Analysis of molecular variance of *Batrachochytrium dendrobatidis* in the Vilcanota.

	Sum of square deviations	Mean square deviations	Degrees of Freedom	σ^2	p-value
Watershed	47.9	24.0	2	0.058	0.428
Sites	398.4	22.1	18	-2.449	0.999
Individuals	560.3	31.1	18	7.100	0.001
Error	660.1	16.9	39	16.925	
Total	1666.7	21.6	77		

Table S 2. Redundancy analysis of *Batrachochytrium dendrobatidis* in the Vilcanota on 459 SNPs.

MissForest	Number of iterations		NRMSE					
	5		0.5404669					
Vegan RDA	Inertia	Proportion	Rank	F	Pr(>F)	r^2		Adj. r^2
Constrained	15.93	0.04	1	1.46	0.031	0.038		0.012
Unconstrained	403.07	0.96	37					
Total	419.00	1						

Figure S 3. Adult counts along the elevational gradient for all sites where any life stage of that species was detected. Slope and confidence intervals are displayed when predictors were significant and the model was well fit. **(a)** *Pleurodema marmoratum* adult counts varied from 0—15 with a mean of 4.98. (n_{sites} = 63). **(b)** *Telmatobius marmoratus* adult counts varied from 0—9 with a mean of 1.92 (n_{sites} = 17). **(c)** *Rhinella spinulosa* adult counts varied from 0—12 with a mean of 2.85 (n_{sites} = 25). *R. spinulosa* adults counts declined by about 6.4 animals per 1000m increase in elevation.
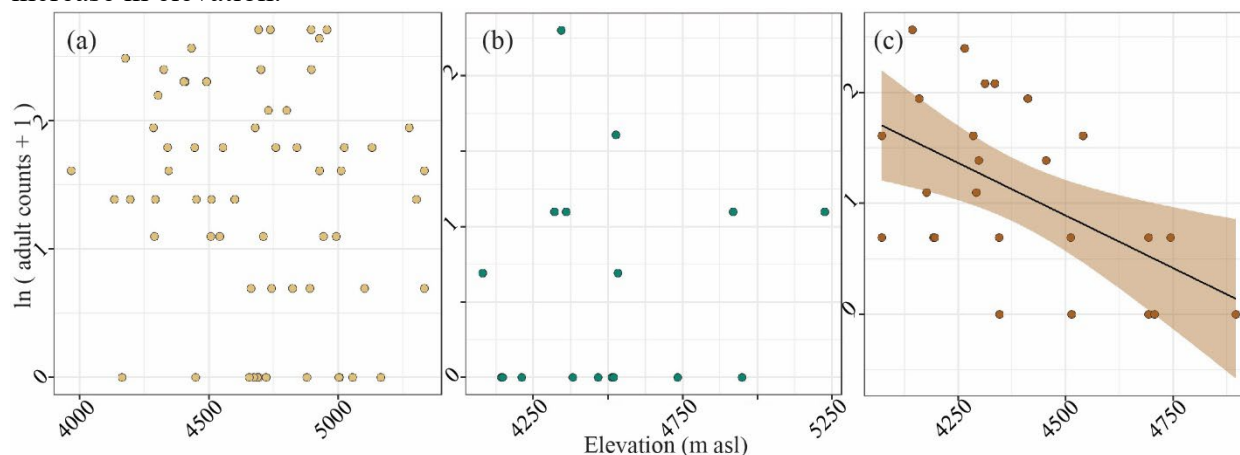
Table S 3. AIC table and model summary for negative binomial regression of adult counts of *Rhinella spinulosa* along the elevational gradient ("ele"). Deviance shown is the residual deviance for the model including elevation and the null deviance for the saturated model.

		K	AIC	ΔAIC	Coefficient	Intercept	Deviance (*df*)	r^2
ln(n_{adults}) ~	ele	3	111.40	0.00	$-3.185 \cdot 10^{-3}$**	14.915***	26.015 (23)	0.150
	1	2	117.47	6.07		1.215***	35.130	

Figure S 4. The relationship between the date at which a site was sampled and elevation. Sites sampled in 2018 are unfilled, and sites sampled in 2019 are filled.
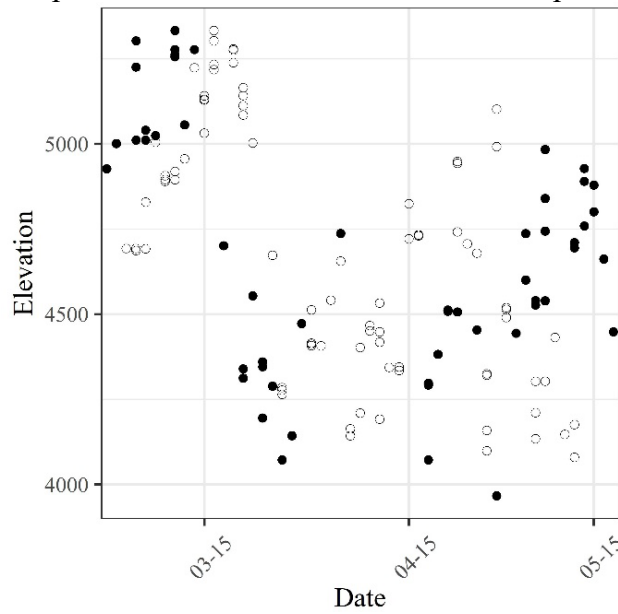
Figure S 5. The relationship between site *Batrachochytrium dendrobatidis* infection metrics in *Pleurodema marmoratum* and elevation (n_{sites} = 18). The infection metrics assessed were **(a)** site prevalence, **(b)** site mean infection intensity, and **(c)** site maximal infection intensity.
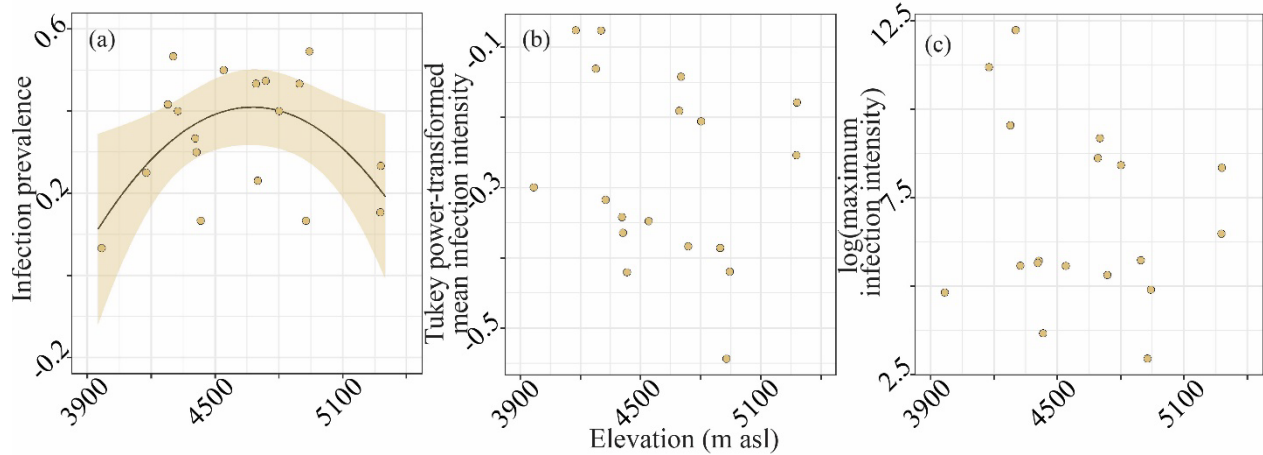
Table S 4. An AIC table for the model relating site *Batrachochytrium dendrobatidis* infection prevalence (n_{sites} = 18) in *Pleurodema marmoratum* to elevation ("ele"). Deviance shown is the residual deviance for models including predictors and the null deviance for the saturated model.

		K	AIC	ΔAIC	Coefficient		Intercept	Residual SE (*df*)	Adj. r^2
prevalence ~	ele + ele²	4	-16.17	0.00	ele	$5.25 \cdot 10^{-3}$*	-11.87*	0.135 (15)	0.200
					ele²	$-5.62 \cdot 10^{-7}$*			
	1	2	-13.90	2.28			0.340***	0.152 (17)	
	ele	3	-11.93	4.24		$1.90 \cdot 10^{-5}$	0.25	0.156 (16)	-0.060

Figure S 6. Linear regression predicting individual SMI from elevation and site *Batrachochytrium dendrobatidis* (*Bd*) infection status for **(a)** *P. marmoratum* tadpoles (*n* = 128, n_{sites} = 15) and **(b)** *P. marmoratum* adults (*n* = 339, n_{sites} = 53).
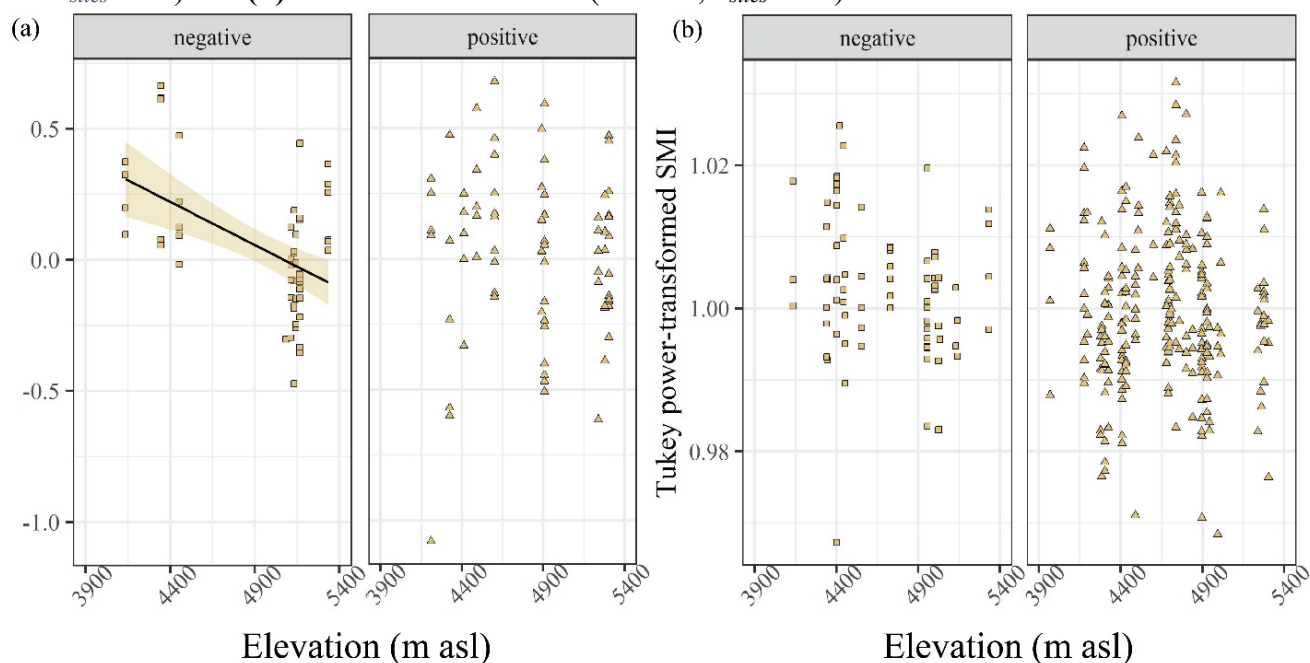
Table S 5. AIC table and model summaries for linear mixed model predicting body condition (SMI) from elevation ("ele"), site *Batrachochytrium dendrobatidis* infection status ("st"), the interaction between those terms, and site as a random effect ("1|site").

Model formula[A]	K	AIC	Δ AIC	Coefficient	Intercept	SE (df)[B]	$r^2_{marginal}$	$r^2_{conditional}$
P. marmoratum tadpoles (n = 128, n_{sites} = 15)								
ln(SMI)~ ele+(1|site)	4	47.21	0.00	ele −1.45·10⁻⁴ ·	0.75·	8.17·10⁻⁵	0.036	0.115
st+ele:st+(1|site)[c]	6	47.42	0.02	st+ −1.37· st-:ele −3.08·10⁻⁴ * st+:ele −3.76·10⁻⁵	1.58**	0.72 (15.5) 1.11·10⁻⁴ (14.7) 9.80·10⁻⁵ (13.1)	0.074	0.113
ele*st+(1|site)[c]	6	47.24	0.02	ele −3.08·10⁻⁴* st+ −1.37· st+:ele 2.71·10⁻⁴·	1.58**	1.11·10⁻⁴ (14.7) 0.72 (15.5) 1.48·10⁻⁴ (14.0)	0.074	0.113
(1|site)	3	47.94	0.72		0.05	0.04 (12.0)	0	0.135
ele+st+(1|site)	5	48.03	0.82	ele −1.50·10⁻⁴· st+ −7.67·10⁻²	0.82·	8.31·10⁻⁵ (16.3) 7.00·10⁻² (12.1)	0.048	0.135
ele+ele:st+(1|site)	5	48.31	1.10	ele −1.42·10⁻⁴ st+:ele −1.39·10⁻⁵	0.78·	8.32·10⁻⁵ (15.3) 1.45·10⁻⁵ (11.0)	0.045	0.133
st+(1|site)	4	48.90	1.69	st+ −0.08	0.10	0.08 (13.8)	0.018	0.154
P. marmoratum adults (n = 339, n_{sites} = 53)								
tuk(SMI)~ ele+st+(1|site)	5		0.00	ele −4.03·10⁻⁶ st+ −3.35·10⁻³	1.02***	2.70·10⁻⁶ (43.5) 2.01·10⁻³ (42.1)	0.031	0.209
ele+ele:st+(1|site)	5		0.12	ele −3.54·10⁻⁶ ele:st+ −7.01·10⁻⁷	1.02***	2.73·10⁻⁶ (42.7) 4.30·10⁻⁷ (41.6)	0.030	0.210
st+(1|site)	4		0.22	st+ −3.36·10⁻³	1.00***	2.02·10⁻³ (40.7)	0.018	0.200
ele+(1|site)	4		0.72	ele −4.14·10⁻⁶	1.02***	2.77·10⁻⁶ (42.9)	0.015	0.209
(1|site)	3		0.95		1.00***	9.26 (36.7)	0	0.196
ele*st+(1|site)[C]	6		1.80	ele −5.90·10⁻⁶ st+ −1.57·10⁻² ele:st+ 2.65·10⁻⁶	1.03***	5.01·10⁻⁶ (50.0) 2.78·10⁻² (47.6) 5.94·10⁻⁶ (46.9)	0.030	0.206
st+ele:st+(1|site)[c]	6		1.80	st+ −1.57·10⁻² st-:ele −5.90·10⁻⁶ st+:ele −3.25·10⁻⁶	1.03***	2.78·10⁻² (47.6) 5.01·10⁻⁶ (50.0) 3.19·10⁻⁶ (40.4)	0.030	0.206

T. marmoratus tadpoles (_n_ = 77, n_{sites} = 6)									
ln(SMI)~	st+ele:st+(1|site) [c,d]	5	-4.70	0.00	st+	-3.08*	4.21***	$1.23 \cdot 10^{-3}$ (77.0)	0.146	0.146
					st-:ele	$-6.42 \cdot 10^{-4}$**		$0.24 \cdot 10^{-3}$ (77.0)		
					st+:ele	$7.77 \cdot 10^{-6}$		$0.12 \cdot 10^{-3}$ (77.0)		
	ele*st+(1|site) [c,d]	5	-4.70	0.00	ele	$-6.42 \cdot 10^{-4}$**	4.21***	$0.24 \cdot 10^{-3}$ (77.0)	0.146	0.146
					st+	-3.08*		$1.23 \cdot 10^{-3}$ (77.0)		
					ele:st+	$6.50 \cdot 10^{-4}$*		$0.27 \cdot 10^{-3}$ (77.0)		
	st+(1|site)	3	-1.71	2.98		-0.12·	1.29***	0.06 (4.96)	0.067	0.081
	ele+st+(1|site) [d]	4	-1.01	3.69	ele	$-1.30 \cdot 10^{-4}$	1.88***	$0.11 \cdot 10^{-3}$ (77.0)	0.080	0.080
					st+	-0.09		$0.06 \cdot 10^{-3}$ (77.0)		
	ele+ele:st+(1|site)	4	-0.67	4.02	ele	$-1.19 \cdot 10^{-4}$	1.83*	$0.12 \cdot 10^{-3}$ (5.55)	0.076	0.078
					ele:st+	$-1.91 \cdot 10^{-5}$		$0.01 \cdot 10^{-3}$ (4.81)		
	ele+(1|site)	3	-0.32	4.38	ele	$-2.09 \cdot 10^{-4}$	2.19*	$1.23 \cdot 10^{-4}$ (48.7)	0.049	0.077
	(1|site)	2	1.129	5.99			1.23***	0.04 (46.0)	0	0.080

[a] Additive effects are shown with a "+", interactive effects are shown with a ":", and a full interactive model including all additive and interactive effects is shown with a "*".

[b] SE shown is for the estimate of the predictor coefficient.

[c] The full interactive model and model including putative site infection status and its interaction with elevation are different parameterizations of the same model, explaining their identical AIC values.

[d] Model is singular and may be overfit.

Figure S 7. Linear regression predicting individual SVL from elevation for **(a)** *P. marmoratum* tadpoles (n = 128, n_{sites} = 15), using residuals from the linear model relating SVL to Gosner developmental stage, and **(b)** *P. marmoratum* adults (*n* = 339, n_{sites} = 53). **(c)** *P. marmoratum* tadpoles (n = 128) were only sampled from the highest parts of the landscape early in the sampling season, despite having visited higher elevations across the sampling season. *P. marmoratum* breed in seasonal ponds, so this temporal-by-elevational sampling association may reflect the fact that higher elevations have shorter hydroperiods—driving the earlier emersion of metamorphs and hence their absence upon visiting high elevation sites later in the season. This association could potentially confound relationships between elevation and SVL or SMI relative to developmental stage in *P. marmoratum*, though it is worth noting that this would impact *Bd+* and *Bd-* sites alike. **(d)** *T. marmoratus* breed in stable stream or peatland environments, perhaps explaining why there was no systematic relationship between Gosner stage, elevation, and time of sampling for *T. marmoratus* tadpoles (*n* = 77).
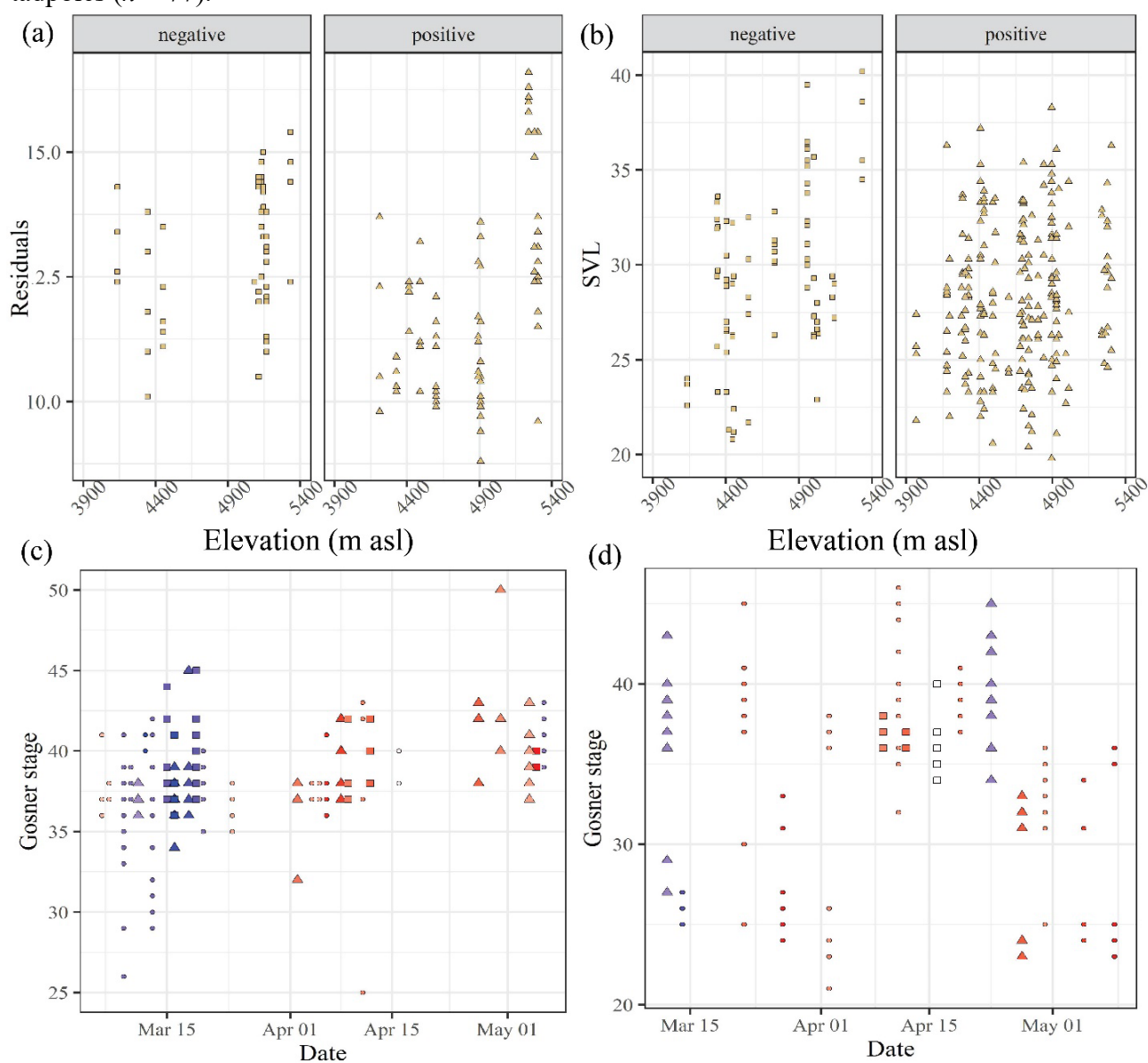
Table S 6. AIC table and model summaries for linear mixed model predicting predicting body size (SVL) from elevation ("ele"), site *Bd* infection status ("st"), the interaction between those terms, site as a random effect ("1|site"), and developmental stage ("go") for tadpoles.

Model formula[D]		K AIC	Δ AIC	Coefficient		Intercept	SE (df)[E]	$r^2_{marginal}$	$r^2_{conditional}$
P. marmoratum tadpoles ($n = 128$, $n_{sites} = 15$)									
SVL~	ele+go +(1|site)	5 443.05	0.00	ele	$1.99\cdot10^{-3}$*	0.40	$6.87\cdot10^{-4}$ (16.4)	0.177	0.536
				go	$6.75\cdot10^{-2}$		$5.57\cdot10^{-2}$ (126.4)		
	ele+st+go +(1|site)	6 443.61	0.56	ele	$1.97\cdot10^{-3}$**	1.05	$6.55\cdot10^{-4}$ (16.4)	0.238	0.548
				st+	-0.70		0.57 (15.0)		
				go	$6.36\cdot10^{-2}$		$5.56\cdot10^{-2}$ (126.8)		
	ele*st+go +(1|site) [F]	7 443.82	0.77	ele	$1.05\cdot10^{-3}$	5.28	$9.20\cdot10^{-4}$ (16.7)	0.252	0.536
				st+	-8.81		5.97 (16.6)		
				go	$6.79\cdot10^{-2}$		$5.54\cdot10^{-2}$ (127.0)		
				st+:ele	$1.70\cdot10^{-3}$		$1.24\cdot10^{-3}$ (16.3)		
	st+ele:st +go +(1|site) [g]	7 443.82	0.77	st+	-8.81	5.28	5.97 (16.6)	0.252	0.536
				go	$6.79\cdot10^{-2}$		$5.54\cdot10^{-2}$ (127.0)		
				st-:ele	$1.05\cdot10^{-3}$		$9.20\cdot10^{-4}$ (16.7)		
				st+:ele	$2.75\cdot10^{-3}$		$8.46\cdot10^{-4}$ (16.5)		
	ele+ele:st +go +(1|site)	6 443.90	0.85	ele	$2.04\cdot10^{-3}$**	0.65	$6.62\cdot10^{-4}$ (16.2)	0.230	0.547
				go	$6.37\cdot10^{-2}$		$5.56\cdot10^{-2}$ (12.7)		
				ele:st+	$-1.31\cdot10^{-4}$		$1.20\cdot10^{-4}$ (14.8)		
	go+(1|site)	4 447.58	4.53	go	0.05	10.39***	0.06 (124.8)	0.005	0.571
	st+go +(1|site)	5 448.60	5.55	st+	-0.73	10.96***	0.72 (14.6)	0.050	0.571
				go	0.05		0.06 (125.1)		
P. marmoratum adults ($n = 339$, $n_{sites} = 53$)									
SVL~	ele*st +(1|site) [g]	6 1835.05	0.00	ele	$6.38\cdot10^{-3}$***	-0.95	$1.81\cdot10^{-3}$ (51.8)	0.081	0.183
				st+	23.56*		9.98 (48.4)		
				ele:st+	$-5.30\cdot10^{-3}$*		$2.13\cdot10^{-3}$ (47.4)		
	st+ele:st + (1|site) [g]	6 1835.05	0.00	st+	23.56*	-0.95	9.98 (48.4)	0.081	0.183
				ele:st-	$6.38\cdot10^{-3}$***		$1.81\cdot10^{-3}$ (51.8)		
				ele:st+	$1.08\cdot10^{-3}$		$1.13\cdot10^{-3}$ (38.3)		
	ele+ele:st +(1|site)	5 1838.43	3.38	ele	$2.78\cdot10^{-3}$**	15.93**	$1.01\cdot10^{-3}$ (38.8)	0.056	0.180
				ele:st+	$-2.82\cdot10^{-4}$·		$1.59\cdot10^{-4}$ (38.16)		
	ele+st + (1|site)	5 1838.99	3.94	ele	$2.58\cdot10^{-3}$*	16.76**	$1.01\cdot10^{-3}$ (39.8)	0.053	0.180
				st+	-1.19		0.75 (38.7)		
	ele+(1|site)	4 1839.40	4.35	ele	$2.60\cdot10^{-3}$*	15.80**	$1.05\cdot10^{-3}$ (40.8)	0.037	0.183
	st+(1|site)	4 1843.16	8.11	st	-1.17	28.78	0.803 (38.0)	0.014	0.177
	(1|site)	3 1843.18	8.13			27.92***	0.37 (36.2)	0	0.186

T. marmoratus tadpoles (n = 77, n_{sites} = 6)										
tuk(SVL) ~	st+ele:st+go +(1|site) [g]	7	1715.58	0.00	st+	$-7.95 \cdot 10^5$***	$5.88 \cdot 10^5$***	$1.15 \cdot 10^5$ (10.6)	0.677	0.691
					ele:st-	$2.06 \cdot 10^3$**		$6.13 \cdot 10^2$ (76.7)		
					ele:st+	$-1.25 \cdot 10^2$***		19.99 (7.2)		
					go	46.01**		13.61 (15.8)		
	ele*st+go +(1|site) [g]	7	1715.58	0.00	ele	$-1.25 \cdot 10^2$***	$5.88 \cdot 10^5$***	19.91 (7.8)	0.677	0.691
					st+	$-7.95 \cdot 10^5$***		$1.15 \cdot 10^5$ (7.2)		
					ele:st+	$2.06 \cdot 10^3$**		$6.13 \cdot 10^2$ (10.6)		
					go	$1.71 \cdot 10^2$***		24.76 (10.1)		
	go+(1|site)	4	1725.32	9.73	go	2028.87	17679.05	612.63 (76.8)	0.114	0.646
	ele+go +(1|site)	5	1726.69	11.11	ele	-5.73	43924.02	30.19 (5.7)	0.103	0.640
					go	2047.81**		618.79 (75.8)		
	st+go +(1|site)	5	1727.28	11.70	st+	-11965.36	23931.55	14810.27 (5.7)	0.192	0.659
					go	2012.25**		612.55 (76.8)		
	ele+st+go + (1|site)	6	1728.66	13.08	ele	5.24	555.30	32.07 (6.1)	0.208	0.665
					st+	-13120.03		16402.47 (5.9)		
					go	1992.005**		625.17 (73.9)		
	ele+ele:st+ go+(1|site)	6	1728.83	13.25	ele	5.53	-1626.23	33.73 (6.0)	0.186	0.661
					ele:st+	2000.43**		624.76 (74.0)		
					go	-2.46		3.63 (5.8)		

[e] Additive effects are shown with a "+", interactive effects are shown with a ":", and a full interactive model including all additive and interactive effects is shown with a "*"

[f] SE shown is for the estimate of the predictor coefficient.

[g] The full interactive model and model including putative site infection status and its interaction with elevation are different parameterizations of the same model, explaining their identical AIC values.

Figure S 8. Hypothesis for how elevation interacts with microhabitat usage by species and life stages studied to impact *Bd* infection outcomes. Lower elevations offer higher average temperatures, but also less extreme daily temperature fluctuations. However, exposure to this thermal variability depend on an organism's microhabitat. Terrestrial habitats are subject to more extreme temperature fluctuations than pond habitats, which in turn experience more extreme fluctuations than stream or peat-bog habitats. These temperature regimes influence *Bd* growth rate and exposure to amphibians' physiological tolerance.
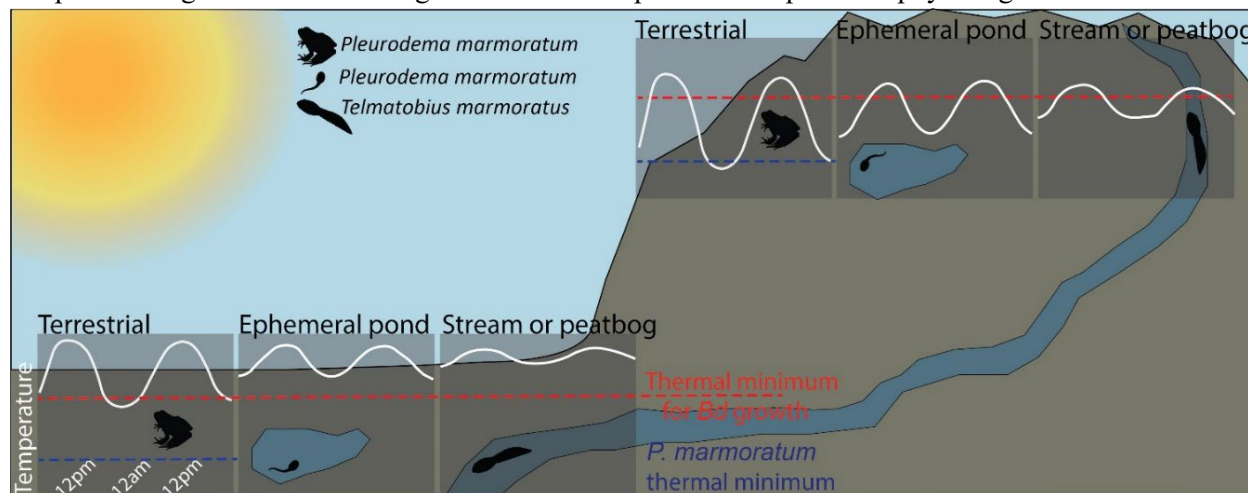
CONCLUSION

As the climate continues to rapidly warm over the coming years, bioclimatic modelling suggests that diverse species will continue to shift their elevational and latitudinal ranges across the world (Corlett et al., 2013; Forero-Media et al. 2011; Elsen and Tingley 2015; Lawler et al., 2013). The potential evolutionary and ecological impacts of these range shifts, therefore, is an issue of widespread relevance to conservation practitioners and to managers. Using the tools of population genomics and disease ecology, my dissertation has explored the following aspects of contemporary, climate-driven range shifts: the spatial signature they leave in whole genome diversity, their influence on genomic adaptation to the new environments colonized, and their implications for host-pathogen dynamics.

Keeping evolution in mind when considering climate-driven range shifts can transform our predictions of their impact on biodiversity (Diamond, 2017). My first chapter adds nuance to the perception of range expansions as a successful response to climate change, since whole genome diversity is perhaps our best proxy for the evolutionary potential of non-model organisms (Kardos et al., 2021) and we document its measurable decline in genomic diversity along a climate-change driven range expansion front. My second chapter additionally finds declines in the frequency of many putatively adaptive variants to the novel environment colonized, suggesting that high drift along the expansion front may be taking a toll on selection efficacy. Since failure to adapt to a physiologically mismatched environment may drive population declines (Bay et al., 2018; Urban et al., 2013), we must consider the possibility that populations inhabiting new range extents may be more susceptible to declines in the present—additional to being less prepared to evolve in the face of future challenges.

Similarly, keeping ecological interactions in mind when considering climate-driven range shifts is crucial if we are to accurately predict how they will impact biodiversity (Berke et al. 2010). With the rising incidence of emerging infectious diseases (EIDs; Fisher et al., 2012; Jones et al., 2008), it is expedient that we improve our understanding of how climate-driven range shifts will modulate host-pathogen dynamics. My third chapter concludes that, though range shifts did not allow hosts to evade infection and did not affect pathogen transmission of the pathogen studied, the novel environment colonized may have mediated infection outcomes for hosts. Improving our understanding of how climate-change driven range expansion influences the disease triangle (disease-host-environment) will be important, not just for biodiversity conservation, but also for public health.

The plummeting costs of high-throughput genomic sequencing (Goodwin et al. 2016) brings the widescale application of the kinds of approaches I have implemented here ever more closely into view. My dissertation work demonstrates the utility of elaborating our understanding of species' responses to climate change with key ecological and evolutionary considerations. In conclusion, I hope we will deploy these approaches to address such problems as detecting range shifting populations in need of genetic rescue, identifying crucial adaptive variants for the long-term persistence of populations in newly colonized ranges, and predicting when range expansions may precipitate disease outbreak events.

REFERENCES

Ahbara, A., Bahbahani, H., Almathen, F., Abri, M. Al, Agoub, M. O., Abeba, A., … Mwacharo, J. M. (2019). Genome-wide variation, candidate regions and genes associated with fat deposition and tail morphology in Ethiopian indigenous sheep. *Frontiers in Genetics*, *10*, 1–21. https://doi.org/10.3389/fgene.2018.00699

Ai, H., Yang, B., Li, J., Xie, X., Chen, H., & Ren, J. (2014). Population history and genomic signatures for high-altitude adaptation in Tibetan pigs. *BMC Genomics*, *15*, 1–14. https://doi.org/10.1186/1471-2164-15-834

Alexa, A., & Rahnenführer, J. (2009). Gene set enrichment analysis with topGO. (R package).

Alvarado-Rybak, M., Acuña, P., Peñafiel-Ricaurte, A., Sewell, T. R., O'Hanlon, S. J., Fisher, M. C., … Azat, C. (2021). Chytridiomycosis outbreak in a Chilean giant frog (*Calyptocephalella gayi*) captive breeding program: genomic characterization and pathological findings. *Frontiers in Veterinary Science*, *8*, 733357. https://doi.org/10.3389/fvets.2021.733357

Arciero, E., Kraaijenbrink, T., Asan, Haber, M., Mezzavilla, M., Ayub, Q., … Tyler-Smith, C. (2018). Demographic history and genetic adaptation in the Himalayan region inferred from genome-wide SNP genotypes of 49 populations. *Molecular Biology and Evolution*, *35*(8), 1916–1933. https://doi.org/10.1093/molbev/msy094

Arenas, M., Ray, N., Currat, M., & Excoffier, L. (2012). Consequences of range contractions and range shifts on molecular diversity. *Molecular Biology and Evolution*, *29*(1), 207–218. https://doi.org/10.1093/molbev/msr187

Bairoch, A. (2000). The ENZYME database in 2000. *Nucleic Acids Research*, *28*(1), 304–305. https://doi.org/10.1093/nar/28.1.304

Basanta, M. D., Byrne, A. Q., Rosenblum, E. B., Piovia-Scott, J., & Parra-Olea, G. (2021). Early presence of *Batrachochytrium dendrobatidis* in Mexico with a contemporary dominance of the global panzootic lineage. *Molecular Ecology*, *30*, 424–437. https://doi.org/10.1111/mec.15733

Battista, V. M. (2022). *Genetic and morphological evidence for local climate adaptation in the Americas*. University of Michigan. (Doctoral dissertation).

Bay, R. A., Harrigan, R. J., Underwood, V. Le, Gibbs, H. L., Smith, T. B., & Ruegg, K. (2018). Genomic signals of selection predict climate-driven population declines in a migratory bird. *Science*, 359(6371), 83–86. https://doi.org/10.1126/science.aan4380

Becker, C. G., Rodriguez, D., Lambertini, C., Toledo, L. F., & Haddad, C. F. B. (2016). Historical dynamics of *Batrachochytrium dendrobatidis* in Amazonia. *Ecography*, *39*(10), 954–960. https://doi.org/10.1111/ecog.02055

Berger, L., Speare, R., Daszak, P., Green, D. E., Cunningham, A. A., Goggin, C. L., … Parkes, H. (1998). Chytridiomycosis causes amphibian mortality associated with population declines in the rain forests of Australia and Central America. *Proceedings of the National Academy of Sciences*, *95*(15), 9031–9036. https://doi.org/10.1073/pnas.95.15.9031

Berger, L., Speare, R., Hines, H. B., Marantelli, G., Hyatt, A. D., McDonald, K. R., … Tyler, M. J. (2004). Effect of season and temperature on mortality in amphibians due to chytridiomycosis. *Australian Veterinary Journal*, *82*(7), 31–36. https://doi.org/10.1111/j.1751-0813.2004.tb11137.x

Berke, S. K., Mahon, A. R., Lima, F. P., Halanych, K. M., Wethey, D. S., & Woodin, S. a. (2010). Range shifts and species diversity in marine ecosystem engineers: Patterns and

predictions for European sedimentary habitats. *Global Ecology and Biogeography*, 19(2), 223–232. https://doi.org/10.1111/j.1466-8238.2009.00509.x

Bi, K., Linderoth, T., Singhal, S., Vanderpool, D., Patton, J. L., Nielsen, R., … Good, J. M. (2019). Temporal genomic contrasts reveal rapid evolutionary responses in an alpine mammal during recent climate change. *PLOS Genetics*, *15*(5), e1008119. https://doi.org/10.1371/journal.pgen.1008119

Bleymehl, K., Perez-Gomez, A., Omura, M., Moreno-Perez, A., Macias, D., Bai, Z., … Mombaerts, P. (2016). Report a sensor for low environmental oxygen in the mouse main olfactory epithelium report. *Neuron*, *92*, 1196–1203. https://doi.org/10.1016/j.neuron.2016.11.001

Bolger, A. M., Lohse, M., & Usadel, B. (2014). Trimmomatic: a flexible trimmer for Illumina sequence data. *Bioinformatics*, *30*(15), 2114–2120. https://doi.org/10.1093/bioinformatics/btu170

Bosch, J., Carrascal, L. M., Durán, L., Walker, S., & Fisher, M. C. (2007). Climate change and outbreaks of amphibian chytridiomycosis in a montane area of Central Spain; is there a link? *Proceedings of the Royal Society B: Biological Sciences*, *274*(1607), 253–260. https://doi.org/10.1098/rspb.2006.3713

Bossdorf, O., Auge, H., Lafuma, L., Rogers, W. E., Siemann, E., & Prati, D. (2005). Phenotypic and genetic differentiation between native and introduced plant populations. *Oecologia*, *144*(1), 1–11. https://doi.org/10.1007/s00442-005-0070-z

Eidesen, P. B., Alsos, I. G., & Brochmann, C. (2015). Comparative analyses of plastid and AFLP data suggest different colonization history and asymmetric hybridization between *Betula pubescens* and *B. nana*. *Molecular Ecology*, *24*, 3993–4009. https://doi.org/10.1111/mec.13289

Boyle, D. G., Boyle, D. B., Olsen, V., Morgan, J. A. T., & Hyatt, A. D. (2004). Rapid quantitative detection of chytridiomycosis (*Batrachochytrium dendrobatidis*) in amphibian samples using real-time Taqman PCR assay. *Diseases of Aquatic Organisms*, *60*(2), 141–148. https://doi.org/10.3354/dao060141

Bradnam, K. R., Fass, J. N., Alexandrov, A., Baranay, P., Bechner, M., Birol, I., … Korf, I. F. (2013). Assemblathon 2: evaluating de novo methods of genome assembly in three vertebrate species. *GigaScience*, *2*, 10. https://doi.org/https://doi.org/10.1186/2047-217X-2-10

Bredeson, J. V., Mudd, A. B., Medina-Ruiz, S., Mitros, T., Smith, O. K., Miller, K. E., … Rokhsar, D. S. (2021). Conserved chromatin and repetitive patterns reveal slow genome evolution in frogs. *BioRxiv*, 1–59. https://doi.org/https://doi.org/10.1101/2021.10.18.464293

Brem, F. M. R., & Lips, K. R. (2008). *Batrachochytrium dendrobatidis* infection patterns among Panamanian amphibian species, habitats and elevations during epizootic and enzootic stages. *Diseases of Aquatic Organisms*, *81*(3), 189–202. https://doi.org/10.3354/dao01960

Brodeur, J. C., Damonte, M. J., Vera Candioti, J., Poliserpi, M. B., D'Andrea, M. F., & Bahl, M. F. (2020). Frog body condition: Basic assumptions, comparison of methods and characterization of natural variability with field data from *Leptodactylus latrans*. *Ecological Indicators*, *112*, 106098. https://doi.org/10.1016/j.ecolind.2020.106098

Burrowes, P. A., & De la Riva, I. (2017). Unraveling the historical prevalence of the invasive chytrid fungus in the Bolivian Andes: Implications in recent amphibian declines. *Biological Invasions*, *19*, 1781–1794. https://doi.org/10.1007/s10530-017-1390-8

Burrowes, P. A., James, T. Y., Jenkinson, T. S., & De la Riva, I. (2020). Genetic analysis of post-epizootic amphibian chytrid strains in Bolivia: Adding a piece to the puzzle.

Transboundary and Emerging Diseases, *67*, 2163–2171. https://doi.org/10.1111/tbed.13568

Burrowes, P. A., Joglar, R. L. ., & Green, D. E. . (2004). Potential causes for amphibian declines in Puerto Rico. *Herpetologica*, *60*(2), 141–154. https://doi.org/https://www.jstor.org/stable/3893539

Burrowes, P., & De la Riva, I. (2017). Detection of the amphibian chytrid fungus *Batrachochytrium dendrobatidis* in museum specimens of Andean aquatic birds: Implications for pathogen dispersal. *Journal of Wildlife Diseases*, *53*(2), 349–355. https://doi.org/10.7589/2016-04-074

Bustamante, M. R., Ron, S. R., & Coloma, L. A. (2005). Cambios en la diversidad en siete comunidades de anuros en los Andes de Ecuador. *Biotropica*, *37*(2), 180–189. https://doi.org/10.1111/j.1744-7429.2005.00025.x

Byrne, A. Q., Richards-Zawecki, C. L., Voyles, J., Bi, K., Ibáñez, R., & Rosenblum, E. B. (2021). Whole exome sequencing identifies the potential for genetic rescue in iconic and critically endangered Panamanian harlequin frogs. *Global Change Biology*, *27*, 50–70. https://doi.org/10.1111/gcb.15405

Byrne, A. Q., Rothstein, A. P., Poorten, T. J., Erens, J., Settles, M. L., & Rosenblum, E. B. (2017). Unlocking the story in the swab: A new genotyping assay for the amphibian chytrid fungus *Batrachochytrium dendrobatidis*. *Molecular Ecology Resources*, *17*(6), 3218–3221. https://doi.org/10.1111/ijlh.12426

Byrne, A. Q., Vredenburg, V. T., Martel, A., Pasmans, F., Bell, R. C., Blackburn, D. C., … Rosenblum, E. B. (2019). Cryptic diversity of a widespread global pathogen reveals expanded threats to amphibian conservation. *Proceedings of the National Academy of Sciences*, *116*(41), 20382–20387. https://doi.org/10.1073/pnas.1908289116

Cahill, A. E., Aiello-Lammens, M. E., Fisher-Reid, M. C., Hua, X., Karanewsky, C. J., Yeong Ryu, H., … Wiens, J. J. (2012). How does climate change cause extinction? *Proceedings of the Royal Society B: Biological Sciences*, *280*(1750), 1–9. https://doi.org/10.1098/rspb.2012.1890

Cai, L. X., Alkassis, F. F., & Kasahara, H. (2020). Defective coronary vessel organization and reduction of VEGF-A in mouse embryonic hearts with gestational mild hypoxia. *Developmental Dynamics*, *249*, 636–645. https://doi.org/10.1002/dvdy.149

Cantalapiedra, C. P., Herṇandez-Plaza, A., Letunic, I., Bork, P., & Huerta-Cepas, J. (2021). eggNOG-mapper v2: Functional Annotation, Orthology Assignments, and Domain Prediction at the Metagenomic Scale. *Molecular Biology and Evolution*, *38*(12), 5825–5829. https://doi.org/10.1093/molbev/msab293

Capblancq, T., Luu, K., Blum, M. G. B., & Bazin, E. (2018). Evaluation of redundancy analysis to identify signatures of local adaptation. *Molecular Ecology Resources*, *18*(6), 1223–1233. https://doi.org/10.1111/1755-0998.12906

Caron, C., Degeer, J., Fournier, P., Duquette, P. M., Luangrath, V., Ishii, H., & Karimzadeh, F. (2016). CdGAP/ARHGAP31, a Cdc42/Rac1 GTPase regulator, is critical for vascular development and VEGF- mediated angiogenesis. *Nature Publishing Group*, *6*, 27485. https://doi.org/10.1038/srep27485

Catenazzi, A., von May, R., & Vredenburg., V. T. (2013a). Conservation of the high Andean frog *Telmatobius jelskii* along the PERU LNG pipeline in the regions of Ayacucho and Huancavelica, Peru. In A. Alonso, F. Dallmeier, & G. Servat (Eds.), *Monitoring biodiversity: Lessons from a Trans-Andean megaproject* (pp. 172–182). Washington DC: Smithsonian Scholarly Press.

Catenazzi, A., Lehr, E., Rodriguez, L. O., & Vredenburg, V. T. (2011). *Batrachochytrium*

dendrobatidis and the collapse of anuran species richness and abundance in the Upper Manu National Park, Southeastern Peru. *Conservation Biology*, *25*(2), 382–391. https://doi.org/10.1111/j.1523-1739.2010.01604.x

Catenazzi, A., Swei, A., Finkle, J., Foreyt, E., Wyman, L., & Vredenburg, V. T. (2017). Epizootic to enzootic transition of a fungal disease in tropical Andean frogs: Are surviving species still susceptible? *PLoS ONE*, *12*(10), e0186478. https://doi.org/10.1371/journal.pone.0186478

Catenazzi, A., von May, R., & Vredenburg, V. T. (2013b). High prevalence of infection in tadpoles increases vulnerability to fungal pathogen in high-Andean amphibians. *Biological Conservation*, *159*, 413–421. https://doi.org/10.1016/j.biocon.2012.11.023

Catenazzi, A., Vredenburg, V. T., & Lehr, E. (2010). *Batrachochytrium dendrobatidis* in the live frog trade of Telmatobius (Anura: Ceratophryidae) in the tropical Andes. *Diseases of Aquatic Organisms*, *92*, 187–191. https://doi.org/10.3354/dao02250

Caye, K., Jumentier, B., Lepeule, J., & François, O. (2019). LFMM 2: Fast and accurate inference of gene-environment associations in genome-wide studies. *Molecular Biology and Evolution*, *36*(4), 852–860. https://doi.org/10.1093/molbev/msz008

Chang, W., Cui, J., Li, Y., Zang, K., Zhang, X., & Zhang, Z. (2023). Transcriptomic analysis of the cerebral hippocampal tissue in spontaneously hypertensive rats exposed to acute hypobaric hypoxia : associations with inflammation and energy metabolism. *Scientific Reports*, (13), 3681. https://doi.org/10.1038/s41598-023-30682-0

Chen, I., Hill, J. K., Ohlemüller, R., Roy, D. B., & Thomas, C. D. (2011). Rapid range shifts of species of climate warming. *Science*, *333*, 1024–1026. https://doi.org/10.1126/science.1206432

Chen, W., Tang, Z. H., Fan, X. G., Wang, Y., & Pike, D. A. (2013). Maternal investment increases with altitude in a frog on the Tibetan Plateau. *Journal of Evolutionary Biology*, *26*(12), 2710–2715. https://doi.org/10.1111/jeb.12271

Chen, Y., Tan, S., & Fu, J. (2022). Modified metabolism and response to UV radiation: gene expression variations along an elevational gradient in the Asiatic toad (*Bufo gargarizans*). *Journal of Molecular Evolution*, *90*(5), 389–399. https://doi.org/10.1007/s00239-022-10070-4

Chen, Z. L., Meng, J. M., Cao, Y., Yin, J. L., Fang, R. Q., Fan, S. B., … He, S. M. (2019). A high-speed search engine pLink 2 with systematic evaluation for proteome-scale identification of cross-linked peptides. *Nature Communications*, *10*(1), 3404. https://doi.org/10.1038/s41467-019-11337-z

Cheng, J. Y., Mailund, T., & Nielsen, R. (2017). Fast admixture analysis and population tree estimation for SNP and NGS data. *Bioinformatics*, *33*(14), 2148–2155. https://doi.org/10.1093/bioinformatics/btx098

Cheviron, Z. A., & Brumfield, R. T. (2012). Genomic insights into adaptation to high-altitude environments. *Heredity*, *108*(4), 354–361. https://doi.org/10.1038/hdy.2011.85

Cingolani, P., Platts, A., Wang, L. L., Coon, M., Nguyen, T., Wang, L., … Ruden, D. M. (2012). A program for annotating and predicting the effects of single nucleotide polymorphisms, SnpEff. *Fly*, *6*(2), 80–92. https://doi.org/10.4161/fly.19695

Cohen, J. M., McMahon, T. A., Ramsay, C., Roznik, E. A., Sauer, E. L., Bessler, S., … Rohr, J. R. (2019). Impacts of thermal mismatches on chytrid fungus *Batrachochytrium dendrobatidis* prevalence are moderated by life stage, body size, elevation and latitude. *Ecology Letters*, *22*(5), 817–825. https://doi.org/10.1111/ele.13239

Cohen, J. M., Venesky, M. D., Sauer, E. L., Civitello, D. J., McMahon, T. A., Roznik, E. A., &

Rohr, J. R. (2017). The thermal mismatch hypothesis explains host susceptibility to an emerging infectious disease. *Ecology Letters*, *20*(2), 184–193. https://doi.org/10.1111/ele.12720

Corlett, R. T., & Westcott, D. A. (2013). Will plant movements keep up with climate change? *Trends in Ecology and Evolution*, *28*(8), 482–488. https://doi.org/10.1016/j.tree.2013.04.003

Corre, V. Le, & Kremer, A. (2012). The genetic differentiation at quantitative trait loci under local adaptation. *Molecular Ecology*, *21*, 1548–1566. https://doi.org/10.1111/j.1365-294X.2012.05479.x

Crawford, A. J. (2003). Relative rates of nucleotide substitution in frogs. *Journal of Molecular Evolution*, *57*(6), 636–641. https://doi.org/10.1007/s00239-003-2513-7

Danecek, P., Bonfield, J. K., Liddle, J., Marshall, J., Ohan, V., Pollard, M. O., … Davies, R. M. (2021). Twelve years of SAMtools and BCFtools. *GigaScience*, *10*(2), 1–4. https://doi.org/10.1093/gigascience/giab008

Daskin, J. H., Bell, S. C., Schwarzkopf, L., & Alford, R. A. (2014). Cool temperatures reduce antifungal activity of symbiotic bacteria of threatened amphibians - Implications for disease management and patterns of decline. *PLoS ONE*, *9*(6), e100378. https://doi.org/10.1371/journal.pone.0100378

De la Riva, I., & Burrowes, P. A. (2011). Rapid assessment of the presence of *Batrachochytrium dendrobatidis* in Bolivian Andean frogs. *Herpetological Review*, *42*(3), 372–375.

De León, M. E., Zumbado-Ulate, H., García-Rodríguez, A., Alvarado, G., Sulaeman, H., Bolaños, F., & Vredenburg, V. T. (2019). *Batrachochytrium dendrobatidis* infection in amphibians predates first known epizootic in Costa Rica. *PLoS ONE*, *14*(12), 1–14. https://doi.org/10.1371/journal.pone.0208969

De Meester, L., Stoks, R., & Brans, K. I. (2018). Genetic adaptation as a biological buffer against climate change: Potential and limitations. *Integrative Zoology*, *13*(4), 372–391. https://doi.org/10.1111/1749-4877.12298

Dejana, E., Orsenigo, F., & Lampugnani, M. G. (2008). The role of adherens junctions and VE-cadherin in the control of vascular permeability. *Journal of Cell Science*, *121*(13), 2115–2122. https://doi.org/10.1242/jcs.017897

Diamond, S. E. (2017). Contemporary climate-driven range shifts: Putting evolution back on the table. *Functional Ecology*, *32*, 1652–1665. https://doi.org/10.1111/1365-2435.13095

Dlugosch, K. M., & Parker, I. M. (2008). Founding events in species invasions: Genetic variation, adaptive evolution, and the role of multiple introductions. *Molecular Ecology*, *17*(1), 431–449. https://doi.org/10.1111/j.1365-294X.2007.03538.x

Dobin, A., Davis, C. A., Schlesinger, F., Drenkow, J., Zaleski, C., Jha, S., Batut, P., Chaisson, M. & Gingeras, T. R. (2013). STAR: ultrafast universal RNA-seq aligner. *Bioinformatics*, *29*(1), 15—21. https://doi.org/10.1093/bioinformatics/bts635

Domingues, H. S., Cruz, A., Chan, J. R., Relvas, J. B., Rubinstein, B., & Pinto, I. M. (2018). Mechanical plasticity during oligodendrocyte differentiation and myelination. *Glia*, *66*(1), 5–14. https://doi.org/10.1002/glia.23206

Dosek, A., Ohno, H., Acs, Z., Taylor, A. W., & Radak, Z. (2007). High altitude and oxidative stress. *Respiratory Physiology and Neurobiology*, *158*, 128–131. https://doi.org/10.1016/j.resp.2007.03.013

Drula, E., Garron, M., Dogan, S., Lombard, V., Henrissat, B., & Terrapon, N. (2022). The carbohydrate-active enzyme database: functions and literature. *Nucleic Acids Research*, *50*, 571–577. https://doi.org/10.1093/nar/gkab1045

Dudney, J., Willing, C. E., Das, A. J., Latimer, A. M., Nesmith, J. C. B., & Battles, J. J. (2021). Nonlinear shifts in infectious rust disease due to climate change. *Nature Communications*, *12*(1), 5102. https://doi.org/10.1038/s41467-021-25182-6

Edelaar, P., & Bolnick, D. I. (2012). Non-random gene flow: An underappreciated force in evolution and ecology. *Trends in Ecology and Evolution*, *27*(12), 659–665. https://doi.org/10.1016/j.tree.2012.07.009

Edgar, R. C. (2004). MUSCLE: Multiple sequence alignment with high accuracy and high throughput. *Nucleic Acids Research*, *32*(5), 1792–1797. https://doi.org/10.1093/nar/gkh340

Eichstaedt, C. A., Antao, T., Cardona, A., Pagani, L., Kivisild, T., & Mormina, M. (2015). Genetic and phenotypic differentiation of an Andean intermediate altitude population. *Physiological Reports*, *3*(5), 1–15. https://doi.org/10.14814/phy2.12376

El-gebali, S., Mistry, J., Bateman, A., Eddy, S. R., Potter, S. C., Qureshi, M., … Finn, R. D. (2019). The Pfam protein families database in 2019. *Nucleic Acids Research*, *47*, 427–432. https://doi.org/10.1093/nar/gky995

Elsen, P. R., & Tingley, M. W. (2015). Global mountain topography and the fate of montane species under climate change. *Nature Climate Change*, 5, 772–776. https://doi.org/10.1038/nclimate2656

Emery, E. D. (2015). *Regulation of stem cell marker LGR5 by hypoxia in colorectal cancer*. University of Bristol. (Doctoral dissertation).

Enriquez-Urzelai, U., Bernardo, N., Moreno-Rueda, G., Montori, A., & Llorente, G. (2019). Are amphibians tracking their climatic niches in response to climate warming? A test with Iberian amphibians. *Climatic Change*, *154*, 289–301. https://doi.org/10.1007/s10584-019-02422-9

Excoffier, L., Foll, M., & Petit, R. J. (2009). Genetic consequences of range expansions. *Annual Review of Ecology, Evolution, and Systematics*, *40*, 481–501. https://doi.org/10.1146/annurev.ecolsys.39.110707.173414

Farber, D. L., Hancock, G. S., Finkel, R. C., & Rodbell, D. T. (2005). The age and extent of tropical alpine glaciation in the Cordillera Blanca, Peru. *Journal of Quaternary Science*, *20*(7–8), 759–776. https://doi.org/10.1002/jqs.994

Farrer, R. A., Weinert, L. A., Bielby, J., Garner, T. W. J., Clare, F., Bosch, J., … Fisher, M. C. (2011). Multiple emergences of genetically diverse amphibian infecting chytrids include a globalized hypervirulent recombinant lineage. *PNAS*, *108*(46), 1–6. https://doi.org/10.1073/pnas-1111915108

Ferris, K. G., Chavez, A. S., Suzuki, T. A., Beckman, E. J., Phifer-Rixey, M., Bi, K., & Nachman, M. W. (2021). The genomics of rapid climatic adaptation and parallel evolution in North American house mice. *PLoS Genetics*, *17*(4), 1–25. https://doi.org/10.1371/journal.pgen.1009495

Fick, S. E., & Hijmans, R. J. (2017). WorldClim 2 new 1-km spatial resolution climate surfaces for global land areas-annotated. *International Journal of Climatology*, *37*, 4302–4315. https://doi.org/10.1002/joc.5086

Fisher, M. C., Henk, D. A., Briggs, C. J., Brownstein, J. S., Madoff, L. C., McCraw, S. L., & Gurr, S. J. (2012). Emerging fungal threats to animal, plant and ecosystem health. *Nature*, *484*(7393), 1–18. https://doi.org/10.1038/nature10947

Fisher, R. A. (1930). *The genetical theory of natural selection*. Oxford: Oxford University Press. https://doi.org/10.5962/bhl.title.27468

Flantua, S. G. A., O'Dea, A., Onstein, R. E., Giraldo, C., & Hooghiemstra, H. (2019). The flickering connectivity system of the north Andean páramos. *Journal of Biogeography*,

46(8), 1808–1825. https://doi.org/10.1111/jbi.13607

Fletcher, D. A., & Mullins, R. D. (2010). Cell mechanics and the cytoskeleton. *Nature*, *463*(7280), 485–492. https://doi.org/10.1038/nature08908

Flynn, J. M., Hubley, R., Goubert, C., Rosen, J., Clark, A. G., Feschotte, C., & Smit, A. F. (2020). RepeatModeler2 for automated genomic discovery of transposable element families. *Proceedings of the National Academy of Sciences*, *117*(17), 9451–9457. https://doi.org/10.1073/pnas.1921046117

Forester, B. R., Beever, E. A., Darst, C., Szymanski, J., & Funk, W. C. (2022). Linking evolutionary potential to extinction risk: applications and future directions. *Frontiers in Ecology and the Environment*, *20*(9), 507–515. https://doi.org/10.1002/fee.2552

Forester, B. R., Lasky, J. R., Wagner, H. H., & Urban, D. L. (2018). Comparing methods for detecting multilocus adaptation with multivariate genotype–environment associations. *Molecular Ecology*, *27*(9), 2215–2233. https://doi.org/10.1111/mec.14584

Fox, E. A., Wright, A. E., Fumagalli, M., & Vieira, F. G. (2019). ngsLD: Evaluating linkage disequilibrium using genotype likelihoods. *Bioinformatics*, *35*(19), 3855–3856. https://doi.org/10.1093/bioinformatics/btz200

François, O., Martins, H., Caye, K., & Schoville, S. D. (2016). Controlling false discoveries in genome scans for selection. *Molecular Ecology*, *25*, 454–469. https://doi.org/10.1111/mec.13513

Freeman, B. G., Scholer, M. N., Ruiz-Gutierrez, V., & Fitzpatrick, J. W. (2018). Climate change causes upslope shifts and mountaintop extirpations in a tropical bird community. *Proceedings of the National Academy of Sciences*, *115*(47), 11982–11987. https://doi.org/10.1073/pnas.1804224115

Fu, T. T., Sun, Y. B., Gao, W., Long, C. B., Yang, C. H., Yang, X. W., … Che, J. (2022). The highest-elevation frog provides insights into mechanisms and evolution of defenses against high UV radiation. *Proceedings of the National Academy of Sciences of the United States of America*, *119*(46). https://doi.org/10.1073/pnas.2212406119

Gao, W., Fu, T., & Che, J. (2019). High-altitude adaptive evolution in amphibians and reptiles: Status and prospect. *Scientia Sinica Vitae*, *49*(4), 345–360. https://doi.org/10.1360/n052018-00216

Garnier, J., & Lewis, M. A. (2016). Expansion under climate change : The genetic consequences. *Bulletin of Mathematical Biology*, *78*, 2165–2185. https://doi.org/10.1007/s11538-016-0213-x

Garroway, C. J., Bowman, J., Cascaden, T. J., Holloway, G. L., Mahan, C. G., Malcolm, J. R., … Wilson, P. J. (2010). Climate change induced hybridization in flying squirrels. *Global Change Biology*, *16*(1), 113–121. https://doi.org/10.1111/j.1365-2486.2009.01948.x

Garroway, C. J., Bowman, J., Holloway, G. L., Malcolm, J. R., & Wilson, P. J. (2011). The genetic signature of rapid range expansion by flying squirrels in response to contemporary climate warming. *Global Change Biology*, *17*(5), 1760–1769. https://doi.org/10.1111/j.1365-2486.2010.02384.x

Gilbert, K. J., Peischl, S., & Excoffier, L. (2018). Mutation load dynamics during environmentally-driven range shifts. *PLoS Genetics*, *14*(9), e1007450. https://doi.org/10.1371/journal.pgen.1007450

Gonzalez-Garrido, A., Rosas-madrigal, S., Rojo-dom, A., Arellanes-Robledo, J., Lopez-Mora, E., Carnevale, A., … Villarreal-Molina, M. T. (2022). Leukocyte nuclear morphology alterations in dilated cardiomyopathy caused by a lamin AC truncating mutation (LMNA/Ser431*) are modified by the presence of a LAP2 missense polymorphism

(TMPO/Arg690Cys). *International Journal of Molecular Sciences*, *23*, 13626. https://doi.org/10.3390/ ijms232113626

González-Martínez, S. C., Ridout, K., & Pannell, J. R. (2017). Range expansion compromises adaptive evolution in an outcrossing plant. *Current Biology*, *27*(16), 2544–2551. https://doi.org/10.1016/j.cub.2017.07.007

Goodwin, S., McPherson, J. D., & McCombie, W. R. (2016). Coming of age: Ten years of next-generation sequencing technologies. Nature Reviews Genetics, 17(6), 333–351. https://doi.org/10.1038/nrg.2016.49

Gosner, K. L. (1960). A simplified table for staging anuran embryos and larvae with notes on identification. *Herpetologica*, *16*(3), 183–190. Retrieved from https://www.jstor.org/stable/3890061

Grupstra, C. G. B., Coma, R., Ribes, M., Leydet, K. P., Parkinson, J. E., McDonald, K., … Coffroth, M. A. (2017). Evidence for coral range expansion accompanied by reduced diversity of Symbiodinium genotypes. *Coral Reefs*, *36*, 981–985. https://doi.org/10.1007/s00338-017-1589-2

Gunderson, A. R., & Stillman, J. H. (2015). Plasticity in thermal tolerance has limited potential to buffer ectotherms from global warming. *Proceedings of the Royal Society B: Biological Sciences*, *282*(1808). https://doi.org/10.1098/rspb.2015.0401

Gutenkunst, R. N., Hernandez, R. D., Williamson, S. H., & Bustamante, C. D. (2009). Inferring the joint demographic history of multiple populations from multidimensional SNP frequency data. *PLoS Genetics*, *5*(10), e1000695. https://doi.org/10.1371/journal.pgen.1000695

Habibi, P., Ostad, S. N., Heydari, A., Aliebrahimi, S., Montazeri, V., Foroushani, A. R., … Golbabaei, F. (2022). Effect of heat stress on DNA damage: a systematic literature review. *International Journal of Biometeorology*, *66*(11), 2147–2158. https://doi.org/10.1007/s00484-022-02351-w

Haddad, N. M., Brudvig, L. A., Damschen, E. I., Evans, D. M., Johnson, B. L., Levey, D. J., … Weldon, A. J. (2014). Potential negative ecological effects of corridors. *Conservation Biology*, *28*(5), 1178–1187. https://doi.org/10.1111/cobi.12323

Hampe, A., & Petit, R. J. (2005). Conserving biodiversity under climate change: the rear edge matters. *Ecology Letters*, *8*(5), 461–467. https://doi.org/https://doi.org/10.1111/j.1461-0248.2005.00739.x

Harvell, M. C. E., Ward, J. R., Altizer, S., Dobson, A. P., Ostfeld, R. S., & Samuel, M. D. (2002). Climate warming and disease risks for terrestrial and marine biota. *Science*, *296*(5576), 2158–2162. https://doi.org/10.1126/science.1063699

Heallen, T., Zhang, M., Wang, J., Bonilla-Claudio, M., Klysik, E., Johnson, R. L., & Martin, J. F. (2011). Hippo pathway inhibits Wnt signaling to restrain cardiomyocyte proliferation and heart size. *Science*, *332*, 458–461. https://doi.org/10.1126/science.1199010

Hector, K. L., Bishop, P. J., & Nakagawa, S. (2012). Consequences of compensatory growth in an amphibian. *Journal of Zoology*, *286*(2), 93–101. https://doi.org/10.1111/j.1469-7998.2011.00850.x

Hermisson, J., & Pennings, P. S. (2017). Soft sweeps and beyond: understanding the patterns and probabilities of selection footprints under rapid adaptation. *Methods in Ecology and Evolution*, *8*(6), 700–716. https://doi.org/10.1111/2041-210X.12808

Hewitt, G. M. (2004). Genetic consequences of climatic oscillations in the Quaternary. *Philosophical Transactions of the Royal Society of London*, *359*(1442), 183–195. https://doi.org/10.1098/rstb.2003.1388

Hirashima, N., & Zasshi, Y. (2000). Molecular mechanism of exocytosis in neural and immune system. *Journal of the Pharmaceutical Society of Japan*, *120*(12), 1419–1427. https://doi.org/10.1248/yakushi1947.120.12_1419

Hoberg, E. P., & Brooks, D. R. (2015). Evolution in action: climate change, biodiversity dynamics and emerging infectious disease. *Philosophical Transactions of the Royal Society B-Biological Sciences*, *370*, 20130553. https://doi.org/10.1098/rstb.2013.0553

Hobohm, L., Kölmel, S., Niemann, C., Kümpers, P., Krieg, V. J., Bochenek, M. L., … Lankeit, M. (2021). Role of angiopoietin-2 in venous thrombus resolution and chronic thromboembolic disease. *European Respiratory Journal*, *58*, 2004196. https://doi.org/10.1183/13993003.04196-2020

Hoffmann, A. A., Sgrò, C., & M. (2011). Climate change and evolutionary adaptation. *Nature*, *470*(7335), 479–485. https://doi.org/10.1038/nature09670

Horvath, S., Haghani, A., Zoller, J. A., Naderi, A., Soltanmohammadi, E., Farmaki, E., & Kaza, V. (2022). Methylation studies in Peromyscus: aging, altitude adaptation, and monogamy. *GeroScience*, *44*, 447–461. https://doi.org/10.1007/s11357-021-00472-5

Hyatt, A. D., Boyle, D. G., Olsen, V., Boyle, D. B., Berger, L., Obendorf, D., … Colling, A. (2007). Diagnostic assays and sampling protocols for the detection of *Batrachochytrium dendrobatidis*. *Diseases of Aquatic Organisms*, *73*(3), 175–192. https://doi.org/10.3354/dao073175

Iturra-Cid, M., Ortiz, J. C., & Ibargüengoytía, N. R. (2010). Age, size, and growth of the chilean frog *Pleurodema thaul* (Anura: Leiuperidae): Latitudinal and altitudinal effects. *Copeia*, (4), 609–617. https://doi.org/10.1643/CG-09-193

Jackson, J., & Tinsley, R. (2002). Effects of environmental temperature on the susceptibility of *Xenopus laevis* and *X. wittei* (Anura) to *Protopolystoma xenopodis* (Monogenea). *Parasitology Research*, *88*(7), 632–638. https://doi.org/10.1007/s00436-002-0629-0

Jacobsen, D. (2008). Tropical high-altitude streams. In D. Dudgeon (Ed.), *Tropical Stream Ecology* (pp. 219–256). San Francisco: Academic Press. https://doi.org/10.1016/B978-012088449-0.50010-8

Jaenson, T. G. T., & Lindgren, E. (2011). The range of *Ixodes ricinus* and the risk of contracting *Lyme borreliosis* will increase northwards when the vegetation period becomes longer. *Ticks and Tick-Borne Diseases*, *2*(1), 44–49. https://doi.org/10.1016/j.ttbdis.2010.10.006

Jaiswal, A. S., Kim, H.-S., Schärer, O. D., Sharma, N., Williamson, E. A., Srinivasan, G., … Hromas, R. (2023). EEPD1 promotes repair of oxidatively-stressed replication forks. *NAR Cancer*, *5*(1), 1–20. https://doi.org/10.1093/narcan/zcac044

James, T. Y., Toledo, L. F., Rödder, D., da Silva Leite, D., Belasen, A. M., Betancourt-Román, C. M., … Longcore, J. E. (2015). Disentangling host, pathogen, and environmental determinants of a recently emerged wildlife disease: Lessons from the first 15 years of amphibian chytridiomycosis research. *Ecology and Evolution*, *5*(18), 4079–4097. https://doi.org/10.1002/ece3.1672

Jenkinson, T. S., Rodriguez, D., Clemons, R. A., Michelotti, L. A., Zamudio, K. R., Toledo, L. F., … James, T. Y. (2018). Globally invasive genotypes of the amphibian chytrid outcompete an enzootic lineage in coinfections. *Proceedings of the Royal Society B*, *285*, 20181894.

Jiang, M., & Zhang, J. (2002). Involvement of plasma-membrane NADPH oxidase in abscisic acid- and water stress-induced antioxidant defense in leaves of maize seedlings. *Planta*, *215*(6), 1022–1030. https://doi.org/10.1007/s00425-002-0829-y

Jombart, T. I. and A. (2011). adegenet 1.3-1: new tools for the analysis of genome-wide SNP

data. *Bioinformatics.*, *27*(21), 3070–3071. https://doi.org/10.1093/bioinformatics/btr521

Jones, K. E., Patel, N. G., Levy, M. A., Storeygard, A., Balk, D., Gittleman, J. L., & Daszak, P. (2008). Global trends in emerging infectious diseases. *Nature*, *451*(7181), 990–993. https://doi.org/10.1038/nature06536

Jones, P., Binns, D., Chang, H. Y., Fraser, M., Li, W., McAnulla, C., … Hunter, S. (2014). InterProScan 5: Genome-scale protein function classification. *Bioinformatics*, *30*(9), 1236–1240. https://doi.org/10.1093/bioinformatics/btu031

Jørsboe, E. (2022). Efficient approaches for large-scale GWAS with genotype uncertainty. *G3: Genes, Genomes, Genetics*, *12*(1), jkab385. https://doi.org/10.1093/g3journal/jkab385

Kamvar, Z., Tabima, J., & Grünwald, N. (2014). Poppr: an R package for genetic analysis of populations with clonal, partially clonal, and/or sexual reproduction. *PeerJ*, *2*, e281. https://doi.org/10.7717/peerj.281

Kardos, M., Armstrong, E. E., Fitzpatrick, S. W., Hauser, S., Hedrick, P. W., Miller, J. M., … Chris Funk, W. (2021). The crucial role of genome-wide genetic variation in conservation. *Proceedings of the National Academy of Sciences of the United States of America*, 118(48). https://doi.org/10.1073/pnas.2104642118

Keilwagen, J., Hartung, F., & Grau, J. (2019). GeMoMa: Homology-based gene prediction utilizing intron position conservation and RNA-seq data . In M. Kollmar (Ed.), *Gene Prediction: Methods and Protocols* (pp. 161–179). New York, New York: Humana Press. https://doi.org/10.15373/2249555x/mar2012/39

Kirkpatrick, M., & Barton, N. H. (1997). Evolution of a species' range. *The American Naturalist*, *150*(1), 1–23.

Klopfstein, S., Currat, M., & Excoffier, L. (2006). The fate of mutations surfing on the wave of a range expansion. *Molecular Biology and Evolution*, *23*(3), 482–490. https://doi.org/10.1093/molbev/msj057

Knapp, R. A., Briggs, C. J., Smith, T. C., & Maurer, J. R. (2011). Nowhere to hide: impact of a temperature-sensitive amphibian pathogen along an elevation gradient in the temperate zone. *Ecosphere*, *2*(8), 1–26. https://doi.org/10.1890/es11-00028.1

Kolby, J. E., Ramirez, S. D., Berger, L., Griffin, D. W., Jocque, M., & Skerratt, L. F. (2015). Presence of amphibian chytrid fungus (*Batrachochytrium dendrobatidis*) in rainwater suggests aerial dispersal is possible. *Aerobiologia*, *31*(3), 411–419. https://doi.org/10.1007/s10453-015-9374-6

Korneliussen, T. S., Albrechtsen, A., & Nielsen, R. (2014). ANGSD: Analysis of Next Generation Sequencing data. *BMC Bioinformatics*, *15*, 356. https://doi.org/10.1186/s12859-014-0356-4

Korneliussen, T. S., Moltke, I., Albrechtsen, A., & Nielsen, R. (2013). Calculation of Tajima's D and other neutrality test statistics from low depth next-generation sequencing data. *BMC Bioinformatics*, *14*(1), 289. https://doi.org/10.1186/1471-2105-14-289

Kusrini, M. D., Lubis, M. I., Endarwin, W., Yazid, M., Darmawan, B., Ul-Hasanah, A. U., … Rachmadi, R. (2017). Elevation range shift after 40 years: The amphibians of Mount Gede Pangrango National Park revisited. *Biological Conservation*, *206*, 75–84. https://doi.org/10.1016/j.biocon.2016.12.018

Lai, Y. T., Yeung, C. K. L., Omland, K. E., Pang, E. L., Hao, Y., Liao, B. Y., … Li, S. H. (2019). Standing genetic variation as the predominant source for adaptation of a songbird. *Proceedings of the National Academy of Sciences of the United States of America*, *116*(6), 2152–2157. https://doi.org/10.1073/pnas.1813597116

Lampo, M., Rodriguez-Contreras, A., La Marca, E., & Daszak, P. (2006). A chytridiomycosis

epidemic and a severe dry season precede the disappearance of Atelopus species from the Venezuelan Andes. *The Herpetological Journal*, *16*(4), 395–402.

Larson, J., Schomberg, S., Schroeder, W., & Carpenter, T. C. (2008). Endothelial EphA receptor stimulation increases lung vascular permeability. *American Journal of Physiology - Lung Cellular and Molecular Physiology*, *295*(3), 431–439. https://doi.org/10.1152/ajplung.90256.2008

Lawler, J. J., Ruesch, A. S., Olden, J. D., & Mcrae, B. H. (2013). Projected climate-driven faunal movement routes. *Ecology Letters*, 16(8), 1014–1022. https://doi.org/10.1111/ele.12132

Lee, J.-W., Bae, S.-H., Jeong, J.-W., Kim, S.-H. & Kim, K.-W. (2004). Hypoxia-inducible factor (HIF-1) α: its protein stability and biological functions. *Experimental and Molecular Medicine*, *36*(1), 1–12. https://doi.org/10.1038/emm.2004.1

Lefouili, M., & Nam, K. (2022). The evaluation of Bcftools mpileup and GATK HaplotypeCaller for variant calling in non-human species. *Scientific Reports*, *12*, 11331. https://doi.org/10.1038/s41598-022-15563-2

Lewontin, R. C. (1974). *The genetic basis of evolutionary change*. New York: Columbia University Press. (Doctoral dissertation).

Li, F., Qiao, Z., Duan, Q., & Nevo, E. (2021). Adaptation of mammals to hypoxia. *Animal Models in Experimental Medicine*, *4*, 311–318. https://doi.org/10.1002/ame2.12189

Li, H. (2013). Aligning sequence reads, clone sequences and assembly contigs with BWA-MEM. *ArXiv*, *00*(00), 1–3. https://doi.org/https://doi.org/10.48550/arXiv.1303.3997

Li, M., Lu, Y., Li, Y., Tong, L., Gu, X. chuan, Meng, J., … Tong, X. (2019). Transketolase deficiency protects the liver from DNA damage by increasing levels of ribose 5-phosphate and nucleotides. *Cancer Research*, *79*(14), 3689–3701. https://doi.org/10.1158/0008-5472.CAN-18-3776

Li, Y., Cohen, J. M., & Rohr, J. R. (2013). Review and synthesis of the effects of climate change on amphibians. *Integrative Zoology*, *8*(2), 145–161. https://doi.org/10.1111/1749-4877.12001

Liang, L., & Gong, P. (2017). Climate change and human infectious diseases: A synthesis of research findings from global and spatio-temporal perspectives. *Environment International*, *103*, 99–108. https://doi.org/10.1016/j.envint.2017.03.011

Liao, W. B., Lu, X., & Jehle, R. (2014). Altitudinal variation in maternal investment and trade-offs between egg size and clutch size in the Andrew's toad. *Journal of Zoology*, *293*(2), 84–91. https://doi.org/10.1111/jzo.12122

Licht, E. (1975). Comparative life history features of the western spotted frog, *Rana pretiosa*, from low- and high-elevation populations. *Canadian Journal of Zoology*, *53*(9), 1254–1257. https://doi.org/10.1139/z75-150

Lincoln, T. M., Dey, N., & Sellak, H. (2001). cGMP-dependent protein kinase signaling mechanisms in smooth muscle: from the regulation of tone to gene expression. *Journal of Applied Physiology*, *91*, 1421–1430. https://doi.org/10.1152/jappl.2001.91.3.1421

Linderoth, T. (2018). *Identifying population histories, adaptive genes, and genetic duplication from population-scale next generation sequencing*. University of California, Berkeley. (Doctoral dissertation).

Lips, K. R., Diffendorfer, J., Mendelson, J. R., & Sears, M. W. (2008). Riding the wave: Reconciling the roles of disease and climate change in amphibian declines. *PLoS Biology*, *6*(3), 441–454. https://doi.org/10.1371/journal.pbio.0060072

Loarie, S. R., Duffy, P. B., Hamilton, H., Asner, G. P., Field, C. B., & Ackerly, D. D. (2009). The velocity of climate change. *Nature*, *462*(7276), 1052–1055.

https://doi.org/10.1038/nature08649

Lobos, G., Rebolledo, N., Sandoval, M., Canales, C., & Perez-Quezada, J. F. (2018). Temporal gap between knowledge and conservation needs in high Andean anurans: The case of the Ascotán salt flat frog in Chile. *South American Journal of Herpetology*, *13*(1), 33–43. https://doi.org/10.2994/SAJH-D-16-00062.1

Lou, R. N., Jacobs, A., Wilder, A. P., & Therkildsen, N. O. (2021). A beginner's guide to low-coverage whole genome sequencing for population genomics. *Molecular Ecology*, *30*(23), 5966–5993. https://doi.org/10.1111/mec.16077

Lowry, D. B., Hoban, S., Kelley, J. L., Lotterhos, K. E., Reed, L. K., Antolin, M. F., & Storfer, A. (2016). Breaking RAD: An evaluation of the utility of restriction site associated DNA sequencing for genome scans of adaptation. *Molecular Ecology Resources*, *17*, 142–152. https://doi.org/10.1111/1755-0998.12596

Lu, B., Jin, H., & Fu, J. (2020). Molecular convergent and parallel evolution among four high-elevation anuran species from the Tibetan region. *BMC Genomics*, *21*(1), 1–14. https://doi.org/10.1186/s12864-020-07269-4

Lu, H., Wang, R., Li, W., Xie, H., Wang, C., Hao, Y., … Jia, Z. (2016). Cytokine arrays analysis of plasma from acute mountain sickness susceptible and resistant individuals. *International Journal of Clinical Experimental Medicine*, *9*(9), 18443–18450.

Lüddecke, H. (2002). Variation and trade-off in reproductive output of the Andean frog *Hyla labialis*. *Oecologia*, *130*(3), 403–410. https://doi.org/10.1007/s00442-001-0820-5

Lundby, C., Pilegaard, H., Van Hall, G., Sander, M., Calbet, J., Loft, S., & Møller, P. (2003). Oxidative DNA damage and repair in skeletal muscle of humans exposed to high-altitude hypoxia. *Toxicology*, *192*(2–3), 229–236. https://doi.org/10.1016/S0300-483X(03)00328-7

Maccracken, J. G., & Stebbings, J. L. (2012). Test of a body condition index with amphibians. *Journal of Herpetology*, *46*(3), 346–350. https://doi.org/10.1670/10-292

Magoč, T., & Salzberg, S. L. (2011). FLASH: Fast length adjustment of short reads to improve genome assemblies. *Bioinformatics*, *27*(21), 2957–2963. https://doi.org/10.1093/bioinformatics/btr507

Majmundar, A. J., Lee, D. S. M., Skuli, N., Mesquita, R. C., Kim, M. N., Yodh, A. G., … Simon, M. C. (2015). HIF modulation of wnt signaling regulates skeletal myogenesis in vivo. *Development*, *142*(14), 2405–2412. https://doi.org/10.1242/dev.123026

Marçais, G., Delcher, A. L., Phillippy, A. M., Coston, R., Salzberg, S. L., & Zimin, A. (2018). MUMmer4: A fast and versatile genome alignment system. *PLoS Computational Biology*, *14*(1), 1–14. https://doi.org/10.1371/journal.pcbi.1005944

Mark, B. G., Seltzer, G. O., & Rodbell, D. T. (2004). Late Quaternary glaciations of Ecuador, Peru and Bolivia. *Developments in Quaternary Science*, *2*, 151–163. https://doi.org/10.1016/S1571-0866(04)80120-9

Martín-Torrijos, L., Sandoval-Sierra, J. V., Muñoz, J., Diéguez-Uribeondo, J., Bosch, J., & Guayasamin, J. M. (2016). Rainbow trout (*Oncorhynchus mykiss*) threaten Andean amphibians. *Neotropical Biodiversity*, *2*(1), 26–36. https://doi.org/10.1080/23766808.2016.1151133

Martini, M. A., Kaplan, M. R., Strelin, J. A., Astini, R. A., Schaefer, J. M., Caffee, M. W., & Schwartz, R. (2017). Late Pleistocene glacial fluctuations in Cordillera Oriental, subtropical Andes. *Quaternary Science Reviews*, *171*, 245–259. https://doi.org/10.1016/j.quascirev.2017.06.033

Martins, F. M. S., Oom, M. do M., Rebelo, R., & Rosa, G. M. (2013). Differential effects of dietary protein on early life-history and morphological traits in natterjack toad (*Epidalea*

calamita) tadpoles reared in captivity. *Zoo Biology*, *32*(4), 457–462. https://doi.org/10.1002/zoo.21067

Mathur, S., & Dewoody, J. A. (2021). Genetic load has potential in large populations but is realized in small inbred populations. *Evolutionary Applications*, *14*, 1540–1557. https://doi.org/10.1111/eva.13216

Meisner, J., & Albrechtsen, A. (2018). Inferring population structure and admixture proportions in low-depth NGS data. *Genetics*, *210*, 719–731. https://doi.org/https://doi.org/10.25386/genetics.6953243

Metcalfe, N. B., & Monaghan, P. (2001). Compensation for a bad start: Grow now, pay later? *Trends in Ecology and Evolution*, *16*(5), 254–260. https://doi.org/10.1016/S0169-5347(01)02124-3

Miscio, G., Milano, E., Aguilar, J., Savia, G., Foffani, G., Mauro, A., … Oliviero, A. (2009). Functional involvement of central nervous system at high altitude. *Experimental Brain Research*, *194*(1), 157–162. https://doi.org/10.1007/s00221-009-1729-1

Mishra, K. P., & Ganju, L. (2010). Influence of high altitude exposure on the immune system: A review. *Immunological Investigations*, *39*(3), 219–234. https://doi.org/10.3109/08820131003681144

Mittan-Moreau, C. S., Kelehear, C., Toledo, L. F., Bacon, J., Guayasamin, J. M., Snyder, A., & Zamudio, K. R. (2022). Cryptic lineages and standing genetic variation across independent cane toad introductions. *Molecular Ecology*, *31*(24), 6440–6456. https://doi.org/10.1111/mec.16713

Monier-Gavelle, F., & Duband, J. L. (1997). Cross talk between adhesion molecules: Control of N-cadherin activity by intracellular signals elicited by β1 and β3 integrins in migrating neural crest cells. *Journal of Cell Biology*, *137*(7), 1663–1681. https://doi.org/10.1083/jcb.137.7.1663

Mörch, P. R., Höglund, J., Luquet, E., Meyer, Y., Alex, L., Boix, R., & Laurila, A. (2019). Latitudinal divergence in a widespread amphibian: Contrasting patterns of neutral and adaptive genomic variation. *Molecular Ecology*, *28*, 2996–3011. https://doi.org/10.1111/mec.15132

Moritz, C., Patton, J. L., Conroy, C. J., Parra, J. L., White, G. C., & Beissinger, S. R. (2008). Impact of a century of climate change on small-mammal communities in Yosemite National Park, USA. *Science*, *322*(5899), 261–264. https://doi.org/DOI 10.1126/science.1163428

Mottet, D., Ruys, S. P. D., Demazy, C., Raes, M., & Michiels, C. (2005). Role for casein kinase 2 in the regulation of HIF-1 activity. *International Journal of Cancer*, *117*(5), 764–774. https://doi.org/10.1002/ijc.21268

Muir, A. P., Biek, R., Thomas, R., & Mable, B. K. (2014). Local adaptation with high gene flow: Temperature parameters drive adaptation to altitude in the common frog (*Rana temporaria*). *Molecular Ecology*, *23*(3), 561–574. https://doi.org/10.1111/mec.12624

Muths, E., Pilliod, D. S., & Livo, L. J. (2008). Distribution and environmental limitations of an amphibian pathogen in the Rocky Mountains, USA. *Biological Conservation*, *141*(6), 1484–1492. https://doi.org/10.1016/j.biocon.2008.03.011

Naeije, R. (2010). Physiological adaptation of the cardiovascular system to high altitude. *Progress in Cardiovascular Diseases*, *52*(6), 456–466. https://doi.org/10.1016/j.pcad.2010.03.004

Noskova, E., Abramov, N., Iliutkin, S., Sidorin, A., Dobrynin, P., & Ulyantsev, V. (2023). GADMA2: more efficient and flexible demographic inference from genetic data. *BioRxiv*, 1–11. https://doi.org/https://doi.org/10.1101/2022.06.14.496083

O'Hanlon, S. J., Rieux, A., Rhys A. Farrer, Rosa, G. M., Waldman, B., Bataille, A., Kosch, T. A., Murray, K. A., Brankovics, B., Fumagalli, M., Martin, M. D., Wales, N., Alvarado-Rybak, M., Bates, K. A., Berger, L., Böll, S., Brookes, L., Frances, C. W., Wombwell, E., Zamudio, K. R., Aanensen, D. M., … Fisher, M. C. (2018). Recent Asian origin of chytrid fungi causing global amphibian declines. *Science*, *360*(6389), 621–627. https://doi.org/10.1126/science.aar1965

Oksanen, J. (2012). Constrained ordination: tutorial with R and vegan. *R- Packace Vegan*, 1–10. Retrieved from https://www.mooreecology.com/uploads/2/4/2/1/24213970/constrained_ordination.pdf

Olechnowicz, S. W. Z., Fedele, A. O., & Peet, D. J. (2012). Hypoxic induction of the regulator of G-protein signalling 4 gene is mediated by the Hypoxia-Inducible Factor pathway. *PLoS ONE*, *7*(9), 1–12. https://doi.org/10.1371/journal.pone.0044564

Ortega, H., & Hidalgo, M. (2008). Freshwater fishes and aquatic habitats in Peru: Current knowledge and conservation. *Aquatic Ecosystem Health and Management*, *11*(3), 257–271. https://doi.org/10.1080/14634980802319135

Palmer, J., & Stajich, J. E. (2016). Funannotate: a fungal genome annotation and comparative genomics pipeline. *Funannotate: Eukaryotic Genome Annotation Pipeline*. Retrieved from https://funannotate.readthedocs.io/

Parmesan, C, Ryrholm, N., Stefanescu, C., Hill, J. K., Thomas, C. D., Descimon, H., … Warren, M. (1999). Poleward shifts in geographical ranges of butterfly species associated with regional warming. *Nature*, *399*, 579–583. https://doi.org/10.1038/21181

Parmesan, C. (2006). Ecological and evolutionary responses to recent climate change. *Annual Review of Ecology, Evolution, and Systematics*, *37*(1), 637–669. https://doi.org/10.1146/annurev.ecolsys.37.091305.110100

Parris, M. J., & Cornelius, T. O. (2004). Fungal pathogen causes compatititve and developmental stress in larval amphibian communities. *Ecology*, *85*(12), 3385–3395. https://doi.org/10.1890/04-0383

Pearman, P. B., & Garner, T. W. J. (2005). Susceptibility of Italian agile frog populations to an emerging strain of Ranavirus parallels population genetic diversity. *Ecology Letters*, *8*(4), 401–408. https://doi.org/10.1111/j.1461-0248.2005.00735.x

Peig, J., & Green, A. J. (2009). New perspectives for estimating body condition from mass/length data: The scaled mass index as an alternative method. *Oikos*, *118*(12), 1883–1891. https://doi.org/10.1111/j.1600-0706.2009.17643.x

Peischl, S., & Excoffier, L. (2015). Expansion load: Recessive mutations and the role of standing genetic variation. *Molecular Ecology*, *24*(9), 2084–2094. https://doi.org/10.1111/mec.13154

Peischl, S., Kirkpatrick, M., & Excoffier, L. (2015). Expansion load and the evolutionary dynamics of a species range. *American Naturalist*, *185*(4), E81–E93. https://doi.org/10.1086/680220

Pennington, L. K., Slatyer, R. A., Ruiz-Ramos, D. V., Veloz, S. D., & Sexton, J. P. (2021). How is adaptive potential distributed within species ranges? *Evolution*, *75*(9), 2152–2166. https://doi.org/10.1111/evo.14292

Pereira, H. M., Ferrier, S., Walters, M., Geller, G. N., Jongman, R. H. G., Scholes, R. J., … Wegmann, M. (2020). Essential Biodiversity Variables. *Science*, *339*, 277–279. https://doi.org/10.1126/science.1229931

Perry, L. B., Seimon, A., & Kelly, G. M. (2014). Precipitation delivery in the tropical high Andes of southern Peru: New findings and paleoclimatic implications. *International Journal of Climatology*, *34*(1), 197–215. https://doi.org/10.1002/joc.3679

Peter, B. M., & Slatkin, M. (2015). The effective founder effect in a spatially expanding population. *Evolution*, *69*(3), 721–734. https://doi.org/10.1111/evo.12609

Piotrowski, J. S., Annis, S. L., & Longcore, J. E. (2004). Physiology of *Batrachochytrium dendrobatidis*, a chytrid pathogen of amphibians. *Mycologia*, *96*(1), 9–15. https://doi.org/10.1080/15572536.2005.11832990

Polechová, J., & Barton, N. H. (2015). Limits to adaptation along environmental gradients. *Proceedings of the National Academy of Sciences of the United States of America*, *112*(20), 6401–6406. https://doi.org/10.1073/pnas.1421515112

Poremba, R. J., Perry, L. B., Seimon, A., Martin, D. T., & Tupayachi, A. (2015). Meteorological characteristics of heavy snowfall in the Cordillera Vilcanota, Peru. In *72nd Eastern Snow Conference* (pp. 167–180). Sherbrooke, Canada. Retrieved from https://static1.squarespace.com/static/58b98f7bd1758e4cc271d365/t/5d41dd82e3638b00018150fc/1564597635718/20+Poremba+et+al.pdf

Pounds, A. J., Bustamante, M. R., Coloma, L. A., Consuegra, J. A., Fogden, M. P. L., Foster, P. N., … Young, B. E. (2006). Widespread amphibian extinctions from epidemic disease driven by global warming. *Nature*, *439*(7073), 161–167. https://doi.org/10.1038/nature04246

Price, T. D., Qvarnström, A., & Irwin, D. E. (2003). The role of phenotypic plasticity in driving genetic evolution. *Proceedings of the Royal Society B: Biological Sciences*, *270*(1523), 1433–1440. https://doi.org/10.1098/rspb.2003.2372

Pyo, J., Ryu, J., Kim, W., Choi, J. S., Jeong, J. W., & Kim, J. E. (2018). The protein phosphatase PPM1G destabilizes HIF-1α expression. *International Journal of Molecular Sciences*, *19*(8), 1–13. https://doi.org/10.3390/ijms19082297

Rachowicz, L. J., & Vredenburg, V. T. (2004). Transmission of *Batrachochytrium dendrobatidis* within and between amphibian life stages. *Diseases of Aquatic Organisms*, *61*(1–2), 75–83. https://doi.org/10.3354/dao061075

Raffel, T. R., Romansic, J. M., Halstead, N. T., McMahon, T. A., Venesky, M. D., & Rohr, J. R. (2013). Disease and thermal acclimation in a more variable and unpredictable climate. *Nature Climate Change*, *3*(2), 146–151. https://doi.org/10.1038/nclimate1659

Raghavan, M., Fee, D., & Barkhaus, P. E. (2019). *Generation and propagation of the action potential*. *Handbook of Clinical Neurology* (1st ed., Vol. 160). Elsevier B.V. https://doi.org/10.1016/B978-0-444-64032-1.00001-1

Ramos, J. E., Pecl, G. T., Moltschaniwskyj, N. A., Semmens, J. M., Souza, C. A., & Strugnell, J. M. (2018). Population genetic signatures of a climate change driven marine range extension. *Scientific Reports*, *8*, 9558. https://doi.org/10.1038/s41598-018-27351-y

Räsänen, K., Laurila, A., & Merilä, J. (2005). Maternal investment in egg size: Environment- and population-specific effects on offspring performance. *Oecologia*, *142*(4), 546–553. https://doi.org/10.1007/s00442-004-1762-5

Rawlings, N. D., Barrett, A. J., Thomas, P. D., Huang, X., Bateman, A., & Finn, R. D. (2018). The MEROPS database of proteolytic enzymes, their substrates and inhibitors in 2017 and a comparison with peptidases in the PANTHER database. *Nucleic Acids Research*, *46*, 624–632. https://doi.org/10.1093/nar/gkx1134

Raxworthy, C. J., Pearson, R. G., Rabibisoa, N., Rakotondrazafy, A. M., Ramanamanjato, J. B., Raselimanana, A. P., … Stone, D. A. (2008). Extinction vulnerability of tropical montane endemism from warming and upslope displacement: A preliminary appraisal for the highest massif in Madagascar. *Global Change Biology*, *14*(8), 1703–1720. https://doi.org/10.1111/j.1365-2486.2008.01596.x

Razgour, O., Juste, J., Ibáñez, C., Kiefer, A., Rebelo, H., Puechmaille, S. J., … Jones, G. (2013). The shaping of genetic variation in edge-of-range populations under past and future climate change. *Ecology Letters*, *16*(10), 1258–1266. https://doi.org/10.1111/ele.12158

Reed, D. H., & Frankham, R. (2003). Correlation between fitness and genetic diversity. *Conservation Biology*, *17*(1), 230–237. https://doi.org/http://www.jstor.org/stable/3095289

Rehm, E. M., Olivas, P., Stroud, J., & Feeley, K. J. (2015). Losing your edge: Climate change and the conservation value of range-edge populations. *Ecology and Evolution*, *5*(19), 4315–4326. https://doi.org/10.1002/ece3.1645

Reider, K. E. (2018). *Survival at the summits: Amphibian responses to thermal extremes, disease, and rapid climate change in the high tropical Andes*. Florida International University. (Doctoral dissertation). Retrieved from https://digitalcommons.fiu.edu/etd/3919%0A

Reider, K. E., Larson, D. J., Barnes, B. M., & Donnelly, M. A. (2020). Thermal adaptations to extreme freeze–thaw cycles in the high tropical Andes. *Biotropica*, *53*(1), 296–306. https://doi.org/10.1111/btp.12875

Rellstab, C., Gugerli, F., Eckert, A. J., Hancock, A. M., & Holderegger, R. (2015). A practical guide to environmental association analysis in landscape genomics. *Molecular Ecology*, *24*, 4348–4370. https://doi.org/10.1111/mec.13322

Riris, P., & Arroyo-Kalin, M. (2019). Widespread population decline in South America correlates with mid-Holocene climate change. *Scientific Reports*, *9*(1), 1–10. https://doi.org/10.1038/s41598-019-43086-w

Rohr, J. R., & Raffel, T. R. (2010). Linking global climate and temperature variability to widespread amphibian declines putatively caused by disease. *Proceedings of the National Academy of Sciences*, *107*(18), 8269–8274. https://doi.org/10.1073/pnas.0912883107

Romanello, M., McGushin, A., Di Napoli, C., Drummond, P., Hughes, N., Jamart, L., … Milne, I. (2021). The 2021 report of the Lancet Countdown on health and climate change. *The Lancet*, *398*(10311), 1619–1662. https://doi.org/10.1016/S0140-6736(21)01787-6

Ron, S. R. (2005). Predicting the distribution of the amphibian pathogen *Batrachochytrium dendrobatidis* in the new world. *Biotropica*, *37*(2), 209–221. https://doi.org/10.1111/j.1744-7429.2005.00028.x

Rosenblum, E. B., James, T. Y., Zamudio, K. R., Poorten, T. J., Ilut, D., Rodriguez, D., … Stajich, J. E. (2013). Complex history of the amphibian-killing chytrid fungus revealed with genome resequencing data. *Proceedings of the National Academy of Sciences*, *110*(23), 9385–9390. https://doi.org/10.1073/pnas.1300130110

Rothstein, A. P., Byrne, A. Q., Knapp, R. A., Briggs, C. J., Voyles, J., Richards-Zawacki, C. L., & Rosenblum, E. B. (2021). Divergent regional evolutionary histories of a devastating global amphibian pathogen. *Proceedings of the Royal Society B*, *288*, 20210782. https://doi.org/10.1098/rspb.2021.0782

Rowe, C. L., Kinney, O. M., Fiori, A. P., & Congdon, J. D. (1996). Oral deformities in tadpoles (*Rana catesbeiana*) associated with coal ash deposition: effects on grazing ability and growth. *Freshwater Biology*, *36*, 727–730. https://doi.org/10.1046/j.1365-2427.1996.00123.x

Rubidge, E. M., Patton, J. L., Lim, M., Burton, a. C., Brashares, J. S., & Moritz, C. (2012). Climate-induced range contraction drives genetic erosion in an alpine mammal. *Nature Climate Change*, *2*(4), 285–288. https://doi.org/10.1038/nclimate1415

Rubio, A. O. (2019). *Effects of the fungal pathogen Batrachochytrium dendrobatidis on the trophic ecology of tadpoles of Andean water frogs*. Southern Illinois University Carbondale.

(Master's thesis).

Russell, I. D., Larson, J. G., von May, R., Holmes, I. A., James, T. Y., and Robosky, A. R. (2019). Widespread chytrid infection across frogs in the Peruvian Amazon suggests critical role for low elevation in pathogen spread and persistence. *PLoS ONE*, *14*(10), e0222718. https://doi.org/10.1371/journal.pone.0222718

Saarikettu, J., Lehmusvaara, S., Pesu, M., Junttila, I., Partanen, J., Sipilä, P., … Silvennoinen, O. (2023). The RNA-binding protein Snd1/Tudor-SN regulates responsive gene expression. *FASEB BioAdvances*, *5*, 183–198. https://doi.org/10.1096/fba.2022-00115

Sakanari, J. A., & Moser, M. (1990). Adaptation of an introduced host to an indigenous parasite. *The Journal of Parasitology*, *76*(3), 420–423. Retrieved from https://www.jstor.org/stable/3282678

Scallen, T. J., & Sanghvi, A. (1983). Regulation of three key enzymes in cholesterol metabolism by phosphorylation/dephosphorylation. *Proceedings of the National Academy of Sciences of the United States of America*, *80*(9), 2477–2480. https://doi.org/10.1073/pnas.80.9.2477

Scheele, B. C., Pasmans, F., Skerratt, L. F., Berger, L., Martel, A., Beukema, W., … Carvalho, T. (2019). Amphibian fungal panzootic causes catastrophic and ongoing loss of biodiversity. *Science*, *1463*, 1459–1463. https://doi.org/10.1126/science.aav0379

Schloegel, L. M., Toledo, L. F., Longcore, J. E., Greenspan, S. E., Vieira, C. A., Lee, M., … James, T. Y. (2012). Novel, panzootic and hybrid genotypes of amphibian chytridiomycosis associated with the bullfrog trade. *Molecular Ecology*, *21*(21), 5162–5177. https://doi.org/10.1111/j.1365-294X.2012.05710.x

Schmidt, S. K., Nemergut, D. R., Miller, A. E., Freeman, K. R., King, A. J., & Seimon, A. (2009). Microbial activity and diversity during extreme freeze–thaw cycles in periglacial soils, 5400 m elevation, Cordillera Vilcanota. *Extremophiles*, *13*, 807–816. https://doi.org/10.1007/s00792-009-0268-9

Schmieder, R., & Edwards, R. (2011). Quality control and preprocessing of metagenomic datasets. *Bioinformatics*, *27*(6), 863–864. https://doi.org/10.1093/bioinformatics/btr026

Scholthof, K. G. (2007). The disease triangle: pathogens, the environment and society. *Nature Reviews Microbiology*, *5*, 152–156. https://doi.org/10.1038/nrmicro1596

Seimon, T. A., Seimon, A., Daszak, P., Halloy, S. R. P., Schloegel, L. M., Aguilar, C. A., … Simmons, J. E. (2007). Upward range extension of Andean anurans and chytridiomycosis to extreme elevations in response to tropical deglaciation. *Global Change Biology*, *13*(1), 288–299. https://doi.org/10.1111/j.1365-2486.2006.01278.x

Seimon, T. A., Seimon, A., Yager, K., Reider, K., Delgado, A., Sowell, P., … Halloy, S. (2017). Long-term monitoring of tropical alpine habitat change, Andean anurans, and chytrid fungus in the Cordillera Vilcanota, Peru: Results from a decade of study. *Ecology and Evolution*, *7*(5), 1527–1540. https://doi.org/10.1002/ece3.2779

Seimon, T., Hoernig, G., Sowell, P., Halloy, S., & Seimon, A. (2005). Identification of chytridiomycosis in *Telmatobius marmoratus* at 4450 m in the Cordillera Vilcanota of southern Peru. *Monografías de Herpetologia*, *7*, 273–281.

Shacter, E., Boon Chock, P., & Stadtman, E. R. (1984). Energy consumption in a cyclic phosphorylation/dephosphorylation cascade. *Journal of Biological Chemistry*, *259*(19), 12260–12264. https://doi.org/10.1016/s0021-9258(20)71348-7

Sharma, V., Varshney, R., & Sethy, N. K. (2022). Human adaptation to high altitude : a review of convergence between genomic and proteomic signatures. *Human Genomics*, *16*, 21. https://doi.org/10.1186/s40246-022-00395-y

Shen, W., Le, S., Li, Y., & Hu, F. (2016). SeqKit: A cross-platform and ultrafast toolkit for

FASTA/Q file manipulation. *PLoS ONE*, *11*(10), 1–10. https://doi.org/10.1371/journal.pone.0163962

Simão, F. A., Waterhouse, R. M., Ioannidis, P., Kriventseva, E. V., & Zdobnov, E. M. (2015). BUSCO: Assessing genome assembly and annotation completeness with single-copy orthologs. *Bioinformatics*, *31*(19), 3210–3212. https://doi.org/10.1093/bioinformatics/btv351

Sinha, R. P., & Häder, D. P. (2002). UV-induced DNA damage and repair: A review. *Photochemical and Photobiological Sciences*, *1*(4), 225–236. https://doi.org/10.1039/b201230h

Skerratt, Lee F., Berger, L., Hines, H. B., McDonald, K. R., Mendez, D., & Speare, R. (2008). Survey protocol for detecting chytridiomycosis in all Australian frog populations. *Diseases of Aquatic Organisms*, *80*(2), 85–94. https://doi.org/10.3354/dao01923

Skerratt, Lee Francis, Berger, L., Speare, R., Cashins, S., McDonald, K. R., Phillott, A. D., … Kenyon, N. (2007). Spread of chytridiomycosis has caused the rapid global decline and extinction of frogs. *EcoHealth*, *4*(2), 125–134. https://doi.org/10.1007/s10393-007-0093-5

Skotte, L., Korneliussen, T. S., & Albrechtsen, A. (2012). Association testing for next-generation sequencing data using score statistics. *Genetic Epidemiology*, *36*, 430–437. https://doi.org/10.1002/gepi.21636

Slatkin, M., & Excoffier, L. (2012). Serial founder effects during range expansion: A spatial analog of genetic drift. *Genetics*, *191*(1), 171–181. https://doi.org/10.1534/genetics.112.139022

Smit, A., Hubley, R., & Green, P. (2022). RepeatMasker Open-4.0. Retrieved from http://www.repeatmasker.org

Solanki, S., Devenport, S. N., Ramakrishnan, S. K., & Shah, Y. M. (2019). Temporal induction of intestinal epithelial hypoxia-inducible factor (HIF)-2a is sufficient to drive colities. *American Journal of Physiology-Gastrointestinal and Liver Physiology*, *317*, G98-107. https://doi.org/10.1152/ajpgi.00081.2019

Steffen, W., Richardson, K., Rockström, J., Cornell, S. E., Fetzer, I., Bennett, E. M., … Sörlin, S. (2015). Planetary boundaries: Guiding changing planet. *Science*, *347*, 1259855. https://doi.org/10.1126/science.1259855

Stepensky, P., Simanovsky, N., Averbuch, D., Gross, M., & Yanir, A. (2013). VPS 45-associated primary infantile myelofibrosis – Successful treatment with hematopoietic stem cell transplantation. *Pediatr Transplantation*, *17*, 820–825. https://doi.org/10.1111/petr.12169

Storey, J. M., Li, Z., & Storey, K. B. (2023). Hypoxia inducible factor-1α responds to freezing, anoxia and dehydration stresses in a freeze-tolerant frog. *Cryobiology*, *110*, 79–85. https://doi.org/10.1016/j.cryobiol.2022.11.242

Sun, Y.-B., Xiong, Z.-J., Xiang, X.-Y., Liu, S.-P., Zhou, W.-W., Tu, X.-L., … Zhang, Y.-P. (2015). Whole-genome sequence of the Tibetan frog *Nanorana parkeri* and the comparative evolution of tetrapod genomes. *Proceedings of the National Academy of Sciences of the United States of America*, *112*(11), E1257-62. https://doi.org/10.1073/pnas.1501764112

Sun, Y. B., Fu, T. T., Jin, J. Q., Murphy, R. W., Hillis, D. M., Zhang, Y. P., & Che, J. (2018). Species groups distributed across elevational gradients reveal convergent and continuous genetic adaptation to high elevations. *Proceedings of the National Academy of Sciences of the United States of America*, *115*(45), E10634–E10641. https://doi.org/10.1073/pnas.1813593115

Taddei, M. L., Chiarugi, P., Cirri, P., Buricchi, F., Fiaschi, T., Giannoni, E., … Ramponi, G. (2002). B-Catenin interacts with low-molecular-weight protein tyrosine phosphatase leading

to cadherin-mediated cell-cell adhesion increase. *Cancer Research*, *62*(22), 6489–6499.

Tajima, F. (1989). Statistical method for testing the neutral mutation hypothesis by DNA polymorphism. *Genetics*, *123*, 585–595. https://doi.org/10.1093/genetics/123.3.585

Takenaka, K., Ogi, T., Okada, T., Sonoda, E., Guo, C., Friedberg, E. C., & Takeda, S. (2006). Involvement of vertebrate Polk in translesion DNA synthesis across DNA monoalkylation damage. *Journal of Biological Chemistry*, *281*(4), 2000–2004. https://doi.org/10.1074/jbc.M506153200

Talaminos-Barroso, A., Roa-Romero, L. M., Ortega-Ruiz, F., Cejudo-Ramos, P., Marquez-Martin, E., & Reina-Tosina, J. (2021). Effects of genetics and altitude on lung function. *The Clinical Respiratory Journal*, *15*, 247–256. https://doi.org/10.1111/crj.13300

Thompson, L. G., Mosley-Thompson, E., Dansgaard, W., & Grootes, P. M. (1986). The Little Ice Age as recorded in the stratigraphy of the tropical Quelccaya ice cap. *Science*, *234*(4774), 361–364. https://doi.org/https://www.jstor.org/stable/1697771

Tiffin, P., & Ross-Ibarra, J. (2014). Advances and limits of using population genetics to understand local adaptation. *Trends in Ecology and Evolution*, *29*(12), 673–680. https://doi.org/10.1016/j.tree.2014.10.004

Urban, M. C. (2015). Accelerating extinction risk from climate change. *Science*, 348, 571–573.

Urban, M. C., Bocedi, G., Hendry, A. P., Mihoub, J. B., Pe'er, G., Singer, A., … Travis, J. M. J. (2016). Improving the forecast for biodiversity under climate change. *Science*, *353*(6304). https://doi.org/10.1126/science.aad8466

Urban, M. C. (2020). Climate-tracking species are not invasive. *Nature Climate Change*, *10*, 382–384. https://doi.org/10.1038/s41558-020-0770-8

Velo-Antón, G, Parra, J. L., Parra-Olea, G., & Zamudio, K. R. (2013). Tracking climate change in a dispersal-limited species: reduced spatial and genetic connectivity in a montane salamander. *Molecular Ecology*, *22*(12), 3261–3278. https://doi.org/10.1111/mec.12310

Velo-Antón, Guillermo, Rodríguez, D., Savage, A. E., Parra-Olea, G., Lips, K. R., & Zamudio, K. R. (2012). Amphibian-killing fungus loses genetic diversity as it spreads across the New World. *Biological Conservation*, *146*, 213–218. https://doi.org/10.1016/j.biocon.2011.12.003

Verma, P., Sharma, A., Sodhi, M., Thakur, K., Kataria, R. S., & Saket, K. (2018). Transcriptome analysis of circulating PBMCs to understand mechanism of high altitude adaptation in native cattle of Ladakh region. *Scientific Reports*, 1–15. https://doi.org/10.1038/s41598-018-25736-7

Vieira, F. G., Fumagalli, M., Albrechtsen, A., & Nielsen, R. (2013). Estimating inbreeding coefficients from NGS data: Impact on genotype calling and allele frequency estimation. *Genome Research*, *23*(11), 1852–1861. https://doi.org/10.1101/gr.157388.113

Voyles, J., Johnson, L. R., Rohr, J., Kelly, R., Barron, C., Miller, D., … Rosenblum, E. B. (2017). Diversity in growth patterns among strains of the lethal fungal pathogen *Batrachochytrium dendrobatidis* across extended thermal optima. *Oecologia*, *184*(2), 363–373. https://doi.org/10.1007/s00442-017-3866-8

Vredenburg, V. T., & Summers, A. P. (2001). Field identification of chytridiomycosis in *Rana muscosa* (Camp 1915). *Herpetological Review*, *32*(3), 151–152.

Wang, G., Murphy, R. W., Wang, G., Zhang, B., Zhou, W., Li, Y., … Yang, H. (2018). Selection and environmental adaptation along a path to speciation in the Tibetan frog *Nanorana parkeri*. *Proceedings of the National Academy of Sciences*, *115*(22), E5056–E5065. https://doi.org/10.1073/pnas.1716257115

Wang, H., Cade, B. E., Chen, H., Gleason, K. J., Saxena, R., Feng, T., … Zhu, X. (2016).

Variants in angiopoietin-2 (ANGPT2) contribute to variation in nocturnal oxyhaemoglobin saturation level. *Human Molecular Genetics*, *25*(23), 5244–5253. https://doi.org/10.1093/hmg/ddw324

Wang, J., Zamar, R., Marazzi, A., Yohai, V., Salibian-Barrera, M., Maronna, R., … Konis, K. (2014). Robust: robust library. Retrieved from https://cran.r-project.org/web/packages/robust/robust.pdf

Wang, M. S., Li, Y., Peng, M. S., Zhong, L., Wang, Z. J., Li, Q. Y., … Zhang, Y. P. (2015). Genomic analyses reveal potential independent adaptation to high altitude in Tibetan chickens. *Molecular Biology and Evolution*, *32*(7), 1880–1889. https://doi.org/10.1093/molbev/msv071

Wang, Q.-W., Hidema, J., & Hikosaka, K. (2014). Is UV-induced DNA damage greater at higher elevation? *American Journal of Botany*, *101*(5), 796–802. https://doi.org/10.3732/ajb.1400010

Wang, Y. L., Han, W. H., Yun, S. M., & Han, J. K. (2023). Identification of protein phosphatase 4 catalytic subunit as a Wnt promoting factor in pan-cancer and Xenopus early embryogenesis. *Scientific Reports*, *13*(1), 1–16. https://doi.org/10.1038/s41598-023-35719-y

Warne, R. W., Crespi, E. J., & Brunner, J. L. (2011). Escape from the pond: Stress and developmental responses to ranavirus infection in wood frog tadpoles. *Functional Ecology*, *25*(1), 139–146. https://doi.org/10.1111/j.1365-2435.2010.01793.x

Wasserman, T. N., Cushman, S. A., Littell, J. S., Shirk, A. J., & Landguth, E. L. (2013). Population connectivity and genetic diversity of American marten (*Martes americana*) in the United States northern Rocky Mountains in a climate change context. *Conservation Genetics*, *14*(2), 529–541. https://doi.org/10.1007/s10592-012-0336-z

Weber, R. E., Ostojic, H., Fago, A., Dewilde, S., Van Hauwaert, M.-L., Moens, L., & Monge, C. (2002). Novel mechanism for high-altitude adaptation in hemoglobin of the Andean frog *Telmatobius peruvianus*. *Am J Physiol Regul Integr Comp Physiol*, *283*(5), R1052-1060. https://doi.org/10.1152/ajpregu.00292.2002

Weisenfeld, N. I., Kumar, V., Shah, P., Church, D. M., & Jaffe, D. B. (2017). Direct determination of diploid genome sequences. *Genome Research*, *27*(5), 757–767. https://doi.org/10.1101/gr.214874.116

White, K., & Someya, S. (2023). The roles of NADPH and isocitrate dehydrogenase in cochlear mitochondrial antioxidant defense and aging. *Hearing Research*, *427*, 108659. https://doi.org/10.1016/j.heares.2022.108659

Wickham, H. (2011). Ggplot2. *Wiley Interdisciplinary Reviews: Computational Statistics*, *3*(2), 180–185. https://doi.org/10.1002/wics.147

Wilkinson, L. J., Neal, C. S., Singh, R. R., Sparrow, D. B., Kurniawan, N. D., Ju, A., … Little, M. H. (2015). Renal developmental defects resulting from in utero hypoxia are associated with suppression of ureteric β-catenin signaling. *Kidney International*, *87*(5), 975–983. https://doi.org/10.1038/ki.2014.394

Willi, Y., Fracassetti, M., Bachmann, O., & Buskirk, J. Van. (2020). Demographic processes linked to genetic diversity and positive selection across a species' range. *Plant Communications*, *1*(6), 100111. https://doi.org/10.1016/j.xplc.2020.100111

Willi, Y., Fracassetti, M., Zoller, S., & Van Buskirk, J. (2018). Accumulation of mutational load at the edges of a species range. *Molecular Biology and Evolution*, *35*(4), 781–791. https://doi.org/10.1093/molbev/msy003

Wilson-Rich, N., & Starks, P. T. (2010). The Polistes war: Weak immune function in the

invasive *P. dominulus* relative to the native *P. fuscatus*. *Insectes Sociaux*, *57*(1), 47–52. https://doi.org/10.1007/s00040-009-0049-6

Winter, S. C., Buffa, F. M., Silva, P., Miller, C., Valentine, H. R., Turley, H., … Harris, A. L. (2007). Relation of a hypoxia metagene derived from head and neck cancer to prognosis of multiple cancers. *Cancer Research*, *67*(7), 3441–3449. https://doi.org/10.1158/0008-5472.CAN-06-3322

Womack, M. C., & Bell, R. C. (2020). Two-hundred million years of anuran body-size evolution in relation to geography, ecology and life history. *Journal of Evolutionary Biology*, *33*(10), 1417–1432. https://doi.org/10.1111/jeb.13679

Woodhams, D. C., Alford, R. A., Briggs, C. J., Johnson, M., & Rollins-Smith, L. A. (2008). Life-history trade-offs influence disease in changing climates: Strategies of an amphibian pathogen. *Ecology*, *89*(6), 1627–1639. https://doi.org/10.1890/06-1842.1

Yang, P., Wang, G., Jiang, S., Chen, M., Zeng, J., Pang, Q., … Zhou, M. (2021). Comparative analysis of genome-wide copy number variations between Tibetan sheep and White Suffolk sheep. *Animal Biotechnology*, *34*(4), 986–993. https://doi.org/10.1080/10495398.2021.2007937

Yang, S., Wang, L., Huang, J., Zhang, X., Yuan, Y., Chen, J.-Q., … Tian, D. (2015). Parent–progeny sequencing indicates higher mutation rates in heterozygotes. *Nature*, *523*, 463. https://doi.org/10.1038/nature14649

Yang, W., Qi, Y., Bi, K., & Fu, J. (2012). Toward understanding the genetic basis of adaptation to high-elevation life in poikilothermic species: A comparative transcriptomic analysis of two ranid frogs, *Rana chensinensis* and *R. kukunoris*. *BMC Genomics*, *13*(1), 1–11. https://doi.org/10.1186/1471-2164-13-588

Yang, W., Qi, Y., & Fu, J. (2014). Exploring the genetic basis of adaptation to high elevations in reptiles: A comparative transcriptome analysis of two toad-headed agamas (genus Phrynocephalus). *PLoS ONE*, *9*(11), 1–8. https://doi.org/10.1371/journal.pone.0112218

Yang, W., Qi, Y., & Fu, J. (2016). Genetic signals of high-altitude adaptation in amphibians: A comparative transcriptome analysis. *BMC Genetics*, *17*(1), 1–10. https://doi.org/10.1186/s12863-016-0440-z

Yang, X., Wang, Y., Zhang, Y., Lee, W., & Zhang, Y. (2016). Rich diversity and potency of skin antioxidant peptides revealed a novel molecular basis for high-altitude adaptation of amphibians. *Scientific Reports*, *6*(Ju), 1–11. https://doi.org/10.1038/srep19866

Yasbin, R. E., Cheo, D., & Bol, D. (1993). DNA Repair Systems. In *Bacillus subtilis and Other Gram-Positive Bacteria* (pp. 529–537). https://doi.org/10.1128/9781555818388

Young, B. E., Josse, C., Stern, M., Vasconez, S., Olander, J., Smyth, R., … Hak, J. (2015). *Ecosystem Profile Technical Summary: Tropical Andes Biodiversity Hotspot*. Retrieved from https://www.cepf.net/sites/default/files/tropicalandes_techsummary.pdf

Yuan, D., Chen, X., Gu, H., Zou, M., Zou, Y., Fang, J., … Wang, Z. (2020). Chromosomal genome of *Triplophysa bleekeri* provides insights into its evolution and environmental adaptation. *GigaScience*, *9*(11), 1–14. https://doi.org/10.1093/gigascience/giaa132

Yuan, Z., Liu, E., Liu, Z., Kijas, J. W., Zhu, C., Hu, S., … Wei, C. (2016). Selection signature analysis reveals genes associated with tail type in Chinese indigenous sheep. *Animal Genetics*, *48*(1), 55–66. https://doi.org/10.1111/age.12477

Zamora-Vilchis, I., Williams, S. E., & Johnson, C. N. (2012). Environmental temperature affects prevalence of blood parasites of birds on an elevation gradient: Implications for disease in a warming climate. *PLoS ONE*, *7*(6), e39208. https://doi.org/10.1371/journal.pone.0039208

Zeng, Y., Zhang, X., Kang, K., Chen, J., Wu, Z., Huang, J., … Gou, D. (2016). MicroRNA-223

attenuates hypoxia-induced vascular remodeling by targeting RhoB/MLC2 in pulmonary arterial smooth muscle cells. *Scientific Reports*, *6*, 1–13. https://doi.org/10.1038/srep24900

Zhang, B., Ban, D., Gou, X., Zhang, Y., Yang, L., Chamba, Y., & Zhang, H. (2019). Genome-wide DNA methylation profiles in Tibetan and Yorkshire pigs under high-altitude hypoxia. *Journal of Animal Science and Biotechnology*, *10*(1), 1–10. https://doi.org/10.1186/s40104-019-0316-y

Zhang, R., Ji, Z., Cai, J., Li, Y., & Ma, G. (2021). Clinical significance of serum kallistatin and ENOX1 levels in patients with coronary heart disease. *Medical Principles and Practice*, *30*(4), 339–346. https://doi.org/10.1159/000510427

Zhang, T., Chen, J., Zhang, J., Guo, Y. T., Zhou, X., Li, M. W., … Shi, P. (2021). Phenotypic and genomic adaptations to the extremely high elevation in plateau zokor (Myospalax baileyi). *Molecular Ecology*, *30*(22), 5765–5779. https://doi.org/10.1111/mec.16174

Zhou, D., Azad, P., Stobdan, T., & Haddad, G. G. (2021). Mechanisms regulating hypoxia tolerance in Drosophila and humans. In *Stress: Genetics, Epigenetics and Genomics* (pp. 241–251). Elsevier Inc. https://doi.org/10.1016/B978-0-12-813156-5.00022-4

Zhou, X., Qiu, W., Sathirapongsasuti, J. F., Cho, M. H., Mancini, J. D., Lao, T., … Silverman, E. K. (2013). Gene expression analysis uncovers novel hedgehog interacting protein (HHIP) effects in human bronchial epithelial cells. *Genomics*, *101*(5), 263–272. https://doi.org/10.1016/j.ygeno.2013.02.010